United States
Environmental Protection
Agency

Industrial Environmental Research
Laboratory
Research Triangle Park NC 27711

EPA-600/7-79-021
January 1979

EPA

Solids Transport Between Adjacent CAFB Fluidized Beds

Interagency Energy/Environment R&D Program Report

RESEARCH REPORTING SERIES

Research reports of the Office of Research and Development, U.S. Environmental Protection Agency, have been grouped into nine series. These nine broad categories were established to facilitate further development and application of environmental technology. Elimination of traditional grouping was consciously planned to foster technology transfer and a maximum interface in related fields. The nine series are:

1. Environmental Health Effects Research
2. Environmental Protection Technology
3. Ecological Research
4. Environmental Monitoring
5. Socioeconomic Environmental Studies
6. Scientific and Technical Assessment Reports (STAR)
7. Interagency Energy-Environment Research and Development
8. "Special" Reports
9. Miscellaneous Reports

This report has been assigned to the INTERAGENCY ENERGY-ENVIRONMENT RESEARCH AND DEVELOPMENT series. Reports in this series result from the effort funded under the 17-agency Federal Energy/Environment Research and Development Program. These studies relate to EPA's mission to protect the public health and welfare from adverse effects of pollutants associated with energy systems. The goal of the Program is to assure the rapid development of domestic energy supplies in an environmentally-compatible manner by providing the necessary environmental data and control technology. Investigations include analyses of the transport of energy-related pollutants and their health and ecological effects; assessments of, and development of, control technologies for energy systems; and integrated assessments of a wide range of energy-related environmental issues.

EPA REVIEW NOTICE

This report has been reviewed by the participating Federal Agencies, and approved for publication. Approval does not signify that the contents necessarily reflect the views and policies of the Government, nor does mention of trade names or commercial products constitute endorsement or recommendation for use.

This document is available to the public through the National Technical Information Service, Springfield, Virginia 22161.

EPA-600/7-79-021

January 1979

Solids Transport Between Adjacent CAFB Fluidized Beds

by

D.M. Bachovchin, P.R. Mulik, R.A. Newby,
and D.L. Keairns

Westinghouse Research and Development Center
Pittsburgh, Pennsylvania 15235

Contract No. 68-02-2142
Program Element No. EHE623A

EPA Project Officer: Samuel L. Rakes

Industrial Environmental Research Laboratory
Office of Energy, Minerals, and Industry
Research Triangle Park, NC 27711

Prepared for

U.S. ENVIRONMENTAL PROTECTION AGENCY
Office of Research and Development
Washington, DC 20460

PREFACE

The Westinghouse Research and Development Center is carrying out a program under contract to the United States Environmental Protection Agency (EPA) to provide experimental and engineering support for the development of the Chemically Active Fluid-Bed (CAFB) process. The process was originally conceived at the Esso Petroleum Company, Ltd., Abingdon, UK (ERCA), as a fluidized-bed gasification process to convert heavy fuel oils to a clean, medium heating-value fuel gas for firing in a conventional boiler. Westinghouse, under contract to EPA, completed an initial evaluation of the process in 1971.[1] Conceptual designs and cost estimates were prepared for new and retrofit utility boiler applications using heavy fuel oil. Westinghouse continued the process evaluation from 1971 to 1973 and formulated an atmospheric pollution control demonstration plant program for retrofit of a utility boiler utilizing a high-sulfur, high-metals content fuel oil (for example, vacuum bottoms).[2] The CAFB process represented an attractive option for use of these low-grade fuels, for which pollution control using hydro-desulfurization or stack-gas cleaning was not economical. Application of a pressurized CAFB concept with combined-cycle power plants was also assessed.[2] Experimental support work was initiated during 1971 to 1973 to investigate two areas of concern - sorbent selection and spent sorbent processing - to achieve an acceptable material for disposal or utilization. The preliminary design and cost estimate for a 50 MWe demonstration plant at the New England System Manchester Street Station in Providence, RI were completed in 1975.[3] Commercial plant costs were projected and development requirements identified. Experimental support on the sulfur removal system continued in order to provide a basis for the detailed plant design. A number of design and operation parameters from the preliminary design study that required further development were identified. Demonstration on a commercial scale of the pulsed-flow solids transport system between

the gasifier and regenerator was identified as one of the areas requiring development. This report presents the results of the program initiated at that time to develop a design basis and operating procedures for the pulsed-flow solids transport system. A solids transport test facility was built and operated to provide an understanding of the pulsed-flow system for plant design and operation. The design and performance projections are applied to the CAFB process designed by Foster Wheeler Energy Corporation (FW) under contract to EPA for retrofit on a 20 MWe gas-fired boiler at a Central Power and Light (CPL) plant in San Benito, Texas.[4]

Additional support work carried out under the present contract (68-02-2142), which will be reported, includes:

- Sorbent selection [5,6]
- Processing spent sorbent to minimize environmental impact[5]
- Environmental impact from disposal of processed and unprocessed spent sorbent[5]
- Engineering evaluation of the CAFB process.[7]

ABSTRACT

A pulsed, dense-phase pneumatic transport system for controlled circulation between adjacent fluidized beds was experimentally investigated and a model developed to predict performance. The program provides technical support for the EPA program to demonstrate the Chemically Active Fluid Bed (CAFB), a process being developed to produce a clean, low heating-value fuel gas from fossil fuels.

A cold model test facility capable of transporting up to about 6.3 kg/s (50,000 lb/hr) was built and operated to allow examination of the effects of key parameters. The data generated were utilized in the development of a mathematical model of the system which allows projection of the effects of key variables. Solids flow is controlled by pulsed air input, whose on-time (<0.3 to 0.4 s) and off-time (1.5 to 2.0 s) should be controlled for best performance. The system pressure balance should also be carefully controlled. The expected demonstration plant bed-material density may result in higher air requirements than had been predicted in the plant design. The use of wider legs and more nozzles or greater transport-gas capacity may alleviate this difficulty.

TABLE OF CONTENTS

	Page
SUMMARY	1
1. INTRODUCTION	4
2. CONCLUSIONS	7
3. RECOMMENDATIONS	9
3.1 CAFB Plant Operation	9
3.2 Further Study	10
4. BACKGROUND AND PLANT REQUIREMENTS	11
5. TEST FACILITY	14
5.1 Design Basis	14
5.2 Specifications	19
5.2.1 Fluidized-Bed Vessels	20
5.2.2 Transfer Legs	20
5.2.3 Centrifugal Blower	20
5.2.4 Cyclone Collectors	21
5.2.5 Dust Collector	21
5.2.6 Pulsation Control System	21
5.2.7 Instrumentation and Control Package	22
5.2.8 Additional Specifications	23
5.3 Construction and Costs	23
6. TEST PROGRAM	24
6.1 Summary	24
6.2 Test Material	24
6.3 Procedures	27
6.3.1 Experimental Technique	27
6.3.2 Solids Flow Rate Determination	28
6.4 First Test Series - Inserted Pipe Sparger	30
6.4.1 Introduction	30
6.4.2 Results and Discussion	30
6.5 Second Test Series - Recessed Nozzle Sparger	38
6.5.1 Introduction	38
6.5.2 Results and Discussion	38

TABLE OF CONTENTS (Cont)

7. SOLIDS TRANSPORT MODEL 60

7.1 Model Development 60

7.1.1 Time Sequence 60
7.1.2 Steady State Assumptions 62
7.1.3 Mass Balances 63
7.1.4 Momentum Balance 65
7.1.5 Horizontal Pressure Drop 66
7.1.6 Dilute Phase Flow Area 67
7.1.7 Fluidizing Time 69
7.1.8 Vertical Section Voidage 70
7.1.9 Dilute Phase Voidage 71
7.1.10 Model Summary and Procedure 72

7.2 Model Performance 75

8. DEMONSTRATION PLANT PERFORMANCE PROJECTIONS 79

8.1 Total Transport Gas Flow Rate 79
8.2 Pulse Gas On- and Off-Times 79
8.3 Process Related Parameters 82
8.4 Particulate Properties 85
8.5 Leg Geometry Variation 87

9. ASSESSMENT 91

10. REFERENCES 94

APPENDICES

A. SOLIDS TRANSPORT TEST FACILITY SPECIFICATION DETAILS 96

A.1. Drawings and Photographs 96
A.2. Instruments and Auxiliary Equipment 111

B. SUPPLEMENTAL TEST DATA 119

C. MODEL DEVELOPMENT DETAIL 134

C.1. Jet Area 134
C.2. Fluidizing Time 137
C.3. Defluidizing Behavior and Vertical Section Voidage Estimation 140

D. MODEL PROGRAM LISTING 142

E. MODEL PREDICTIONS 149

LIST OF FIGURES

1. CAFB Material Circulation System 12

2. Test Facility Schematic 15

3. Test Facility Fluid-Bed Vessels 16

4. Test Facility Transport Leg 18

5. Inserted Pipe Sparger 31

6. Recessed Nozzle Sparger 39

7. Effect of Pulse Air Rate 52

8. Effect of Pulse Air Rate 52

9. Effect of Pulse Air Rate 53

10. Effect of Pulse Air Rate 53

11. Effect of Off-Time 54

12. Effect of Off-Time 54

13. Effect of Pulse Air Rate at Constant On-Off Times 55

14. Effect of Off-Time at Lower Fluidizing Velocities 55

15. Effect of Off-Time at Lower Fluidizing Velocities 56

16. Effect of Off-Time at Lower Fluidizing Velocities 56

17. Observed Transport Flow Profile 59

18. Nomenclature for Transport Model 61

19. Solids Transport Model Flow Profile 64

20. Jet Expansion Model 68

21. Transport Leg Model Flow Sheet 73

22. CAFB Demonstration Plant Transport Leg Design 77

LIST OF TABLES

1. Particle Size Distribution at Beginning of Final Test Series 26

2. Particle Size Distribution at Conclusions of Final Test Series 26

3. Transport Data - First Test Series 33

4. Transport Data - Second Test Series 41

5. Transport Leg Model - Variables 74

6. Comparison of FWEC Final Design Data and Model Predictions 78

7. Effect of Total Gas Flow Rate 80

8. Effect of On- and Off-Times at Constant Total Gas Flow Rate 81

9. Effect of On- and Off-Times at Constant Gas Flow Rate during Pulse 83

10. Effect of Temperature 83

11. Effect of Receiving Vessel Absolute Pressure 85

12. Effect of Pressure Gradient across Transfer Leg 85

13. Effect of Average Particle Size 86

14. Effect of Particle Density 86

15. Effect of Horizontal Slot Height 88

16. Effect of Vertical Height at Constant $\Delta P/L$ 88

17. Effect of Horizontal Length 90

NOMENCLATURE

Note: The model computer program listing features different nomenclature, which is detailed in the listing. Different unit multiples (e.g., μm) are noted in text.

Symbol	Definition	Dimensions
A	Projected area of rising slug or bubble (Appendix C.2)	m^2
A_B	Fluid-bed cross-sectional area	m^2
A_r	Relative entrainment interface area	m^2
C_D	Drag coefficient of fluid bed on rising gas slug (Appendix C.2)	-
d_o	Nozzle diameter	m
d_p	Average particle dimension	m
d_{pi}	Particle dimension of ith sieve fraction	m
D_t	Four times mean hydraulic radius	m
g	Gravitational acceleration	m/s^2
g_c	Conversion constant	$1\ kg\ m/(N\ s^2)$
G_A	Overall average pulse gas input rate	kg/s
G_S	Solids flow rate	kg/s
h	Final height of plane jet (Fig. C-1)	m
H_h	Horizontal slot height	m
k	$\equiv v_{s3}/v_3$	-
L_H	Length of horizontal leg section	m
L_S	Length of vertical leg section	m

NOMENCLATURE (Cont)

Symbol	Definition	Dimensions
L_V	Vertical component of L_S	m
M	Gas molecular weight	-
N	Number of nozzles per leg	-
P	Pressure	N/m^2
P_1	Pressure at leg bend	N/m^2
P_2	Transport gas pressure issuing from nozzles	N/m^2
P_3	Pressure at leg discharge	N/m^2
P_4	Pressure at top of leg	N/m^2
ΔP	$\equiv P_1 - P_4$	N/m^2
$\Delta P°$	$\equiv P_3 - P_4$	N/m^2
ΔP_L	Level recorder pressure drop	N/m^2
r	Radius of noninterfering circular jets	m
S_1	Cross-sectional area of leg	m^2
S_2	Inside area of N nozzles	m^2
S_3	Area of dilute phase horizontal flow	m^2
t	Time	s
t_M	Fluidizing time in response to imposed ΔP	s
t_{OFF}	Pulse off-time	s
t_{ON}	Pulse on-time	s
t_P	Time required for repacking	s
t_R	Response time for defluidization	s
t_S	Time during which solids may flow: minimum of t_M, t_{ON}	s
T	Gas temperature	K

NOMENCLATURE (Cont)

Symbol	Definition	Dimensions
T.R.	Transport ratio = mass of solids moved per mass of transport gas required	-
U_f	Fluidizing velocity (superficial)	m/s
U_{mf}	Minimum fluidizing velocity (superficial)	m/s
U_r	Interstitial gas velocity relative to solids	m/s
U_s	Superficial horizontal solids velocity (eq. 13)	m/s
v	Rise velocity of slug	m/s
v_1	Downward velocity of gas in leg vertical section	m/s
v_2	Pulse gas nozzle exit velocity	m/s
v_3	Velocity of gas exiting leg in dilute phase	m/s
v_R	$\equiv v_{s1} - v_1$	m/s
v_{RH}	Interstitial gas velocity in stagnant solid area of horizontal leg section	m/s
v_{s1}	Downward solids velocity in leg vertical section	m/s
v_{s3}	Velocity of solids in dilute phase at leg discharge	m/s
W	Leg width	m
W_H	Horizontal air rate during pulse	kg/s
W_P	Transport air rate during pulse	kg/s
x_1	Distance from nozzle plane to plane of mutual jet interference	m
x_h	Distance from nozzle plane to plane of horizontal ceiling lip	m
x_i	Weight fraction of ith sieve size	-

NOMENCLATURE (Cont)

Symbol	Definition	Dimensions
x_n	Center-to-center nozzle separation	m
y_1	Distance from virtual origin of plane jet to nozzle plane (Fig. C-1)	m
y_2	Distance from virtual origin of circular jet to nozzle plane (Fig. C-2)	m
z	Upward height of rise of bubble (Fig. C-2)	m
Δz	Packed-bed slab thickness (Fig. C-2)	m
α	Angle of leg downcomer from vertical	Deg.
β	Plane jet half-angle	Deg.
ε_1	Vertical section voidage	-
ε_3	Dilute phase discharge voidage	-
ε_p	Packed bed voidage	-
θ	Circular jet half-angle	Deg.
μ	Gas viscosity	kg/m/s
ρ_1	Gas density at transfer leg bend	kg/m^3
ρ_2	Gas density issuing from nozzles	kg/m^3
ρ_3	Gas density at transfer leg discharge	kg/m^3
ρ_B	Bulk density	kg/m^3
ρ_{DS}	Superficial bulk density of horizontal section material	kg/m^3
ρ_{FB}	Fluid-bed density	kg/m^3
ρ_g	Gas density	kg/m^3
ρ_p	Particle density	kg/m^3

ACKNOWLEDGEMENT

The authors acknowledge the contributions and support of Mr. S. L. Rakes who served as the EPA project officer. Mr. P. P. Turner and Mr. R. P. Hangebrauck, Industrial Environmental Research Laboratory, EPA, are acknowledged for their continuing contributions and support of the program.

The following Westinghouse personnel made significant contributions to the design, construction and operation of the facility: M. J. Balogh, T. R. Dristas, W. J. Havener, W. K. Hess, R. B. Mitchell, R. D. Novak, and E. J. Vidt. R. G. Ballinger, W. D. Ciprella, and E. P. Tully of the Peter F. Loftus Corporation performed the detailed mechanical design and equipment specification for the facility.

SUMMARY

The chemically Active Fluid Bed (CAFB) process is being developed as a retrofit to existing boilers to allow the efficient use of high-sulfur liquid or solid fuels in an environmentally acceptable manner. This atmospheric-pressure fluidized-bed gasification process utilizes limestone feed to the gasifier to achieve desulfurization. During the gasification process, fuel sulfur is absorbed by lime, which is the major bed material constituent. The spent lime can be regenerated in a separate vessel and the regenerated material returned to the gasifier. Regeneration of the spent sulfur sorbent offers the opportunity to minimize the quantity of limestone required to meet the sulfur emission standards.

The regeneration of the bed material requires the controllable, efficient, and nonmechanical transfer of high-temperature particulate between vessels featuring different chemical environments. During the early development work on the CAFB process by the Esso Research Centre at Abingdon, UK (ERCA),[8] a pulsed transfer technique evolved for the simultaneous transfer of material to and from the regenerator.

Westinghouse has designed, built, and operated a large cold model test unit to examine the transport process, as part of a broad CAFB engineering support program sponsored by the U. S. Environmental Protection Agency (EPA). The purpose of this program is to gain an understanding of the transport technique, its limitations, and the associated physical phenomena. With such an understanding projections of performance under different sets of conditions could be made, with more confident scale-up and optimization possible. The test facility was also designed to be able to support the CAFB demonstration plant program at the Central Power and Light Company (CPL). A 20 MWe gas-fixed boiler at the CPL La Palma Power Station in San Benito, Texas is being retrofitted with the CAFB process.[9]

Transport system optimization must deal with the following desirable features: high solids capacity, minimum air requirement, controllability, a seal against reactor gas exchange, and freedom from plugging or other malfunction.

Pulsed transport air is added to the junction of the horizontal and vertical sections of each transport leg. In the first method of air introduction tested, air was supplied internally to the leg via a pipe sparger. Then a method was tested whereby air was supplied through nozzles in the back wall of the transfer slot elbow. This method was clearly superior in terms of both solids capacity and efficiency.

Variables tested included pulse on-time, off-time, and flow rate; and fluidizing velocity. A mathematical model of the system was developed on the basis of a momentum balance. The model allows the projection of demonstration plant transport system performance at various conditions.

Each pulse of nozzle gas was found to cause the vertical seal between vessels to be destroyed. This takes a short time (0.4s), during which effective solids flow can take place. Gas added after this time is wasted, passing upward. Exchange of reactor gas may also occur after this point. Between pulses sufficient time (>1.5 s) must be allowed for the repacking of vertical leg solids. At given pulse on- and off-times, higher gas input will produce more solids flow at reduced efficiency. The pressure gradient across a leg will determine whether a leg will fluidize and how long it will take. The gradient should therefore be minimized. The model predicts that higher solids densities allow better transport performance.

On the basis of this model we project that, as currently designed, the desired particulate flow can be achieved in the demonstration plant, but the efficiency (i.e., the solids-to-gas ratio) will be lower than those optimally obtained in the FW and Westinghouse experimental programs. The air requirement may be reduced by using wider legs and more nozzles. Every effort to control pulse on- and off- times near the optimum conditions

identified in this study should be made. Further study, concentrating on particle density, particle size, nozzle configuration, leg dimensions, and simulation of operational problems is recommended.

1.0 INTRODUCTION

The controlled transport of high-temperature solids is required for the successful commercialization of many advanced fossil fuel processing systems. An application that illustrates this need is the circulation of sulfur sorbents in high-temperature sulfur removal systems that regenerate the sorbent for reutilization in the desulfurizer.[2,3,10]

Westinghouse, under contract to EPA, is providing experimental and engineering support for the development of such a process, the Chemically Active Fluid Bed (CAFB). The work performed is in support of the EPA program to demonstrate this technology.[6] The CAFB process was originally conceived by ERCA to gasify high-sulfur residual oil to produce a clean, low heating-value fuel gas. The current demonstration program includes the use of lignite as a fuel.

In the CAFB process, fuel is gasified in a fluid bed composed of lime, which will chemically capture fuel sulfur. Regeneration of the lime will require simultaneous transfer of solids to and from the gasifier vessel and the adjacent regenerator vessel. A method has been developed whereby this transfer is caused and controlled by the pulsed introduction of transport gas.

A preliminary design and cost estimate for a 50 MWe demonstration plant for the CAFB process carried out by Westinghouse reviewed alternative solids transport systems.[3] The need for a compact transport system with the potential for reduced gas transport requirements resulted in the selection of a pulsed, dense-phase transport system that ERCA was using on a 1 MWe equivalent CAFB pilot facility.[8] Westinghouse recommended that simulation tests be carried out on the demonstration scale to develop design and operating data. The purpose of this program was to gain an understanding of the transport technique, its limitations, and the

associated physical phenomena. With such an understanding projections of performance under different sets of conditions could be made, with more confident scale-up and optimization possible. The test facility was also conceived to be able to test proposed solutions for demonstration plant troubles that might arise.

The design of the solids transport test facility was initiated in 1975 on the basis of the available information from the ERCA pilot plant facility and discussions with ERCA personnel, as a direct scale to the 50 MWe plant design. The 50 MWe demonstration plant program, however, was not continued, primarily because of the decision to minimize the use of oil in boilers capable of firing coal in the Northeast following the oil embargo. The EPA program to demonstrate the CAFB process was continued in 1975 with a contract to Foster Wheeler Energy Corporation (FW) to retrofit a CAFB process on a 20 MWe gas-fired boiler at Central Power and Light's (CPL) plant in San Benito, Texas.[4] The CPL plant is designed to utilize residual oil as fuel. CPL, however, is interested in using lignite coal as a fuel, and the test program includes the use of lignite. The pulsed-flow solids transport system remains an area of concern. Westinghouse, as part of a CAFB engineering support program sponsored by EPA, continued with the support program to build the solids transport test facility for development of information useful for the plant design and operation.

The program objectives were directed toward developing a sufficient understanding of the solids transport system to provide a basis for projection, improvement, and correction of the performance of the CAFB demonstration plant now scheduled for operation in 1979. Transport system optimization must deal with the following desirable features: high solids capacity, minimum air requirement, controllability, a seal against reactor gas exchange, and freedom from plugging or other malfunction.

The transport test facility has been built to provide data for this investigation. Pulsed transport air is added to the junction of the horizontal and vertical sections of each transport leg. In the first

method of air introduction tested, air was supplied internally to the leg via a pipe sparger. Then a method was tested whereby air was supplied through nozzles in the back wall of the transfer slot elbow.

Variables tested included pulse on-time, off-time, and flow rate; and fluidizing velocity. A mathematical model of the system was developed on the basis of a momentum balance. The model allows the projection of demonstration plant transport system performance at various conditions. Design and performance projections reported are related to the CPL plant design. Previous solids transport data collected by FW on a cold model are also compared with the model projections.[11]

2.0 CONCLUSIONS

- The inserted pipe sparger tests were not satisfactory with regard to solids flow capacity and transfer efficiency. Presumed reasons were obstruction of the solids flow stream and limited transport gas interface for solids entrainment.
- The recessed nozzle system similar to that being used in the CAFB demonstration plant yielded solids flows of 80 to 110 kg/s-m^2. This compares with projected needs of 110 to 150 kg/s-m^2 with the current demonstration plant design. Transfer ratios (mass of solids to mass of air) in excess of 100 were frequently obtained.
- Each pulse of transport gas imposes a pressure drop upon the vertical section of a transport leg that is in excess of that needed to fluidize the leg. The nonequilibrium state existing during the short time required to fluidize the leg is a vertical seal only during which transfer of solids may occur. This time is about 0.3 to 0.4 s. Longer on-times only waste transport gas.
- If a pulse is long enough to complete fluidization, a minimum time is required to complete defluidization and repacking of solids prior to the next pulse. This time is about 1.5 s. Proportionately less time is needed at shorter on-times. Excessive off-time may result in overpacking and resistance to new pulse jets.
- Unless both beds are highly expanded, adequate solids flow in each direction simultaneously is not possible under continuous (i.e., not pulsed) aeration control.

- A model has been developed that allows the projection of transport system performance under different conditions and sets of variables. The model is essentially a momentum balance with appropriate assumptions. The following points are model predicted trends:
  - Other conditions being constant, a higher gas input rate will yield increased solids flow and reduced transport efficiency.
  - Temperature, pressure level, and particle size have only moderate effects upon performance.
  - The pressure gradient across a leg is important in that it determines whether a leg will fluidize or not during a pulse. Within either of these regimes the imposed pressure gradient does not seem to have a major effect.
  - Both solids flow rate and transport ratio (mass of solids to gas) are sensitive to particle density. Heavier particles are more rapidly moved than lighter ones.
  - The model predicts that increasing any of several leg dimensions (vertical height, horizontal length, horizontal depth) will improve capacity and efficiency.
- It is projected that, if the solids density is as low as expected, transport gas requirements will be high relative to those optimally obtained in the FW and Westinghouse test programs (transport mass ratios of about 40). Necessary flow should still be achievable.
- On-times in excess of the leg fluidizing times may result in significant transfer of reactor gases from one vessel to another, particularly from the higher pressure bed.
- The stagnant solids region at the base of the horizontal section is the most likely place for caking of solids to occur.
- The solids transport legs seem to have a preference for the larger bed particles. This may result in the build-up of unreactive fines in either bed.

3.0 RECOMMENDATIONS

3.1 CAFB PLANT OPERATION

- Every effort should be made to keep the pulse on-time slightly lower than the leg fluidizing time (~0.3 s), yielding substantially improved efficiency and preventing massive flows of reactor gas between the two vessels. This procedure may be practical using two solenoid valves in series, with offset phases.
- For maximum efficiency and capacity the off-time should be 1.5 to 2.0 s, depending on the on-time used.
- Piping volume between the pulsation control and delivery systems should be minimized to reduce capacitance effects and allow the actual and desired pulse wave forms to be alike.
- Within other process constraints the pressure gradients across the transfer legs should be minimized by manipulation of bed operating pressures, bed levels, and fluidizing velocities. Furthermore, if the pulse duration is longer than the fluidizing time, the beds should be operated at as nearly the same pressures as possible because gas will be exchanged between the two vessels when seals are blown.
- Bed compositions should be periodically monitored to ascertain whether or not untransportable fines are building up in either system. If so, recycle of cyclone fines to opposite beds (if possible within system pressure balance and other constraints) may remedy this problem.
- Wider legs of similar design, with proportionately more nozzles, and with less gas input per nozzle, should produce higher capacity and require much less transport gas.

3.2 FURTHER STUDY

- The effect of particle density should be experimentally confirmed. In conjunction, particle size effects should be investigated.
- The effects of nozzle diameter, penetration, and spacing should be explored to complete model applicability and provide operating flexibility.
- Further systematic investigations of leg dimension (height, horizontal length, width, horizontal depth, angle of tilt) may confirm better designs.

4.0 BACKGROUND AND PLANT REQUIREMENTS

The material circulation concept for the CAFB process is illustrated schematically in Figure 1. The gasifier and regenerator are to be located in a single rectangular vessel, partitioned to prevent intermixing of the two atmospheres. The partition is pierced by transfer slots to carry controlled amounts of material in each direction. Each slot has a vertical section in which solids move downward as a packed bed to provide at least a partial seal against gas backflow. A horizontal section is needed to allow packing, and, hence, to prohibit "freewheeling" of solids between pulses. Pulsed gas (boiler stack gas) is to blow material from the horizontal section in the proper direction, the transferred material to be replaced with solids from the vertical packed-bed supply line. In each fluid bed a partial obstruction will regulate the circulation of material and provide some control of solids residence time.

Placing the two beds in close contact at the same level has the significant advantages of allowing compact, economical construction, and conserving process heat at the interface and in the transfer duct system. The main disadvantage is that the short vertical legs between relatively dense fluidized vessels cannot provide a complete or stable partial seal in both directions simultaneously. The pulsed transport mode of operation should allow this weakness to be circumvented at some cost in efficiency in comparison to similar designs with continuous control aeration.

The potential problems of blown seals and uncontrollable or unpredictable solids flow rates have required a testing program to identify

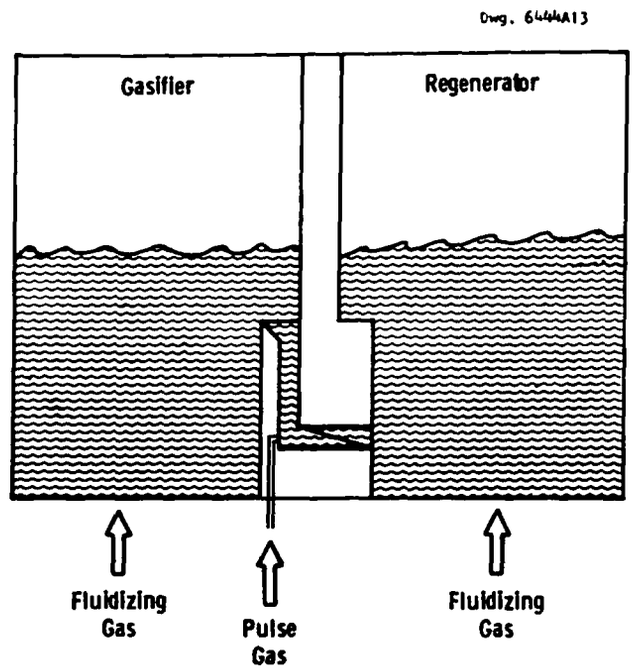

Figure 1a. System Schematic - Side View CAFB Material Circulation

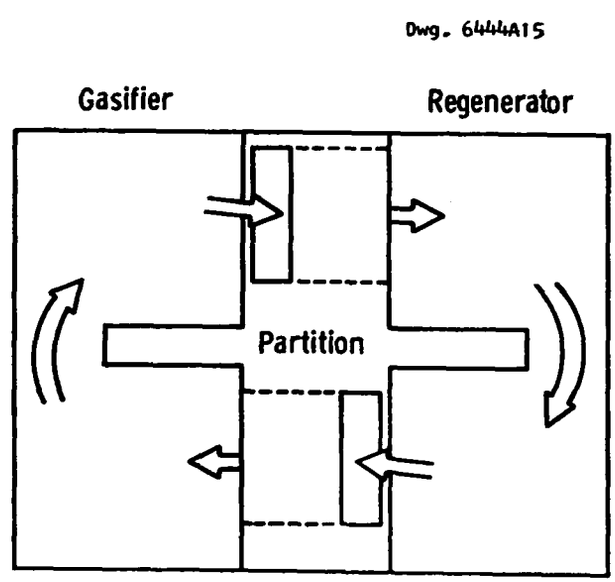

Figure 1b. System Schematic - Top View CAFB Material Circulation

and understand the key parameters and their effects. This knowledge will be useful in optimizing the transfer system performance in the demonstration plant. The specific performance requirements include:

- The capacity to achieve the necessary solids circulation rates (2.5 to 3.8 kg/s) in each direction
- A minimum pulse gas flow requirement (maximum transport efficiency)
- The minimum necessary pulse gas delivery pressure
- A predictable and controllable relationship between gas input rate and solids flow
- The prevention of a significant flux of regenerator gas into the gasifier via the transfer ducts, and the converse
- Freedom from plugging caused by agglomeration, geometric obstacles, and other malfunctions
- The assurance that the full spectrum of material present (particle size, density, etc.) will be periodically transferred to the other bed, in order to prevent the build-up of inactive material in either bed.

In the present study we constructed a large cold test facility to generate data with which to gain a more thorough understanding of the pulse-transport system. The resulting mathematical model should allow projections of the effects of major system variables and more satisfactory extrapolation to hot conditions. With this facility we also hoped to determine whether the above listed qualitative expectations are realistic, to note possible operational problem areas, and to suggest methods to avoid or solve such problems.

5.0 TEST FACILITY

5.1 DESIGN BASIS

The solids transport test facility has been designed to simulate the pulsed, dense-phase pneumatic transport method that has been utilized in the ERCA pilot plant and has been selected for use in the CPL demonstration plant. The scale of the facility was selected to be representative of the demonstration plant and future commercial CAFB plants. The facility was also designed with sufficient flexibility to permit a wide range of operating conditions and transport leg designs, since only small-scale data were available. A schematic of the test facility is presented in Figure 2.

The major design basis considerations specified prior to detailed design are summarized below.

Scale of model - 10–25 MWe

Solids circulation rate expected - 4 kg/s (maximum)

Vessel design (see Figure 3)

- Two identical semicylindrical vessels
- Operating pressure - 120 kPa
- Design pressure - 140 kPa
- Operating temperature - ambient
- Materials of construction - sheet metal with clear sections (Plexiglas, Lucite, glass, etc.) as shown in drawing
- Locations of clear observation sections - one 1.2 m strip on wall of each vessel as shown, one section on each lid, one section above each entrance and exit of two transport legs
- Dimensions - 3 m tall, 0.7 m radius, 1.5 m bed depth (max.), 1.2 m freeboard (min.), transfer leg exit 8 cm above distributor plate (indention in vessel wall)
- Skid mounted to permit transfer leg interchange (maximum separation of 1.2 m)

Dwg. 1699B34

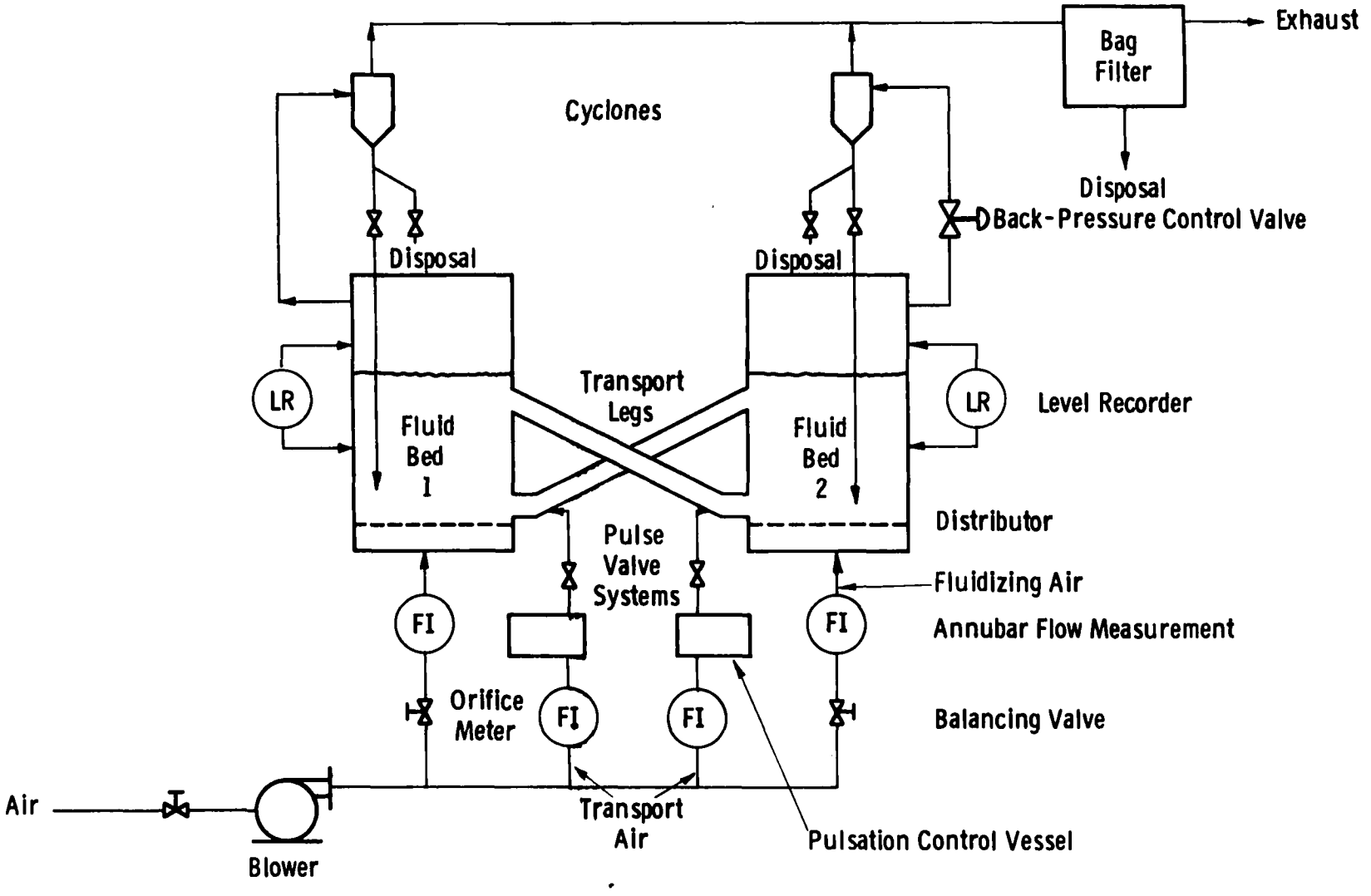

Figure 2. Test Facility Flow Diagram

Dwg. 1699B35

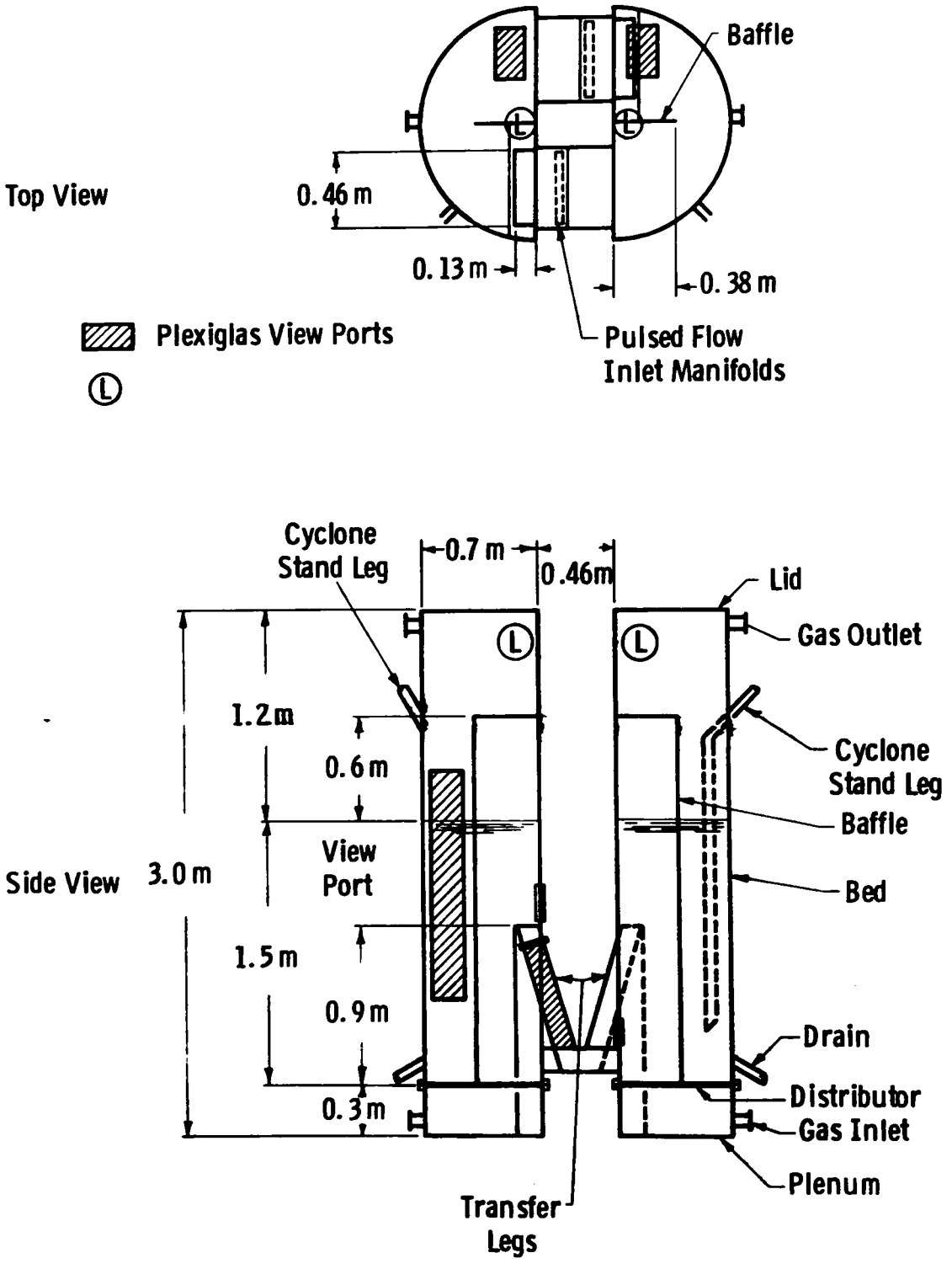

Figure 3. Test Facility Fluid-Bed Vessels

Internals - vertical baffle plate (2.1 m tall) to separate inlet from outlet (should be removable)

Distributor plate is orifice type with 325 mesh screen covering holes. Hole diameter, number, and spacing to be determined based on 3 kPa ΔP at bed operating velocity of 1.2 m/s.

Inlets and Outlets - air to plenum, air exit through wall, cyclone standleg through wall, bed loading port and bed drain through wall; sizes to be determined.

Lid bolted or hinged

Transport legs (see Figure 4)

Two identical transport legs (single design shown)

Design pressure - 140 kPa

Materials of construction - totally clear plastic material or constructed with clear sections for observation

Dimensions - duct height 12.7 cm, duct width 0.456 m, leg height 0.853 m, horizontal leg length 0.37 m (see drawing)

Transport legs are flanged at both ends to permit easy changing of legs.

Transport gas rate (average maximum) - 0.047 m^3/s at $\sim$130 kPa (based on 80 kg solids transferred per 1 m^3 transport gas)

Transport gas pulse duration (s) - 0.5, 1, 2, 3, 4, 5, continuous

Pulse % on time - 100, 75, 50, 40, 30, 20, 10

Instantaneous transport gas rate - 0.12 m^3/s (maximum)

Aeration gas locations as shown in drawing

Aeration gas rate (maximum) - 0.025 m^3/s at standard conditions

Aeration pipes - diameter, hole size, number of holes to be determined on the basis of permissible pressure drop

Transport gas pulse-pipe design - pipe diameter (2.5 to 5 cm), hole size, number to be determined on the basis of permissible pressure drop ($\sim$4 kPa). Pipe should be permitted to rotate to change hole orientation. Alternate locations for pipe provided.

Bed material - crushed brick or other material having proper bulk density. Particle size about 600 to 3000 μm range. Bed pressure drop of about 0.1 kPa/cm bed depth. Minimum fluidization velocity of 0.3 to 0.6 m/s.

Dwg. 1699B36

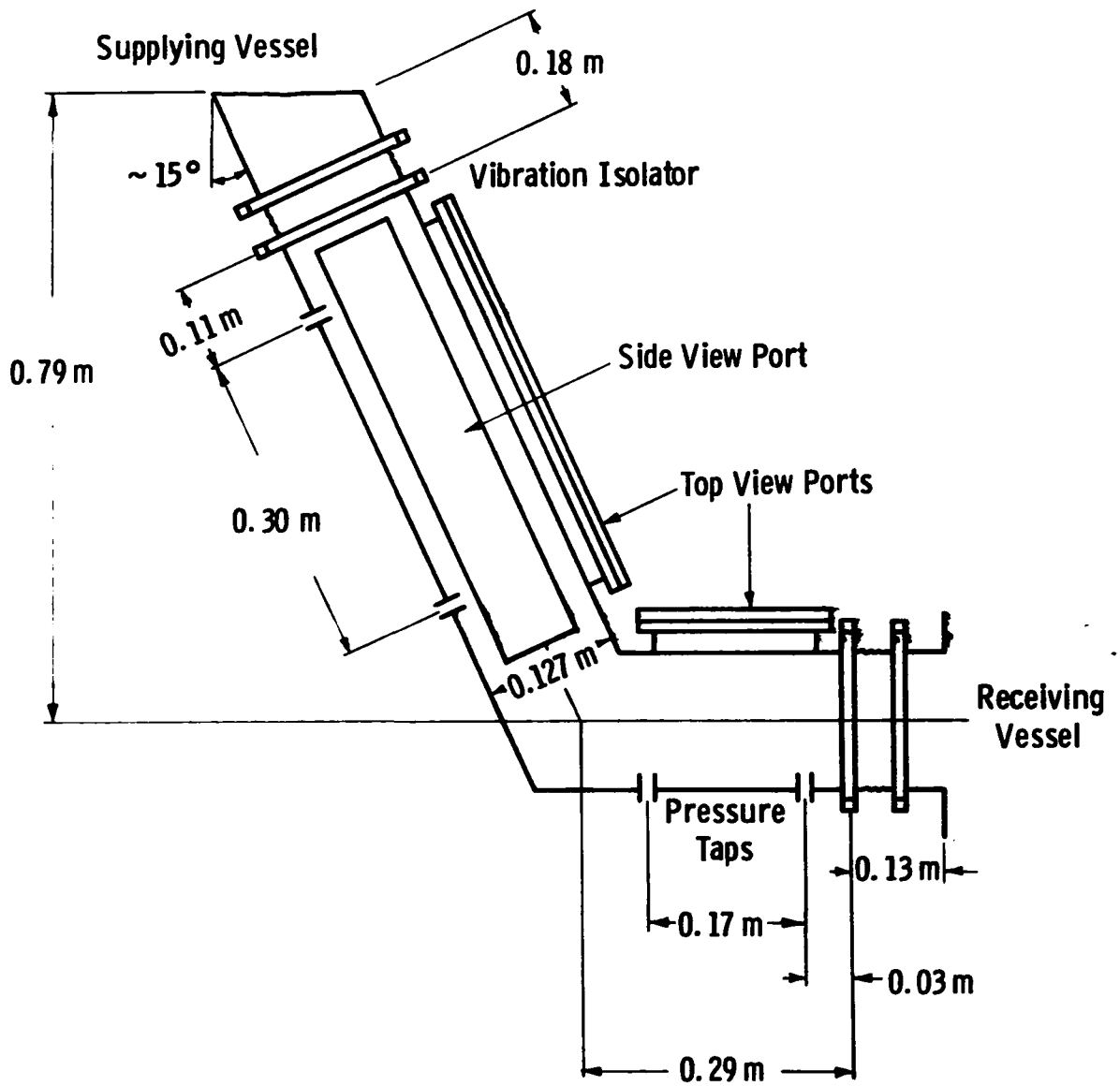

Note: Width = 0.457 m

Figure 4. Test Facility Transport Leg

Air requirements - about 2 standard m^3/s at 130 kPa delivery pressure. Supplied by new blower(s).

Loading and draining system - standard feeder and pneumatic transport system (packaged system) capable of filling or draining beds. Fill both beds through single vessel. Drain both vessels separately.

Cyclone(s) - maximum pressure drop of 3.7 kPa. Collect large material (>400 μm) and recycle to beds. Single cyclone for both beds or two cyclones in parallel.

Filter - collect fines passing through cyclone(s). Sufficient efficiency to meet environmental restrictions. Maximum pressure drop of 3.7 kPa.

Pulsing valves - capable of meeting pulse frequency and duration requirements at specified flow rates by simple adjustments.

Back-pressure valve - capable of providing a pressure differential between the two vessels of 0.25 to 1.25 kPa

Operation - pulse-gas rates will be continuously recorded to provide record of instantaneous and average transport gas usage. Solids transport rates will be determined by recording the bed level change (pressure drop change) of one of the beds as a function of time when one transport leg is shut off. This method will be supplemented by direct observation of the flow in the transport legs or tracer experiments.

5.2 SPECIFICATIONS

A complete set of drawings of the system and its components is in Appendix A-1. These are numbered F940-1 to F940-11. As shown in Figure F940-1, the facility consists of two identical fluidized-bed vessels and the following major support systems:

1. Transfer legs (TL-1 and TL-2)
2. 186 kW centrifugal blower (CB-1)
3. Cyclone collectors (CC-1 and CC-2)
4. Baghouse dust collector (DC-1)
5. Pulsation control system, including pulsation control vessels (PCV-1 and PCV-2)
6. Instrument and control package.

5.2.1 Fluidized Bed Vessels

The two identical semicylindrical vessels are illustrated in Figure 3 and Drawing F940-2 in the Appendix. These 0.7 m radius by 3 m tall vessels have cross-sectional flow areas of 0.63 m^2 below the transfer leg hoppers and 0.74 m^2 above. View ports were included as described under Section 5.1 above. Design parameters were:

Operating pressure	- 140 kPa
Design pressure	- 160 kPa
Operating and design temperature	- 340 K.

One of the units was mounted on a track system to permit the use of different leg designs requiring other vessel separation (maximum separation of 1.8 m).

The distributor plates each contained 252 0.95 cm holes drilled at 4.76 cm triangular pitch (F940-2). Weeping of solids through the distributor holes was prevented by overlaying a 325 mesh stainless steel screen.

5.2.2 Transfer Legs

The transfer legs (Figure 4 and Drawing F940-3) of 0.058 m^2 flow area featured standlegs of 0.85 m vertical height slanted at 15° from the vertical. View ports (Drawing F940-3) were installed to allow observation of solids flow characteristics. There were two pressure taps in both the vertical and horizontal sections of each leg for further examination of the flow behavior. Provision was made to aerate the vertical leg section continuously (maximum rate 0.00566 m^3/s) if desired or necessary. Design and operating temperatures and pressures were the same as for the fluidized-bed vessels.

5.2.3 Centrifugal Blower

Fluidizing and pulse air were supplied by a five-stage centrifugal blower (CB-1), which was Model 1255 supplied by the Lamson Division of Diebold, Inc. This unit is rated to supply 2.83 standard m^3/s at a

delivery pressure of 140 kPa. Blower capacity is regulated by a manual butterfly valve mounted on the intake. The blower will generate 157 kPa at approximately 1.18 m^3/s, and the pressure curve is relatively flat from that point to no delivery.

5.2.4 Cyclone Collectors

Two identical cyclones (CC-1 and CC-2) were used to control emissions and prevent excessive loss of bed material. Each of these units (Model VM810/150, Size 77, supplied by the Ducon Company, Inc.) has a capacity of 1.42 m^3/s of air at 325 K and is rated for positive pressure operation up to a gauge pressure of 7.5 kPa. Adjustable pressure switches, set at 7.5 kPa, are employed to protect the unit. The maximum dust loading on each unit is 1.15 mg/m^3 of particles ranging from 1 to 1500 μm in size. The cyclones are capable of removing 99 percent of all particles larger than 40 μm at a maximum pressure drop of 1.5 kPa at the above dust loading. Collected dust is removed by rotary valves and can be either recycled to the fluid bed or collected for disposal.

5.2.5 Dust Collector

This unit (DC-I) has a capacity of 2.83 m^3/s of air at 320 K, is rated for positive pressure operation up to 5 kPa gauge pressure, and is protected by a rupture disc. The collector (Model 645-10-20, Micropul Division, U. S. Filter Corp.) has a maximum dust loading of 0.46 mg/m^3 of particles 1 to 40 μm in size and is capable of removing 99 percent of the material 1 μm or larger at a maximum pressure loss of 1.5 kPa.

5.2.6 Pulsation Control System

Identical systems draw air from the blower discharge for pulsing each transfer leg. Each system consists of an orifice-type flow measuring device, a pulsation control vessel, a balancing valve, a solenoid valve, and the actual injection configuration. The average maximum transport gas rate is 0.05 m^3/s, with an instantaneous maximum rate of 0.12 m^3/s. The solenoid valves and their control system allow variable pulse frequency (1.5 to 90 pulses/min) with the capability to vary the on-time from 0 to 100 percent of the pulse cycle length.

Pulsation control vessels (PCV-1 and PCV-2) are 1.8 m^3 units located between the flow measuring elements and the control valves. These units dampen pulsations at the flow meters sufficiently to produce accurate measurements of average transport gas flow over the range investigated. Design parameters are:

Operating pressure	- 140 kPa
Design pressure	- 160 kPa
Operating temperature	- 340 K
Design temperature	- 345 K.

5.2.7 Instrumentation and Control Package

Relative locations of all instrument measurement points are found in Drawing F940-1 in Appendix A1. Accurate positions can then be located from the appropriate detailed drawings. A list of instrument and auxiliary equipment specifications is contained in Appendix A2. In the following brief discussion of the instrumentation package, parenthetical codes refer to designations used in these Appendices.

Process temperatures (TI-1 through TI-4) are measured at blower inlet and discharge and between each vessel and the corresponding cyclone. Pressures (PI-1 through PI-4) are measured at blower discharge, cyclone inlets, and at the baghouse inlet.

Fluidization velocities can be independently controlled with 30-cm butterfly valves (V-1). A back-pressure control valve (PC-3) permits maintenance of equal bed pressure levels at different fluidizing velocities or the converse. Flow rates are metered with Annubar (Ellison Instrument Co.) velocity head sensors (FE-1, 4).

Transport gas flow is metered with flange top orifice plates (FRT-2, 3), and the square root of the differential pressure signal is recorded. The signals are computer integrated for average flow rate. The solenoid valves (VFC-2, 3), controllers (FC-2, 3), and hand-operated 10-cm balancing valve (V-1) provide control of the transport gas curve.

Pressure differentials are monitored across the distributor plates and across the fluidized beds. In addition, the level of either bed can be recorded (LR-1) by manipulation of valves between the level recorder and the bed vessels. The rate of bed level decrease (or increase) is used to determine the bed material transfer rate. Finally, pressures at various points in the transport legs can be monitored or recorded (PT-1, 2, PR-1, 2).

5.2.8 Additional Specifications

Diagrams describing system layout, the control panel, electrical plan, instrumentation schematics, and structural details are included as Drawings F940-4 through F940-11 in Appendix A1.

5.3 CONSTRUCTION AND COSTS

Detailed engineering design and construction supervision were performed by Peter F. Loftus Corporation. Site construction was done by Garfield, Inc. The facility was constructed at the Westinghouse Waltz Mill Site. Facility costs included:

Engineering and design (Loftus)	-	$24,000
Site construction (Garfield)	-	79,000
Capital equipment	-	64,000
Alumina (bed material)	-	2,350 .

6.0 TEST PROGRAM

6.1 SUMMARY

An activated alumina catalyst was used as the bed material in our simulation of the CAFB transfer system. Solids flow rates were measured during one-directional tests at points of equal bed height. Independent variables included pulse duration, time between pulses, airflow during pulse, and fluidizing velocity.

The test program was divided into two segments during which two different pulse gas introduction systems were examined. The first sparger (first test series) was a multiorifice pipe distributor inserted directly into the transport leg bend. The second test series used a sparger that was a series of nozzles inserted just through the back wall of the standleg. Extensive data with each system demonstrated the superiority of the second system, in terms of both achievable solids flow and transfer efficiency. The data were used to test a mathematical model (Section 7) that was being developed simultaneously. Optimization of the pulse curve was possible using feedback understanding from the model.

6.2 TEST MATERIAL

Activated alumina was selected as the test material on the basis of its bulk density (specific gravity $\sim$1, as expected for CAFB material), particle size distribution, and availability in bulk. The first alumina used was Alcoa type F-1 with nominal size distribution of 8 to 10 mesh (1680 to 2380 μm).

The high porosity of this material (top pore size 3 to 10 μm) suggested that it would be prone to attrition. A series of tests were performed to determine attrition losses during long-term exposure of the

material to a fluidized-bed environment. In addition, experiments were performed to determine other pertinent data - minimum fluidization velocity, particle size distribution, and bulk density.

Experimental conditions for the attrition test were as follows:

- Test unit - 7.0-cm diameter Plexiglas tube (0.91 m high)
- Distributor - high-velocity orifice type
- Operating velocity - 1.2 m/s (slugging)
- Test duration - 96 hr.

Attrition losses, without recycle, were approximately 10 percent by weight of the initial charge. These data indicate that the greatest attrition loss occurred for particles ranging in size from 2000 to 2800 μm. Elutriation due to slugging may have been responsible for loss of some of the larger particles, but no analysis of the elutriated material was conducted. Due to the shift in particle size distribution, the minimum fluidization velocity was reduced from 0.76 m/s initially to 0.67 m/s in 96 hr. Extrapolation of the test results to a 1.5 m bed depth with operation at 1.2 m/s indicates that the elutriation rate would be approximately 1 percent in 96 hr, with no recycle of fines.

This material was used for the tests on the first sparger configuration (Section 6.4 below). Low fluidizing velocities, just in excess of the minimum as determined in the above tests, were used to prevent excessive entrainment. Entrained fines were not recycled.

At the break during which the transfer leg pulse system was modified, bed material was withdrawn and analyzed for size distribution (Table 1). Despite the low fluidizing velocity, a significant reduction in average size was evident. The size distribution, and the low amount of makeup solids needed during the first series of runs, indicate that, as in the attrition tests above, attrition consists primarily of the breakdown of the very largest particles into moderate sized ones. At the same time, the loose bulk specific gravity was found to be 0.982, and the packed

TABLE 1

PARTICLE SIZE DISTRIBUTION AT BEGINNING OF FINAL TEST SERIES

U. S. Mesh	Average Size, d_{pi} (μm)	Wt %, x_i
+8	2605	0.1
-8 +12	2030	41.0
-12 +16	1435	35.8
-16 +20	1016	11.2
-20 +30	718	6.0
-30 +40	508	2.8
-40	350	3.0
		99.9

Linear mean size $(\Sigma x_i d_{pi})$ = 1530 μm

Surface mean size $(1/(\Sigma x_i/d_{pi}))$ = 1274 μm

TABLE 2

PARTICLE SIZE DISTRIBUTION AT CONCLUSION OF FINAL TEST SERIES

U. S. Mesh	Average Size, d_{pi} (μm)	Wt %, x_i
+8	2605	2.1
-8 +12	2030	12.9
-12 +16	1435	26.0
-16 +20	1016	21.2
-20 +30	718	14.2
-30 +40	508	8.0
-40	350	15.0
		99.9

Linear Mean Size = 1104 μm

Surface Mean Size = 794 μm

specific gravity was 1.133. Effective aerodynamic particle densities could not be measured because the very large pores allowed absorption of even high surface tension immersing fluids (Mercury). Alcoa quoted the true specific gravity (immersion in helium) as 3.3.

The test series with the second sparger design was primarily conducted at higher fluidizing velocities (∿1.0 m/s). Greatly increased attrition and elutriation were very apparent, requiring that we recycle fines continuously. Solids makeup requirements, to replace baghouse fines only in this case, were nonetheless larger when compared to cyclone replacement losses at the lower velocity. When our initial stockpile of alumina was depleted, replacement material was purchased from Reynolds Metals Company because of a large cost difference and the poor performance of the Alcoa material. The Reynolds alumina (RA-1), which was to fare no better, was nominally sized at 8 to 14 mesh (1190 to 2380 μm).

The particle size distribution of the bed material, at the conclusion of the test sequences, is shown in Table 2. The susceptibility of these materials to attrition is obvious by comparison with data in Table 1. The loose bulk specific gravity of the final material was 1.14 and the packed bulk specific gravity was 1.23. Calculations were performed with particle sizes and bulk densities estimated by interpolation between these sets of results.

6.3 PROCEDURES

The experimental technique was largely dictated by the method of solids flow determination. First, the overall technique will be outlined, then the solids flow measurement procedure will be discussed.

6.3.1 Experimental Technique

Prior to a day's series of runs, the bed levels would be noted and adjusted, if desired. Fluidization velocities were then set using the blower intake butterfly valve. Usually, the balancing valves in the transport air lines were set at preselected openings to determine the

approximate levels of airflow desired. The actual average and pulse instantaneous airflow, however, would vary considerably with the pulse on- and off-times selected for the particular run. For the inserted pipe sparger the cyclone discharge valves were set to divert solids into a collecting drum. For the final nozzle configuration runs the valves were set to recycle fines to the source bed.

After starting fluidizing airflow, all but one solenoid valve were isolated via the hand shut-off valves (see Figure 940-1 in Appendix A-1). The desired pulse rate and percent off-time were then set for the test solenoid valve. The shut-off valves for airflow to the transport system for the other leg were then opened, and this leg was pulsed to develop a bed height difference, the deeper bed to be used as the feeding bed in the run. Again, all transport air shut-off valves were closed, except those in the line prepared for the test.

At this point temperatures, pressures, pressure differentials, and fluidizing air rates were recorded and the transport leg pressure transmitter selector switches set to the desired position for recording. Solids flow was then initiated by starting transport air at the preselected pulse rate. While material was being transferred, the transport airflow would be recorded for future integration. Within a few minutes solids flow would stop because of the depletion of material in the feeding bed above the leg hopper. Transport air was then stopped manually and both final bed heights recorded. Pulse rates could now be reset in preparation for the next run. In the second test series a repeat run in the opposite direction was made, both pulse systems having been preset.

6.3.2 Solids Flow Rate Determination

The pulsing, turbulent nature of solids movement in the transport legs would make direct measurement of solids flow in the leg difficult. Several techniques were evaluated as methods to determine rates of solids circulation between the vessels: solid tracer particles based on color, magnetic properties, electric conductivity, etc.; heat transport rate measurement between the vessels; an external, mechanical solids circulation loop as used by FW in their cold model studies;[11] continuous monitoring

techniques based on X ray, γ radiation, microwave, sonic energy, inductance, capacitance probes, light source probes, heat transfer probes, momentum or strain probes. All of these techniques are complex, expensive, and subject to great uncertainty. We decided, therefore, to try measuring the solids flow rate by bed level changes, as recorded by a pneumatic differential pressure transmitter. This decision required that runs be one-way and not steady state with respect to bed levels and, hence, to level-dependent parameters such as the system pressure balance. The level recorder was carefully selected to reduce any response time effect to insignificance. The method proved completely satisfactory except for failure to allow longer, steady-state runs. The rate could be calculated as

$$G_s = -(A_B g_c/g) \frac{d(\Delta P_L)}{dt} \quad .$$

Two potential problems with this method were the random fluctuations in pressure drop characteristic of fluid beds and the possibility that the transport rate might be dependent on bed height and, hence, upon time. It was evident that the transport rate was bed-level dependent mostly at great bed-level differences - that is, the start and finish of each test sequence. The lower-than-characteristic rate at the beginning of the run was attributed to the high degree of packing and consequent resistance to motion of the leg solids when first pulsed. The low rate at the end of the run was due to the inability to fill the solids hoppers as the mean bed level fell below. It was decided to measure the transport rate at the point of equal bed heights. This could be done by noting the two final bed levels and averaging.

For the first test series solids transfer rates were sufficiently low that the bed-level change rate could be accurately approximated by the incremental difference over a 30 s time interval around the equal bed point, during which the rate was fairly constant. The time scale of random fluctuations (about 0.5 to 2 s) was small enough compared to this interval that fluctuations did not cause significant error. The main source of error was in accurately reading the pressure differentials at the two ends of the intervals.

The second test series featured solids transfer rates high enough that runs lasted only 20 to 30 s. Using a long time increment as before was undesirable because the rate would not be nearly constant over the wide variation in bed depth involved. A short interval was not acceptable because the bed fluctuations would obscure the real rate. A technique was developed, therefore, to solve this dilemma. The level recorder curve was fitted to a quadratic equation of ΔP_L versus time, whose slope ($d(\Delta P_L)/dt$) at the required bed-level point could be mathematically computed. This approach proved to be successful.

6.4 FIRST TEST SERIES - INSERTED PIPE SPARGER

6.4.1 Introduction

The first sparger tested was a steel pipe (6.03 cm od, 5.25 cm id) inserted through a flange at the elbow of each transfer slot. The pipe was drilled with 32 0.95-cm diameter holes in a single line from end to end of the transfer width. The holes were located 1.27 cm apart, center-to-center, and were oriented horizontally or angled downward at 45°, depending on the specific test. The holes and pipe were designed for uniform gas distribution. The sparger is illustrated in Figure 5 and detailed in Appendix A-1, drawing F940-3.

The objectives of the initial test program were (chronologically arranged):

- To develop the experimental techniques for maximum benefit. In particular, the suitability of the solids flow measurement method had to be confirmed and its details resolved
- To conduct an initial survey of the effects of major parameters to guide program development for system optimization
- To evaluate the initial design for potential success
- To optimize the performance of the initial design, if it proved acceptable.

6.4.2 Results and Discussion

The results of tests with this system are listed in Table 3. Flow rates obtained were unacceptably low (<1 kg/s in all but one run),

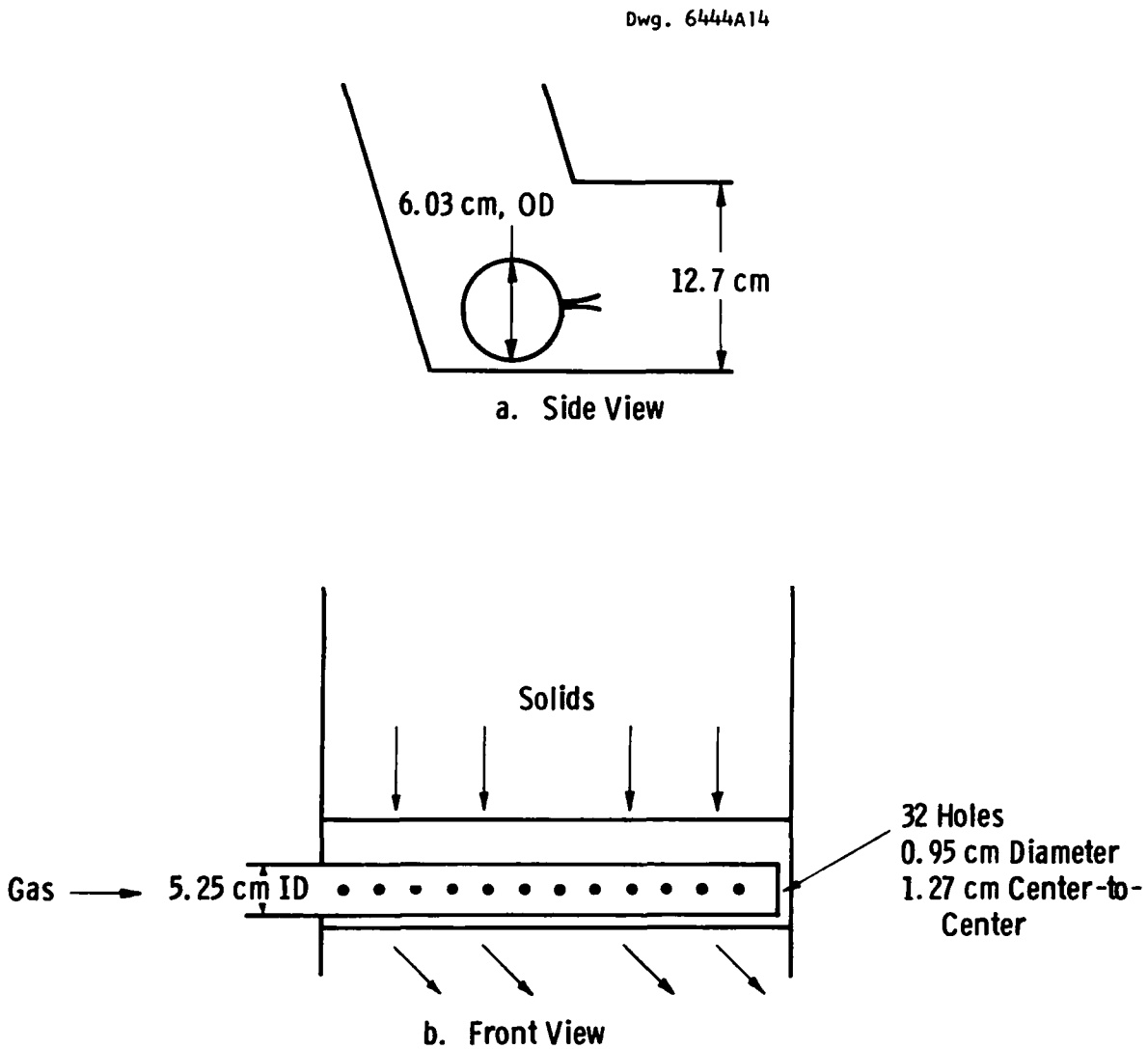

Figure 5. Inserted Pipe Sparger

TABLE 3

TRANSPORT DATA - FIRST TEST SERIES

Run No.	Leg No.	On-Time, s	Off-Time, s	Pulse Rate, kg/s	Solids Rate, kg/s	Transfer Ratio	Fluidizing Velocity, m/s
6	1	3.25	3.2	0.0387	0.10	2.6	0.70
7	2	3.25	3.2	0.0379	0.08	2.1	0.70
8	1	10.60	2.7	0.0614	0.10	1.6	0.70
9	2	10.20	2.6	0.0604	0.18	3.0	0.70
10	1	5.20	1.3	0.0666	0.26	3.9	0.70
11	2	6.80	1.7	0.0623	0.29	4.7	0.70
12	1	2.30	0.6	0.0691	0.00	0.0	0.70
13	2	2.40	0.6	0.0713	0.00	0.0	0.70
14	1	6.40	4.3	0.0479	0.21	4.4	0.70
15	2	5.10	3.4	0.0567	0.26	4.6	0.70
16	1	3.70	2.4	0.0539	0.37	6.9	0.70
17	2	4.10	2.8	0.0520	0.31	6.0	0.70
18	1	2.30	0.6	0.0691	0.00	0.0	0.69
19	2	2.40	0.6	0.0701	0.00	0.0	0.69
20	1	1.80	1.2	0.0667	0.39	5.8	0.69
21	2	1.90	1.2	0.0620	0.37	6.0	0.69
22	1	4.60	6.9	0.0374	0.21	5.6	0.69
23	2	4.30	6.4	0.0388	0.21	5.4	0.69
24	1	2.40	3.7	0.0398	0.21	5.3	0.69
25	2	2.10	3.1	0.0376	0.31	8.2	0.69
26	1	2.40	3.7	0.0469	0.31	6.6	0.69
28	1	1.20	1.9	0.0530	0.42	7.9	0.69
29	2	1.20	1.8	0.0465	0.37	8.0	0.69
30	2	0.80	1.3	0.0548	0.37	6.8	0.69
31	1	0.80	1.3	0.0558	0.39	7.0	0.69
32	2	0.60	0.8	0.0644	0.00	0.0	0.69
33	1	0.50	0.8	0.0656	0.00	0.0	0.69
34	1	2.00	7.8	0.0260	0.18	6.9	0.69

TABLE 3 (Continued)

Run No.	Leg No.	On-Time, s	Off-Time, s	Pulse Rate, kg/s	Solids Rate, kg/s	Transfer Ratio	Fluidizing Velocity, m/s
35	2	2.20	8.7	0.0227	0.18	7.9	0.69
37	1	1.20	4.5	0.0261	0.21	8.0	0.70
38	2	1.20	4.6	0.0262	0.13	5.0	0.70
39	1	0.60	2.4	0.0320	0.23	7.2	0.70
40	2	0.60	2.3	0.0335	0.31	9.3	0.70
41	1	0.40	1.7	0.0382	0.42	11.0	0.70
42	2	0.40	1.5	0.0411	0.37	9.0	0.70
43	1	0.20	1.0	0.0427	0.52	12.2	0.70
44	2	0.20	0.9	0.0616	0.42	6.8	0.70
45	2	7.80	2.0	0.0753	0.16	2.1	0.67
46	1	9.60	2.4	0.0868	0.23	2.6	0.67
47	2	4.90	1.2	0.0820	0.23	2.8	0.67
48	1	5.00	1.3	0.0930	0.57	6.1	0.67
49	2	4.90	1.2	0.0794	0.34	4.3	0.67
50	1	2.30	0.6	0.1050	0.00	0.0	0.67
51	2	2.20	0.5	0.1138	0.00	0.0	0.67
52	2	5.90	3.9	0.0643	0.10	1.6	0.67
53	1	6.20	4.1	0.0786	0.34	4.3	0.67
54	2	4.00	2.7	0.0571	0.26	4.6	0.67
55	1	3.50	2.4	0.0766	0.73	9.5	0.67
56	2	1.60	1.1	0.0796	0.57	7.2	0.67
57	1	1.90	1.3	0.0901	0.99	11.0	0.67
58	2	4.00	6.0	0.0445	0.39	8.8	0.67
59	1	4.40	6.7	0.0584	0.39	6.7	0.67
60	2	2.40	3.7	0.0444	0.31	7.0	0.67
61	1	2.40	3.7	0.0591	0.57	9.6	0.67
62	2	1.20	4.6	0.0409	0.31	7.6	0.68
63	1	3.30	2.2	0.0826	0.73	8.8	0.68
64	2	3.20	2.1	0.0767	0.42	5.5	0.68
65	1	3.30	2.2	0.0816	0.42	5.1	0.68

TABLE 3 (Continued)

Run No.	Leg No.	On-Time, s	Off-Time, s	Pulse Rate, kg/s	Solids Rate, kg/s	Transfer Ratio	Fluidizing Velocity, m/s
66	2	3.20	2.1	0.0781	0.52	6.7	0.68
67	2	3.20	2.1	0.0781	0.37	4.7	0.68
68	1	3.30	2.2	0.0816	0.57	7.0	0.68
69	2	3.20	2.1	0.0781	0.47	6.0	0.68
70	1	3.30	2.2	0.0816	0.52	6.4	0.68
71	2	0.50	2.2	0.0579	0.84	14.5	0.68
72	1	0.60	2.4	0.0788	0.99	12.6	0.68
73	2	0.10	1.1	0.0528	0.94	17.8	0.68
74	1	0.10	1.1	0.0484	0.84	17.4	0.68
75	2	0.10	1.1	0.0451	0.94	20.8	0.68
76	1	0.10	1.1	0.0439	0.78	17.8	0.68
77	1	0.00**	0.0	0.0496	0.00	0.0	0.62
78	2	0.00**	0.0	0.0166	0.00	0.0	0.62
79	1	0.70	2.8	0.0078	0.10	12.8	0.62
80	1	0.70	2.8	0.0268	0.57	21.3	0.74
81	1	4.50	6.8	0.0219	0.13	5.9	0.74
82	2	4.10	6.2	0.0160	0.21	13.1	0.74
83*	2	4.70	7.1	0.0184	0.21	11.4	0.72
84	1	4.40	6.5	0.0250	0.31	12.4	0.72
85	2	4.70	7.1	0.0189	0.21	11.1	0.72
86	1	4.40	6.5	0.0247	0.42	17.0	0.72
87	2	0.50	1.8	0.0141	0.37	26.2	0.72
88	1	0.60	2.5	0.0226	0.52	23.0	0.72
89	1	0.60	11.4	0.0103	0.47	45.6	0.64
90	2	0.60	11.4	0.0087	0.29	33.3	0.64
91	1	0.60	5.5	0.0136	0.34	25.0	0.64

*Runs 83-99: jets directed 45° downward.
**Continuous aeration.

TABLE 3 (Continued)

Run No.	Leg No.	On-Time, s	Off-Time, s	Pulse Rate, kg/s	Solids Rate, kg/s	Transfer Ratio	Fluidizing Velocity, m/s
92	2	0.60	5.3	0.0104	0.31	29.8	0.64
93	1	0.40	3.7	0.0127	0.47	37.0	0.64
94	2	0.40	3.4	0.0127	0.23	18.1	0.64
95	1	1.50	1.0	0.0417	0.05	1.2	0.60
96	2	1.90	1.3	0.0317	0.31	9.8	0.60
97	1	0.10	0.9	0.0215	0.78	36.3	0.60
98	2	0.10	1.1	0.0193	0.52	26.9	0.60
99	1	0.00**	0.0	0.0421	0.00	0.0	0.60

**Continuous aeration.

especially in light of the larger flow area used relative to the CAFB design. Efficiencies, measured as mass ratio of solids transferred to gas required, were correspondingly poor, although much of this is the result of suboptimum combinations of on- and off-times. These results were attributable to the obstruction of the solids flow by the sparger pipe. The design was concluded to be unpromising. Optimization with regard to pulse variables, therefore, was not pursued.

This test series was useful, however, in providing clues to understanding the system and its limitations. At the beginning of the sequence there was little basis for choosing on- and off-times. By trial and error, covering combinations of on-times from 0. 1 to 10.6 s and off-times from 0.5 to 11.4 s, we came to realize several important points:

- The transfer leg fluidizes with each pulse, and large quantities of transport gas are lost upward.
- Solids transport apparently occurred early in each run before fluidization had culminated. Short on-times were therefore desirable.
- No transfer could be achieved with continuous aeration (runs 77, 78, 99), presumably because no time is allowed for defluidizing.
- No transport could be achieved for off-times less than a critical value of around 1.0 s (runs 12, 13, 18, 19, 32, 33, 50, 51), suggesting that a minimum time is required for defluidization.
- Exceptions to the above point are those runs that have very short on-times, 0.1 or 0.2 s, and off-times just less than 1.0 s (runs 43, 44, 97). Less defluidizing time is required if the process of blowing the seal leg has not been completed.
- Angling the sparger holes downward by 45° yielded significant improvement in transport efficiency (runs 83-99), presumably because it prevented the jet from bypassing the horizontal solids. The additional resistance encountered by the air jets resulted in lower overall transport gas rates and, hence, no improvement in net solids flow.

These observations were very useful in planning and analyzing the runs on the subsequent pulse configuration. Other corollary observations were made during this sequence.

- Small differences in leg cross-section, caused by using different sight-glass thicknesses on the two legs, caused noticeable differences in performance before being corrected.
- The level recorder tracings clearly indicated the on-off nature of solids flow. In other words, solids flow does not act to even out over a pulse cycle.
- The transport rate was somewhat dependent on bed level difference, particularly near the beginning and end of each run. The hopper feeding difficulties at low bed-levels and the great initial inertia of the leg solids, both discussed previously, are certainly important. Hindsight now indicates that some dependence of the system performance on system pressure balance changes with bed depth can be expected.
- Solids flow occurs in a fast moving dilute phase above a region of apparently stagnant solids. This void is filled between vessels largely from the receiving vessel side. A brief backflow of solids seems to occur following the blowing of the vertical seal.
- Vertical upflow of transport gas commences soon after the start of a pulse and is composed of large bubbles or slugs apparently adjacent to the upper slanted face of the vertical section.
- "Freewheeling," the flow of solids with no pulse air input, was only seen to occur with great bed depth differences, in which case solids would move so as to partially alleviate the difference. It is probably caused by a very low-pressure gradient across the transfer leg with bed pressure fluctuations causing the gradient to become negative periodically.

6.5 SECOND TEST SERIES - RECESSED NOZZLE SPARGER

6.5.1 Introduction

The fact that FW had finished design of the transfer slot, and the poor performance of the inserted pipe sparger, made it desirable for us to convert to a system similar to the FW design for further study. With the installation of the new test system our objectives were:

- To confirm that the new design would permit the required flow
- To optimize the pulse variables for maximum efficiency and stable operation
- To begin to understand the transport process from a more fundamental vantage point, to allow more confidence in extrapolating to different conditions, particularly those expected in the CAFB plant.

The new nozzle configuration is illustrated in Figure 6. Nine 1.91-cm id nozzles, protected against backflow of solids by 325 mesh screens, are inserted into the back of each transfer leg, near the base of the leg. These nozzles are oriented horizontally and are arranged linearly, spaced 5.08 cm center to center. Additional sets of nozzle inserts (Figure 6d) are available for future testing of additional nozzle diameters and insertion lengths, if desired. This design should allow maximum "bite" of the gas jets into the horizontal solids with minimum obstruction of the downward solids flow path. Nozzle diameter, spacing, and distance from nozzle to the transfer slot overhang are the same as for the CAFB design; the number of nozzles, however, is greater because of the greater width of the transfer leg.

6.5.2 Results and Discussion

A total of 272 formal tests were made with the new transport air injection system. The results and main variables are listed in Table 4. Further details may be found in Appendix B. An extensive matrix of pulse durations of from 0.05 to 4.0 s and off-times of from 0.5 to 3.1 s was tested, chosen because of the results of the previous test series.

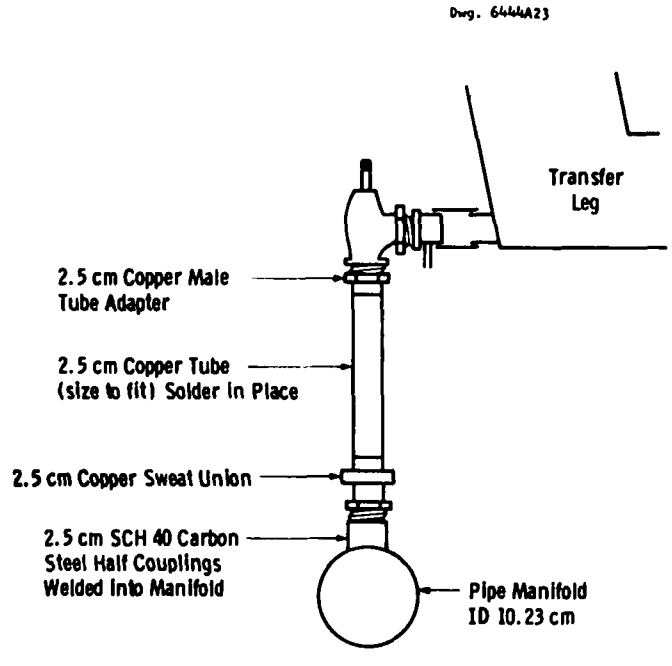

Figure 6a. Sparger Manifold - Side View

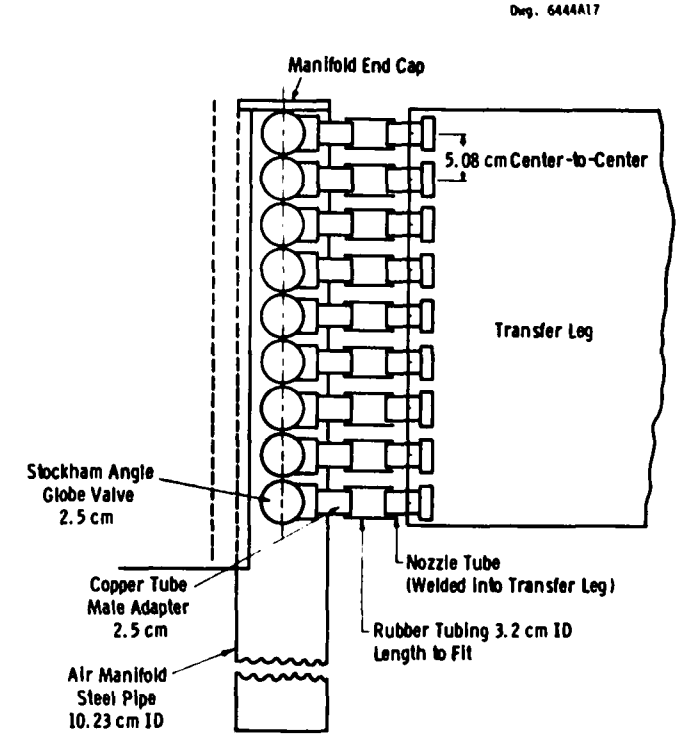

Figure 6b. Sparger Nozzle Configuration and Manifold - Top View

Figure 6. Recessed Nozzle Sparger

Dwg. 6444A19

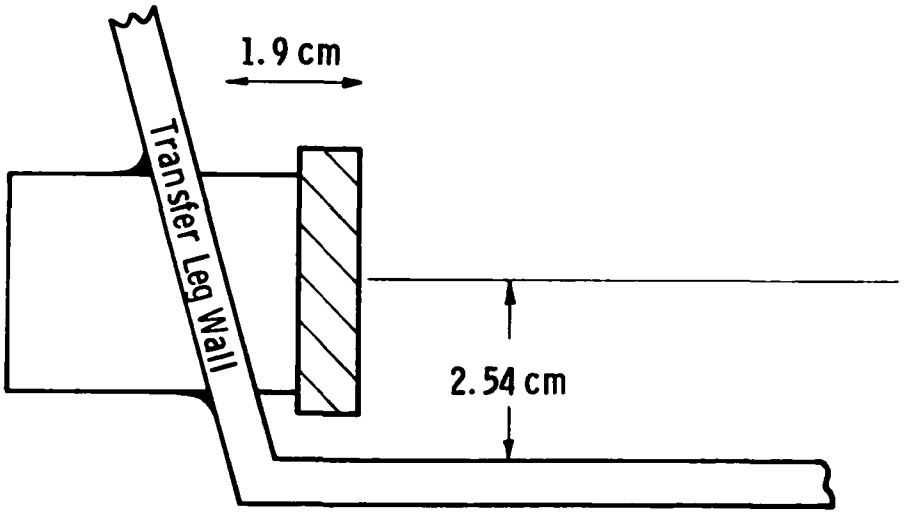

Figure 6c. Nozzle Insertion - Side View

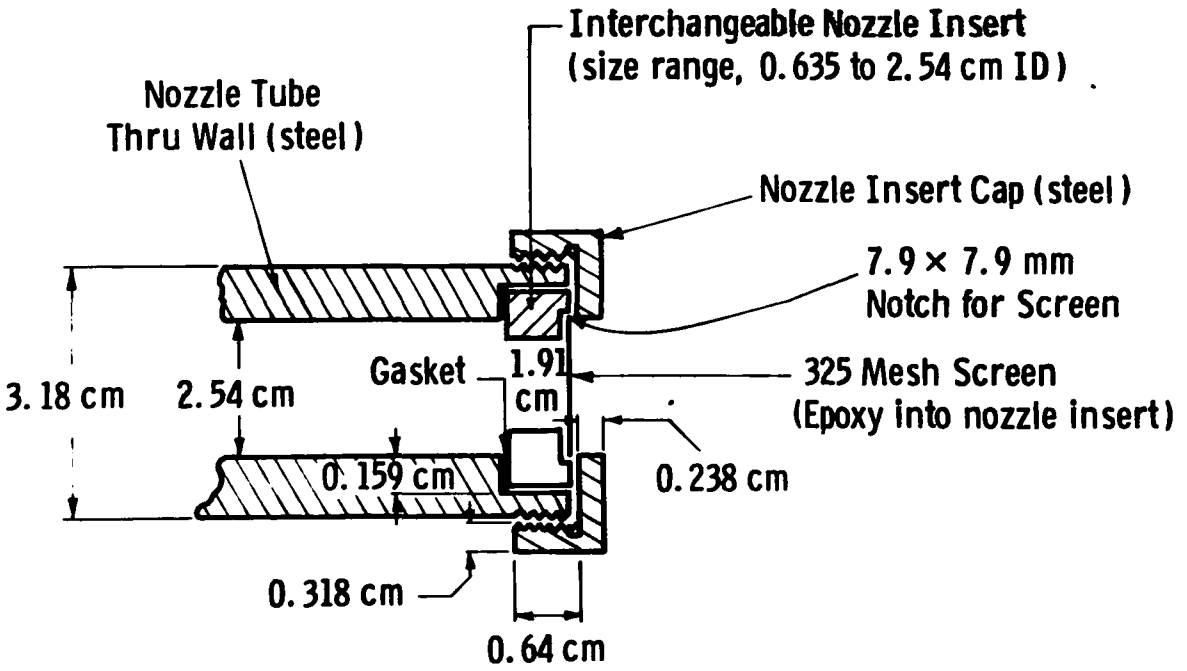

Figure 6d. Nozzle Construction

TABLE 4

TESTS RESULTS - SECOND TEST SERIES

Run No.	Leg No.	On-Time, s	Off-Time, s	Pulse Rate, kg/s	Solids Rate, kg/s	Transfer Ratio	Fluidizing Velocity, m/s
1	1	0.10	2.0	0.0341	1.56	45	1.10
2	2	0.10	2.0	0.0430	2.60	60	1.10
3	1	0.50	2.0	0.0445	3.46	77	1.01
4	2	0.50	2.0	0.0528	2.41	45	1.04
6	2	0.25	2.0	0.0504	1.58	31	1.04
7	1	0.25	2.0	0.0334	2.40	71	1.04
8	2	1.00	2.0	0.0617	2.17	35	1.04
9	1	1.00	2.0	0.0480	2.57	53	1.04
10	2	0.75	2.0	0.0578	2.03	35	1.04
11	1	0.75	2.0	0.0472	2.62	55	1.04
12	2	0.10	2.0	0.0422	2.75	65	1.07
13	1	0.10	2.0	0.0286	2.41	84	1.07
14	2	0.05	2.0	0.0373	2.76	74	1.07
15	1	0.05	2.0	0.0236	1.83	77	1.07
16	1	0.50	2.0	0.0478	2.82	59	1.01
17	2	0.50	2.0	0.0468	1.45	31	1.04
18	1	0.20	2.0	0.0386	2.55	65	1.04
19	2	0.20	2.0	0.0393	1.58	40	1.04
20	1	2.00	2.0	0.0600	3.04	50	1.04
21	2	2.00	2.0	0.0552	1.92	34	1.07
22	1	1.00	2.0	0.0547	2.40	43	1.07
28	1	2.00	2.0	0.0601	1.85	30	1.01
29	2	2.00	2.0	0.0523	2.04	39	1.01
30	2	0.50	2.0	0.0433	3.14	72	1.01
31	1	0.50	2.0	0.0454	2.82	62	1.01
32	1	0.20	2.0	0.0374	3.47	92	1.04
33	2	0.20	2.0	0.0383	2.52	65	1.04
34	2	1.20	2.4	0.0451	2.18	48	1.04

TABLE 4 (Continued)

Run No.	Leg No.	On-Time, s	Off-Time, s	Pulse Rate, kg/s	Solids Rate, kg/s	Transfer Ratio	Fluidizing Velocity, m/s
35	1	1.20	2.4	0.0487	2.59	53	1.04
36	1	0.10	2.0	0.0299	2.81	93	1.04
37	2	0.10	2.0	0.0319	2.38	74	1.04
38	2	3.00	2.0	0.0596	1.82	30	1.04
39	1	2.80	1.8	0.0618	1.15	18	1.04
40	1	1.00	2.0	0.0549	2.14	39	0.98
41	2	1.00	2.0	0.0456	2.76	60	0.98
42	2	1.50	2.0	0.0484	3.19	65	1.01
43	1	1.50	2.0	0.0601	1.98	32	1.01
44	1	2.50	2.0	0.0660	2.16	32	1.01
45	2	2.50	2.0	0.0499	2.28	45	1.01
46	2	4.00	2.0	0.0560	1.51	27	1.04
47	1	4.00	2.0	0.0662	1.13	17	1.04
48	1	1.00	1.0	0.0750	0.06	0	1.04
49	2	1.00	1.0	0.0654	1.27	19	1.04
50	2	2.00	1.0	0.0643	2.06	31	1.04
51	1	2.00	1.0	0.0736	0.21	2	1.04
52	1	0.50	1.0	0.0700	0.14	1	1.04
53	2	0.50	1.0	0.0666	1.13	17	1.04
54	2	3.00	1.0	0.0648	1.88	28	1.04
55	1	3.00	1.0	0.0737	0.88	11	1.04
56	1	0.20	1.0	0.0525	2.88	54	1.04
57	2	0.20	1.0	0.0572	3.11	54	1.04
58	2	1.50	1.0	0.0652	1.79	27	1.04
59	1	1.50	1.0	0.0751	0.32	4	1.04
60	1	0.10	1.0	0.0324	2.75	84	0.98
61	2	0.10	1.0	0.0348	3.06	87	1.01
62	2	2.50	1.0	0.0636	1.84	28	1.04
63	1	2.50	1.0	0.0747	0.33	4	1.04
64	1	0.75	1.0	0.0728	0.00	0	1.04

TABLE 4 (Continued)

Run No.	Leg No.	On-Time, s	Off-Time, s	Pulse Rate, kg/s	Solids Rate, kg/s	Transfer Ratio	Fluidizing Velocity, m/s
65	2	0.75	1.0	0.0576	2.32	40	1.04
66	2	4.00	1.0	0.0643	1.27	19	1.04
67	1	4.00	1.0	0.0741	0.45	6	1.04
68	1	0.50	1.5	0.0548	2.90	52	1.04
69	2	0.50	1.5	0.0494	2.74	55	1.04
70	2	1.00	1.5	0.0528	3.13	59	1.04
71	1	1.00	1.5	0.0616	2.14	34	1.04
72	1	0.20	1.5	0.0404	2.72	67	1.04
73	2	0.20	1.5	0.0427	2.98	69	1.04
74	2	1.50	1.5	0.0561	2.23	39	1.04
75	1	1.50	1.5	0.0650	2.27	34	1.04
76	1	0.20	1.5	0.0384	4.09	106	0.91
77	2	0.20	1.5	0.0379	3.06	80	0.94
78	2	2.00	1.5	0.0530	2.14	40	0.94
79	1	2.00	1.5	0.0648	2.36	36	0.98
80	1	0.10	1.5	0.0325	3.40	104	0.98
81	2	0.10	1.5	0.0318	3.13	98	0.98
82	2	3.10	1.5	0.0567	1.50	26	0.98
83	1	3.10	1.5	0.0652	1.77	27	0.98
84	1	0.40	1.5	0.0473	2.99	63	0.98
85	2	0.40	1.5	0.0479	3.25	67	0.98
86	1	0.20	3.0	0.0347	3.73	107	0.98
87	2	0.20	3.0	0.0323	2.64	81	1.01
88	2	0.80	3.0	0.0387	2.53	65	1.04
89	1	0.80	3.0	0.0461	3.28	71	1.04
90	1	2.00	3.0	0.0525	2.18	41	1.04
91	2	2.00	3.0	0.0476	1.98	41	1.04
92	2	0.40	2.9	0.0319	2.43	76	1.04
93	1	0.40	2.9	0.0380	2.62	69	1.04
94	1	1.00	3.0	0.0479	3.43	71	1.04

TABLE 4 (Continued)

Run No.	Leg No.	On-Time, s	Off-Time, s	Pulse Rate, kg/s	Solids Rate, kg/s	Transfer Ratio	Fluidizing Velocity, m/s
95	2	1.00	3.0	0.0413	2.94	71	1.04
96	2	0.60	2.9	0.0358	3.18	88	1.04
97	1	0.60	2.9	0.0429	3.87	90	1.04
98	1	1.50	3.1	0.0497	2.24	45	1.04
99	2	1.50	3.1	0.0405	2.11	52	1.04
100	2	0.40	0.5	0.0699	0.34	4	1.04
101	1	0.40	0.5	0.0803	0.00	0	1.04
102	1	0.40	1.6	0.0523	5.45	104	1.04
103	2	0.40	1.6	0.0500	3.83	76	1.04
104	2	0.40	1.0	0.0709	0.77	10	1.04
105	1	0.40	1.0	0.0733	0.52	7	1.04
106	1	0.40	1.8	0.0485	4.88	100	1.04
107	1	0.40	1.8	0.0461	4.16	90	1.04
108	2	0.40	1.4	0.0544	3.38	62	1.04
109	1	0.40	1.4	0.0554	4.04	72	1.04
110	1	0.40	1.2	0.0582	1.84	31	1.04
111	2	0.40	1.2	0.0626	2.79	44	1.04
112	1	0.10	0.5	0.0747	0.57	7	0.98
113	2	0.10	0.5	0.0736	0.92	12	0.98
114	2	0.20	0.5	0.0726	0.00	0	1.04
115	1	0.20	0.5	0.0826	0.00	0	1.04
116	1	0.20	1.6	0.0411	4.85	118	1.04
117	2	0.20	1.6	0.0432	4.34	100	1.04
118	2	0.20	1.2	0.0465	4.10	88	1.04
119	1	0.20	1.2	0.0464	5.88	126	1.04
120	1	0.20	1.0	0.0528	5.13	97	1.04
121	2	0.20	1.0	0.0593	3.90	65	1.04
122	2	0.20	0.8	0.0711	1.29	18	1.04
123	1	0.20	0.8	0.0717	0.53	7	1.04
124	1	0.20	1.4	0.0425	4.91	115	1.04

TABLE 4 (Continued)

Run No.	Leg No.	On-Time, s	Off-Time, s	Pulse Rate, kg/s	Solids Rate, kg/s	Transfer Ratio	Fluidizing Velocity, m/s
125	2	0.20	1.4	0.0434	4.09	94	1.04
126	2	0.20	1.8	0.0406	3.77	92	1.04
127	1	0.20	1.8	0.0409	4.58	111	1.04
128	1	0.10	0.9	0.0432	4.33	100	0.98
129	2	0.10	0.9	0.0480	3.37	70	1.01
130	2	0.10	0.8	0.0595	3.47	58	1.04
131	1	0.10	0.8	0.0516	2.69	52	1.04
132	1	0.10	0.7	0.0533	2.75	51	1.04
133	2	0.10	0.7	0.0717	1.89	26	1.04
134	2	0.10	0.6	0.0724	0.57	7	1.04
135	1	0.10	0.6	0.0610	0.91	14	1.04
136	1	1.00	1.0	0.0854	1.50	17	1.04
137	2	1.00	1.0	0.0729	1.22	16	1.04
138	1	1.00	1.8	0.0669	3.46	51	1.04
139	1	0.40	1.8	0.0914	5.66	61	1.01
140	2	0.40	1.8	0.0797	6.56	82	1.01
141	2	0.20	1.5	0.0829	6.75	81	1.04
142	1	0.20	1.5	0.0788	5.54	70	1.04
143	1	0.60	2.7	0.0816	3.87	47	1.04
144	2	0.60	2.7	0.0676	4.80	71	1.04
145	2	1.00	3.0	0.0746	2.38	31	1.04
146	1	1.00	3.0	0.0931	2.23	23	1.04
147	1	0.40	1.6	0.1013	3.17	31	1.04
148	2	0.40	1.6	0.0849	5.06	59	1.07
149	2	0.40	1.4	0.0888	3.35	37	1.07
150	1	0.40	1.4	0.1092	4.65	42	1.07
151	1	0.20	1.4	0.0899	5.52	61	1.07
152	2	0.20	1.4	0.0811	7.65	94	1.07
153	2	0.20	1.0	0.1070	4.10	38	1.07
154	1	0.20	1.0	0.0977	3.66	37	1.07

TABLE 4 (Continued)

Run No.	Leg No.	On-Time, s	Off-Time, s	Pulse Rate, kg/s	Solids Rate, kg/s	Transfer Ratio	Fluidizing Velocity, m/s
155	1	0.20	0.8	0.1187	3.03	25	1.07
156	2	0.20	0.8	0.1301	1.46	11	1.07
157	2	0.10	1.0	0.0950	4.35	45	1.07
158	1	0.10	1.0	0.0768	3.91	50	1.07
159	1	0.10	0.8	0.0949	0.00	0	1.07
160	2	0.10	0.8	0.1185	0.00	0	1.07
161	2	1.00	2.0	0.0928	2.71	29	1.07
162	1	1.00	2.0	0.1017	1.20	11	1.07
163	1	1.00	1.6	0.1245	4.16	33	1.07
164	2	1.00	1.6	0.1065	1.82	17	1.07
165	2	0.40	2.0	0.0907	5.32	58	1.07
167	1	0.40	2.0	0.0893	4.53	50	1.07
168	2	0.40	2.0	0.0949	3.09	32	1.07
170	1	0.40	2.0	0.0855	4.65	54	1.07
171	2	0.40	2.0	0.0557	5.37	96	1.07
172	1	0.40	2.0	0.0586	4.30	73	1.07
173	2	0.40	2.0	0.0430	3.51	81	1.07
174	1	0.40	2.0	0.0405	3.93	97	1.07
175	1	0.40	2.0	0.0407	3.75	92	0.98
176	2	0.40	2.0	0.0445	2.61	58	0.98
177	1	0.40	2.0	0.0487	3.92	80	0.98
178	2	0.40	2.0	0.0568	4.87	85	0.98
179	1	0.40	2.0	0.0666	4.58	68	0.98
180	2	0.40	2.0	0.0591	3.90	65	0.98
181	1	0.40	2.0	0.0362	3.98	110	0.98
182	2	0.40	2.0	0.0361	3.53	97	0.98
183	1	0.40	2.0	0.0431	3.33	77	1.01
184	2	0.40	2.0	0.0382	3.23	84	1.01
185	1	0.40	2.0	0.0279	1.92	68	1.01
186	2	0.40	2.0	0.0198	1.08	54	1.04

TABLE 4 (Continued)

Run No.	Leg No.	On-Time, s	Off-Time, s	Pulse Rate, kg/s	Solids Rate, kg/s	Transfer Ratio	Fluidizing Velocity, m/s
187	1	0.20	1.2	0.0145	2.37	163	1.04
188	2	0.20	1.2	0.0200	1.12	56	1.04
189	1	0.20	1.2	0.0308	3.76	121	1.04
190	2	0.20	1.2	0.0273	2.90	106	1.04
191	1	0.20	1.2	0.0359	5.41	150	1.04
192	2	0.20	1.2	0.0370	2.99	80	1.04
193	1	0.20	1.2	0.0504	5.80	115	1.04
194	2	0.20	1.2	0.0467	5.07	108	1.04
195	1	0.20	1.2	0.0614	5.09	82	1.04
196	2	0.20	1.2	0.0638	5.11	80	1.04
197	1	0.40	1.8	0.0346	4.59	132	1.04
198	2	0.40	1.8	0.0332	3.53	106	1.04
199	1	0.40	1.8	0.0291	2.55	87	1.04
200	2	0.40	1.8	0.0273	3.49	127	1.04
201	2	0.40	1.6	0.0273	2.40	87	1.04
202	1	0.40	1.6	0.0308	2.64	85	1.04
203	1	0.40	1.4	0.0308	2.71	87	1.04
204	2	0.40	1.4	0.0284	2.53	89	1.04
205	2	0.40	1.2	0.0346	2.88	83	1.04
206	1	0.40	1.2	0.0370	1.84	49	1.04
207	1	0.40	2.0	0.0310	2.74	88	0.37
208	2	0.40	2.0	0.0275	1.89	68	0.37
209	1	0.40	2.0	0.0410	3.87	94	0.79
210	2	0.40	2.0	0.0361	2.90	80	0.79
211	1	0.40	2.0	0.0370	3.06	82	0.55
212	2	0.40	2.0	0.0308	3.37	109	0.55
213	2	0.40	1.8	0.0325	3.63	111	0.55
214	1	0.40	1.8	0.0333	3.20	96	0.55
215	1	0.40	1.6	0.0385	3.57	92	0.55
216	2	0.40	1.6	0.0336	2.66	79	0.55

TABLE 4 (Continued)

Run No.	Leg No.	On-Time, s	Off-Time, s	Pulse Rate, kg/s	Solids Rate, kg/s	Transfer Ratio	Fluidizing Velocity, m/s
217	2	0.40	1.4	0.0375	1.90	50	0.55
218	1	0.40	1.4	0.0403	2.37	58	0.55
219	1	0.40	1.2	0.0403	3.14	77	0.55
220	2	0.40	1.2	0.0378	2.38	63	0.55
221	2	0.40	1.0	0.0316	1.32	41	0.55
222	1	0.40	1.0	0.0493	3.00	60	0.55
223	1	0.20	1.0	0.0357	3.57	99	0.55
224	2	0.20	1.0	0.0357	3.08	86	0.55
225	2	0.20	0.8	0.0469	1.45	30	0.55
226	1	0.20	0.8	0.0447	2.70	60	0.55
227	1	0.20	0.6	0.0582	0.39	6	0.55
228	2	0.20	0.6	0.0514	1.02	19	0.55
229	2	0.20	1.4	0.0287	2.70	94	0.55
230	1	0.20	1.4	0.0305	3.47	113	0.55
231	1	0.20	1.8	0.0263	3.01	114	0.55
232	2	0.20	1.8	0.0260	2.57	98	0.55
233	2	1.00	2.0	0.0349	2.28	65	0.55
234	1	1.00	2.0	0.0450	2.52	56	0.55
235	1	1.00	1.8	0.0464	2.62	56	0.55
236	2	1.00	1.8	0.0361	2.81	77	0.55
237	2	1.00	1.6	0.0377	2.76	73	0.55
238	1	1.00	1.6	0.0477	2.60	54	0.55
239	1	1.00	1.4	0.0501	2.06	41	0.55
240	2	1.00	1.4	0.0367	1.68	45	0.55
241	2	0.40	2.0	0.0261	1.22	46	0.37
242	1	0.40	2.0	0.0279	1.88	67	0.37
243	2	0.40	2.0	0.0361	2.71	75	0.37
244	1	0.40	2.0	0.0391	3.44	88	0.37
245	1	0.40	1.8	0.0386	3.20	82	0.37
246	2	0.40	1.8	0.0360	4.39	121	0.37

TABLE 4 (Continued)

Run No.	Leg No.	On-Time, s	Off-Time, s	Pulse Rate, kg/s	Solids Rate, kg/s	Transfer Ratio	Fluidizing Velocity, m/s
247	2	0.40	1.4	0.0425	3.25	76	0.37
248	1	0.40	1.4	0.0425	3.27	76	0.37
249	1	0.40	1.2	0.0473	2.85	60	0.37
250	2	0.40	1.2	0.0507	2.66	52	0.37
251	2	0.40	1.0	0.0523	1.89	36	0.37
252	1	0.40	1.0	0.0507	2.69	52	0.40
253	1	1.00	2.0	0.0490	2.71	55	0.40
254	2	1.00	2.0	0.0418	3.18	75	0.40
255	2	1.00	1.6	0.0462	3.51	75	0.40
256	1	1.00	1.6	0.0540	2.80	51	0.40
257	1	1.00	1.2	0.0628	0.47	7	0.40
258	2	1.00	1.2	0.0528	2.66	50	0.40
259	2	1.00	1.4	0.0506	2.62	51	0.40
260	1	1.00	1.4	0.0594	3.00	50	0.40
261	1	1.00	1.8	0.0528	2.86	54	0.40
262	2	1.00	1.8	0.0456	4.06	89	0.40
263	2	1.00	1.0	0.0590	2.53	42	0.40
264	1	1.00	1.0	0.0666	0.54	8	0.40
265	1	0.20	1.4	0.0329	3.59	109	0.40
266	2	0.20	1.4	0.0345	3.98	115	0.40
267	2	0.20	1.0	0.0418	3.57	85	0.40
268	1	0.20	1.0	0.0424	3.48	82	0.40
269	1	0.20	0.8	0.0418	3.23	77	0.40
270	2	0.20	0.8	0.0472	3.20	67	0.40
271	2	0.20	0.6	0.0660	0.00	0	0.40
272	1	0.20	0.6	0.0616	0.00	0	0.40

Overall pulse air rates of from 0.015 to 0.13 kg/s were used. The fluidizing velocity was about 1.0 m/s for most runs. This value was selected as a compromise between the desires for maximum bed expansion and for limited attrition and entrainment. Fluidizing velocities as low as 0.37 m/s were tested later.

The results were clearly superior to those of the previous sequence. With proper selection of the pulse pattern, solids transfer rates in excess of 4.0 kg/s were often obtained. Several runs had rates greater than 5.0 kg/s. These values compare with the CAFB expected rate requirement of 3.0 to 4.0 kg/s. A more accurate comparison can be made on a flow per unit area basis. Expressed in this manner our rates were optimally 80 to 110 $kg/s/m^2$. With the existing CAFB design, required rates will be 110 to 150 $kg/s/m^2$. Transfer efficiencies (mass of solids/mass of gas) varied considerably, but values in excess of 100 were frequently obtained.

Important information regarding optimum on- and off-times was obtained. Pulse gas entering after about 0.4 s from the start of an individual pulse is wasted, passing vertically upward through a fluidized stand-leg. For on-times in excess of this value, at least 1.2 s is needed for complete defluidization of the vertical leg prior to the next pulse. For shorter on-times proportionately less defluidizing time is needed. In any case, off-times slightly longer than the minimum defluidizing time will result in a loss of efficiency due to incomplete packing. The optimum configuration, therefore, would have an on-time of less than 0.4 s and an off-time of about 1.6 to 2.0 s. A shorter on-time or a longer on-time would result in a lower fraction of transfer time. This would result in either a lower transfer rate or decreased transfer efficiency, depending on whether the overall flow rate was increased. Longer on-times or shorter off-times result in unacceptable loss of gas upwards. Simultaneous shorter on-times and off-times provide efficient and rapid transfer but would be mechanically difficult. Projected optimum on- and off-times for the demonstration plant are presented in Section 8.0.

The data can best be examined by expressing the transfer efficiency as

$$\frac{\text{Mass Solids Transfer}}{\text{Solids Flow Time}} \div \frac{\text{Mass Gas Transfer}}{\text{Pulse On-Time}} .$$

This is the ratio of instantaneous solid-to-gas flow rates and is termed the modified transfer ratio to distinguish it from the apparent (real) transfer ratio, which is

$$\frac{\text{Mass Solids Transfer}}{\text{Unit Real Time}} \div \frac{\text{Mass Gas Transfer}}{\text{Unit Real Time}} .$$

Note that the solids flow time may be significantly less than the on-time, its maximum value being the fluidizing time of the vertical section. Estimating the maximum solids flow time, t_M, by 0.35 s, the data are summarized in Figures 7 through 16, each of which illustrates a specific sequence of runs. Because of the number of interrelated variables, some of which could not be independently controlled, these graphs should not be interpreted as correlations. They are useful, however, in identifying the key principles in the transport process.

Figures 7 through 10 show how increasing instantaneous gas flow rate affected the transfer efficiency in series of exploratory runs at off-times of 1.0, 1.5, 2.0, and 3.0 s, respectively. Note that on-time is not constant on any of these graphs, but is related to the gas flow rate. The striking feature is that efficiency increases sharply with decreasing gas input rate at the low values of airflow. The two presumed interrelated reasons for this are that 1) high solids mass flow is required to compensate for decreased velocity in the momentum balance, and 2) horizontal transport occurs in a denser phase (i.e., the jets are more persistent). Although the ratios are large here, the low flows result in solids transfer rates not being correspondingly large. Also, the low velocity runs generally correspond to long pulse on-times, so true efficiencies suffer, as actual solids flow time is less than gas input time. This is why the true transfer ratios (Table 4) showed less variation in value.

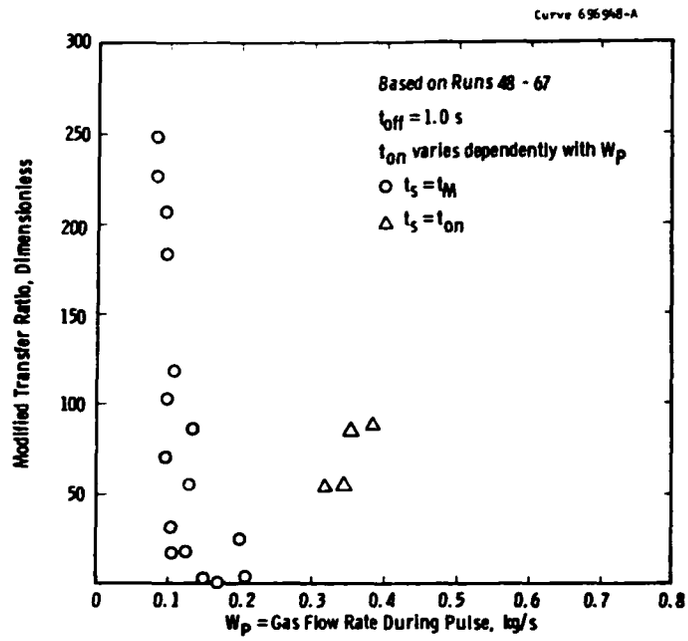

Figure 7. Effect of Pulse Air Rate on Modified Transfer Data

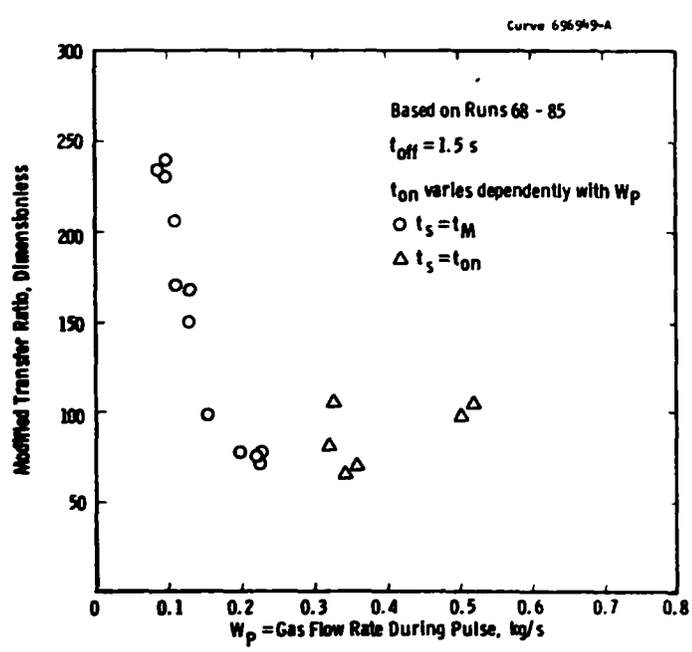

Figure 8. Effect of Pulse Air Rate on Modified Transfer Ratio

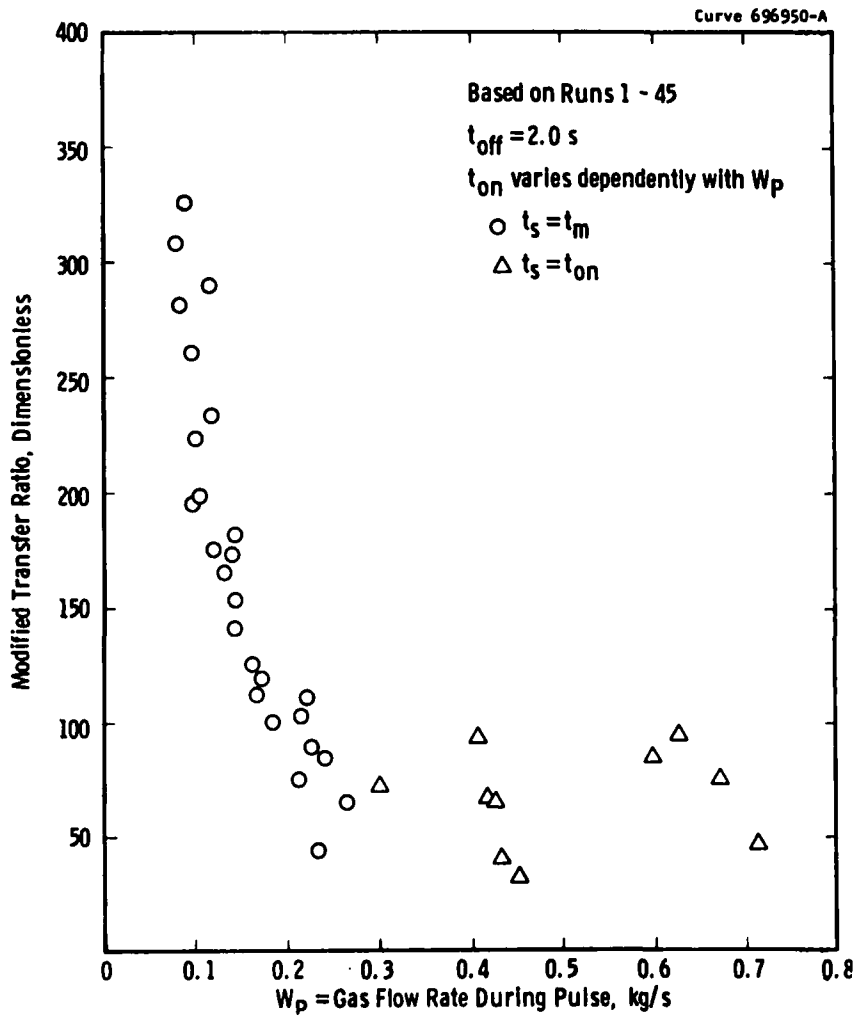

Figure 9. Effect of Pulse Air Rate on Modified Transfer Ratio

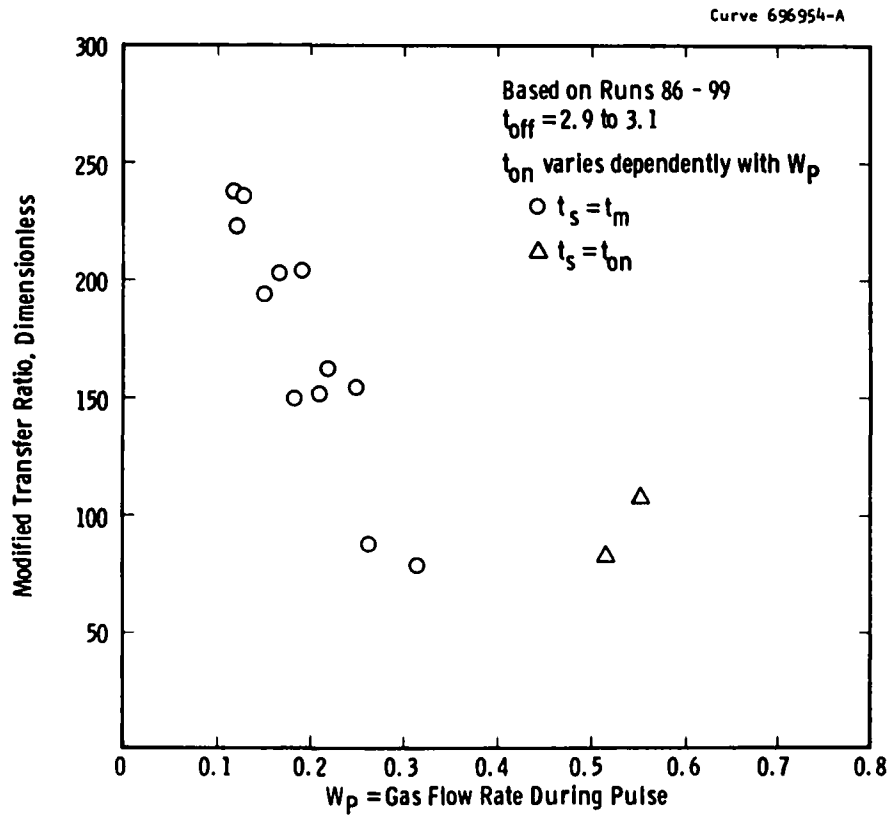

Figure 10. Effect of Pulse Air Rate on Modified Transfer Ratio

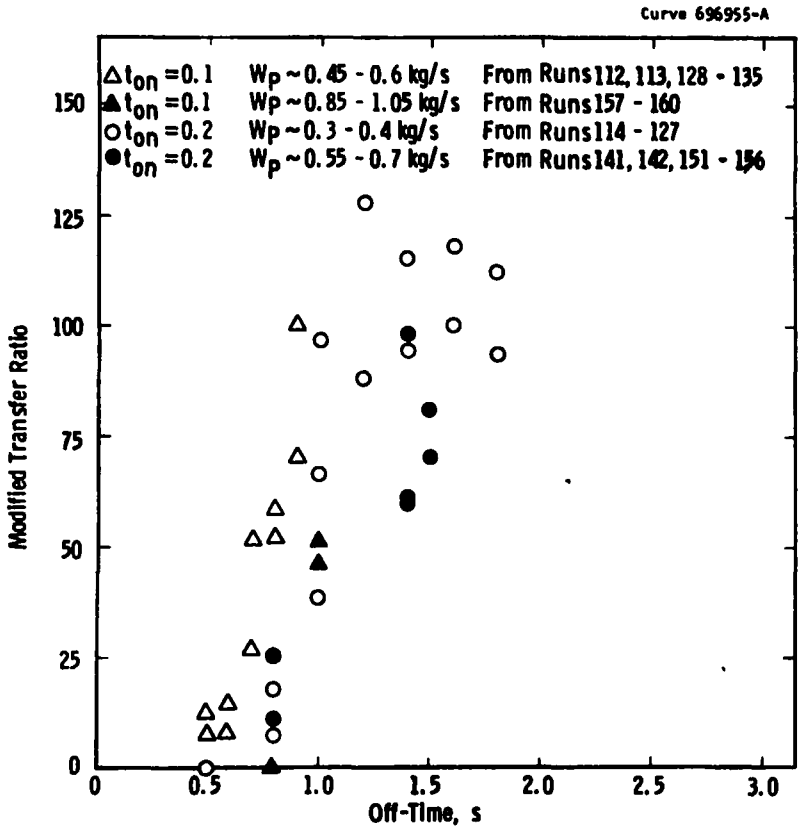

Figure 11. Effect of Off-Time on Modified Transfer Ratio

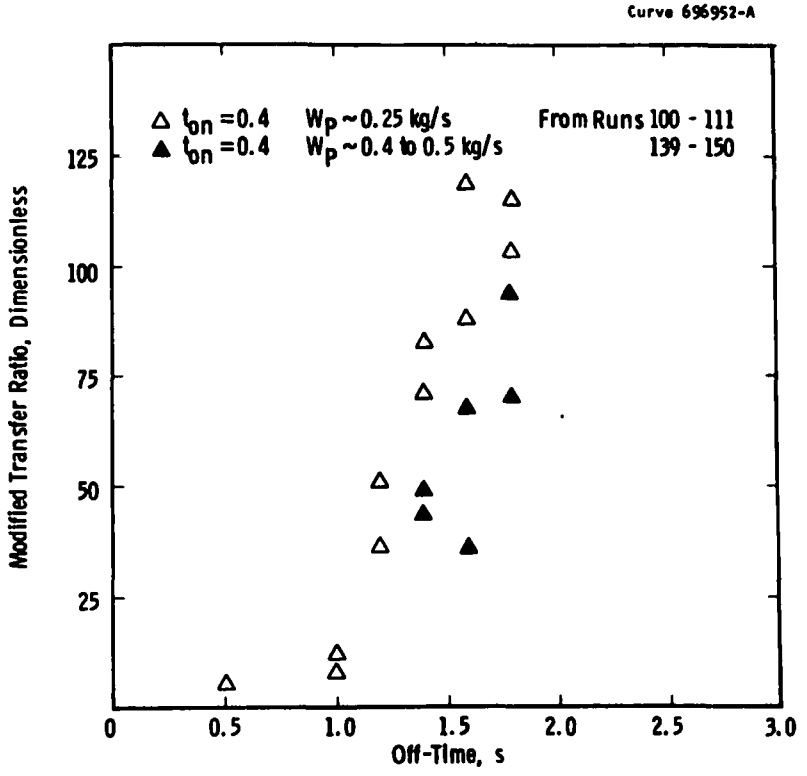

Figure 12. Effect of Off-Time on Modified Transfer Ratio

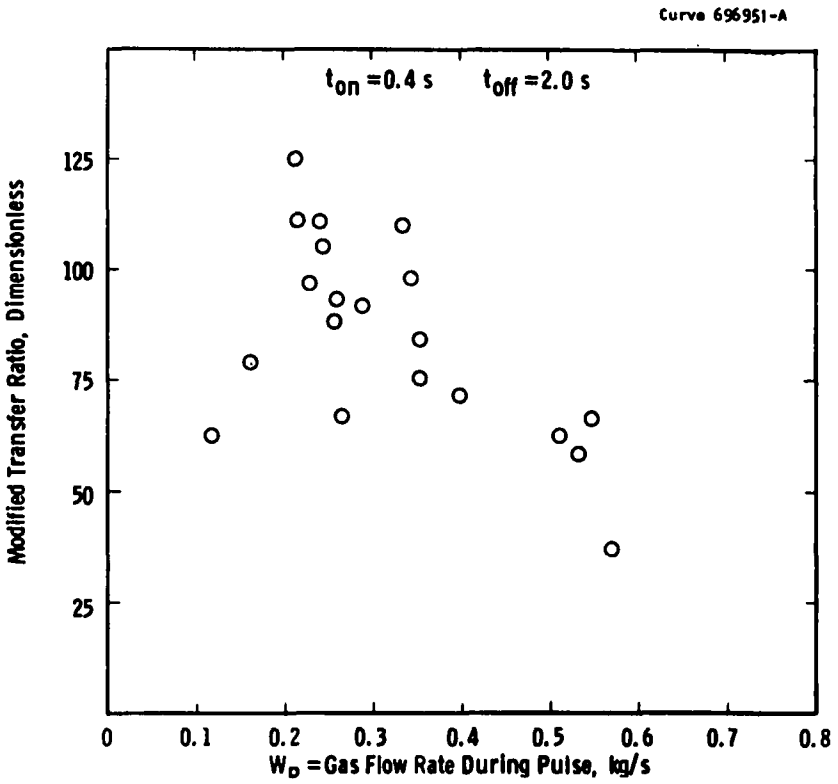

Figure 13. Effect of Pulse Air Rate on Modified Transfer Ratio

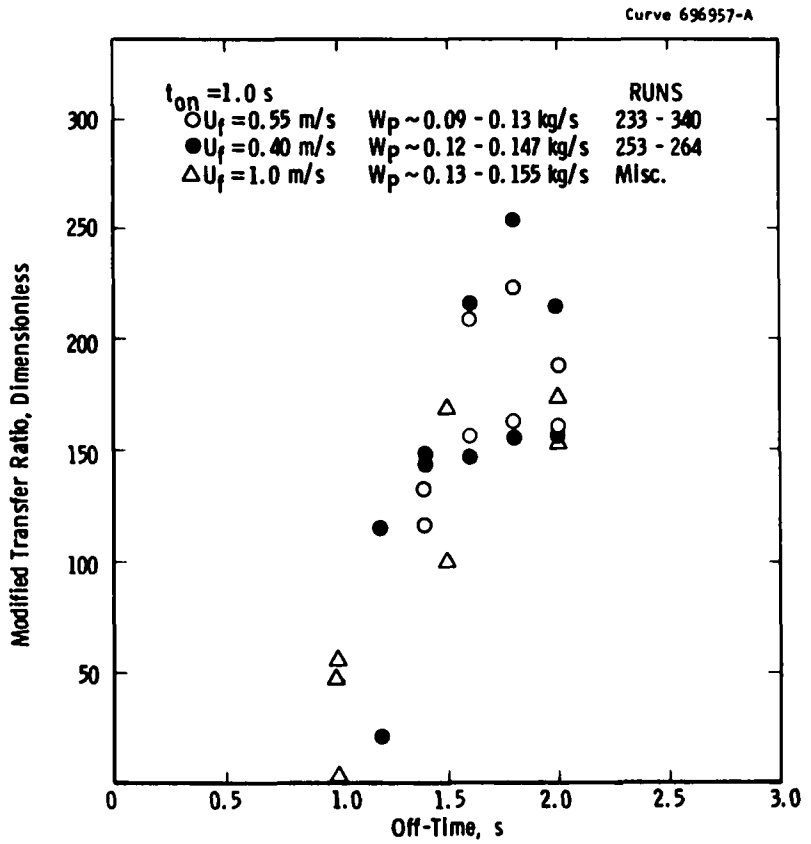

Figure 14. Effect of Off-Time at Lower Fluidizing Velocities

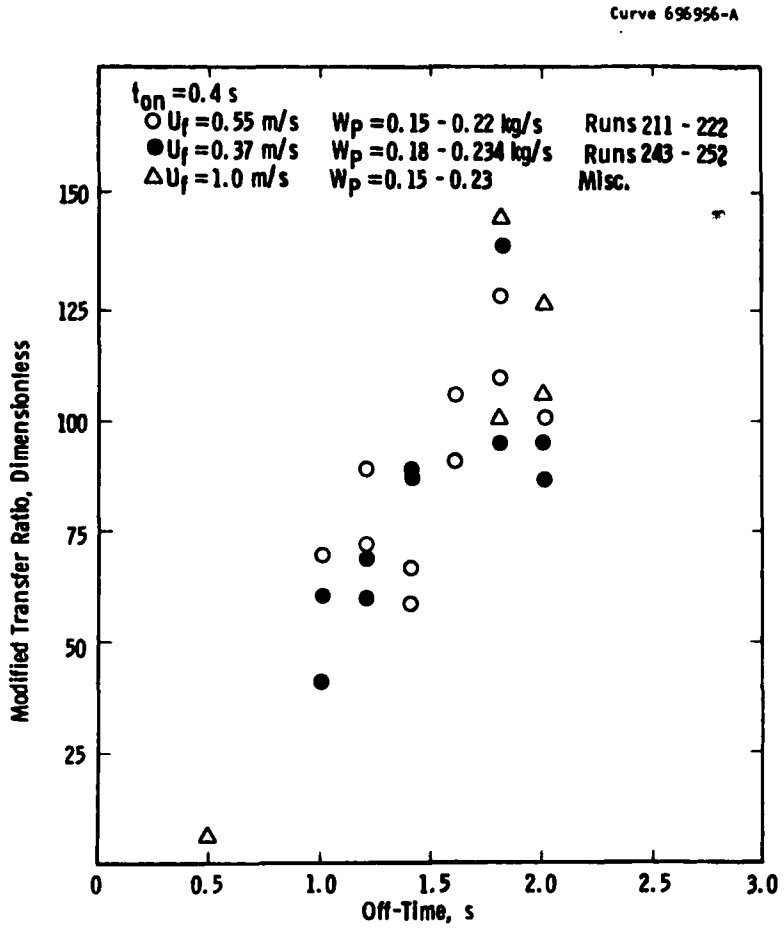

Figure 15. Effect of Off-Time at Lower Fluidizing Velocities

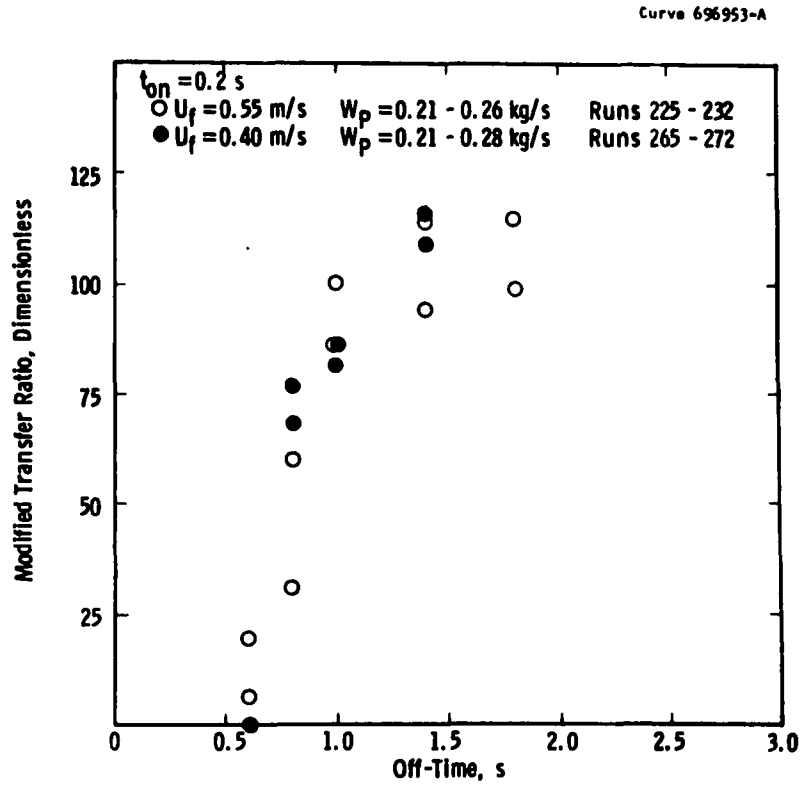

Figure 16. Effect of Off-Time at Lower Fluidizing Velocities

In Figure 7 the curve is displaced substantially lower than those in Figures 8, 9, and 10. This is because with the 1.0 s off-time complete defluidization does not occur, and great efficiency loss occurs as gas blows upward. The exceptions are the cases where fluidization is not completed (Δ in Figure 7). Here the modified transfer ratio is similar to those of the other off-times. The curves for 1.5 s and 2.0 s off-times are similar, indicating that defluidization is substantially complete. The 3.0 s curve has slightly higher efficiencies at corresponding gas inputs. This suggests that we are now seeing effects of increased packing tightness.

Figures 11 and 12 show how important it is to allow sufficient defluidizing time between pulses. The scatter in these diagrams is attributed to variation in the gas flow rate, upon which, we have seen, efficiency strongly depends. It was not feasible to control the gas flow rate rigorously during a pulse, independently of other variables (notably, in this case the off-time). The data, however, were grouped and plotted in reasonably narrow ranges of air input rate. The longer off-times needed for longer pulses are also evident by comparison of these figures, although partially compensated by the air rate variation. One would suspect that the curves would level out at high off-time when no significantly better packing between pulses could be achieved.

Figure 13 illustrates the effect of gas flow rate at constant on- and off-times. This is contrasted with Figure 9, wherein a relationship between on-time and flow rate rather than the on-time value is specified. If the two isolated points in Figure 13 at lower gas flow rate are indeed significant (which is questionable), the drop in efficiency is probably related to the difficulty the weak jets encounter in breaking through the packed solids. This did not occur in Figure 9, presumably because the long pulse durations at low gas flow rates did not accurately represent the amount of time during which the bulk of the pulse flow occurred. In other words, the assumption of a square wave pulse curve is faulty at high pulse lengths.

Several sets of runs were made at fluidizing velocities lower than the 1.0 to 1.1 m/s in the bulk of the tests. These runs were possible because the reduction of particle size during the high velocity runs lowered the minimum fluidizing velocity (U_{mf}) to 0.3 m/s (calculated value) from the initial value of 0.67 m/s (experimental, 0.55 m/s calculated). If sufficient material is used to keep the solids hopper full, the effect of fluidizing velocity should be to determine bed expansion. This would determine the pressure balance across a leg, which would, in turn, determine whether or not the leg solids fluidize, how long it takes to fluidize the solids, and gas loss during a pulse.

The low-fluidizing velocity runs are summarized in Figures 14 to 16. No substantial effect can be noticed from these figures. This is understandable since we were still substantially above the minimum fluidizing velocity, which had changed. Furthermore, the bed pressure drop per unit length in the bed never changed much over the entire run sequence and was also at about the bulk density of the material. This indicates that no significant bed expansion occurred, even during the later higher velocity runs relative to U_{mf}. We were never able to expand the bed sufficiently to affect the fluidizing characteristics of the leg material, and certainly not enough to prevent fluidizing there. That our data show no dependence of the transport performance on the fluidizing velocity does suggest that the bed expansion effect is the only one.

Other findings during this phase of the study include the following:

- Fines entering the transfer leg appear to be blown out more effectively than larger material when the leg fluidizes. Visually, the leg material appeared to contain only very small amounts of fines compared to bed material near windows, and under stagnant conditions. If fines are generated and recycled in the CAFB system, a quantity of nontransferable material may accumulate. A potential solution would be to recycle fines via dip legs to opposite beds.

- The basic flow profile, visually noted, is illustrated in Figure 17. Transport gas is divided into a fast-moving horizontal dilute phase and upward moving slugs or bubbles near the upper vertical face, moving more slowly. Some recirculation seemed to occur near the base of the vertical section. After a short time all gas would apparently rise upward and blow the leg completely. A relatively stagnant area exists below the dilute phase. This may cause possible agglomeration problems if hot.
- Data was collected on pressure profiles in the direction of flow in the transport legs. Appendix B contains more details. Although actual pressure fluctuated significantly (±5 kPa) with pulsing at any point within a leg, the horizontal pressure drop was about 2 to 2.5 kPa, and the average total pressure drop across a leg 7 to 7.5 kPa, independent of run conditions.

Dwg. 6444A18

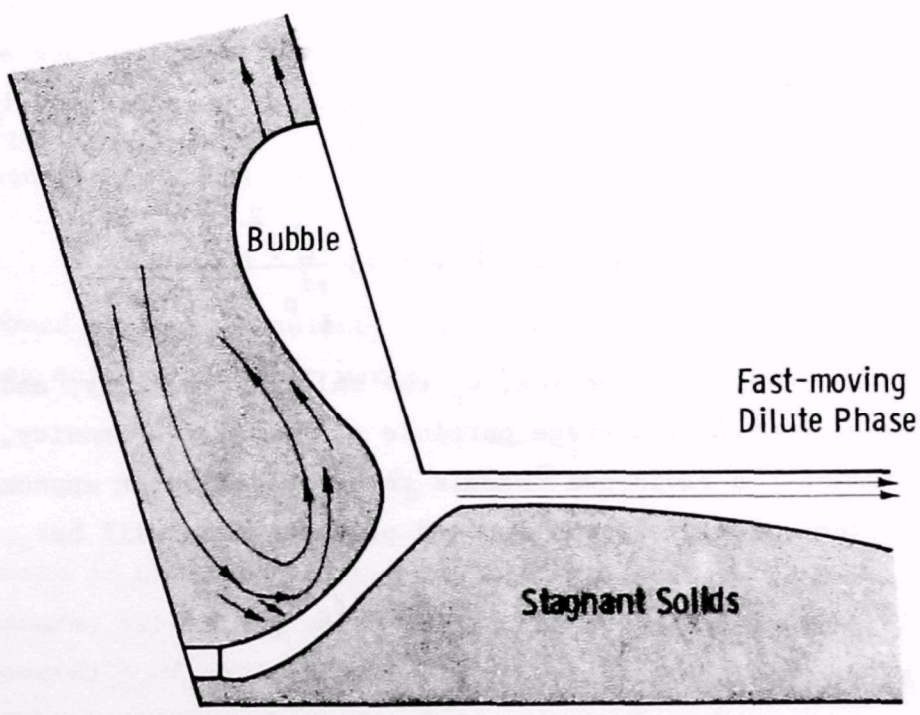

Figure 17. Observed Transport Flow Profile

7.0 SOLIDS TRANSPORT MODEL

7.1 DEVELOPMENT

7.1.1 Time Sequence

Using the data generated with the second pulse air introduction system, a mathematical model of the solids transport system was developed. This model is basically a momentum balance corrected for some of the major unsteady aspects of the flow behavior. We will first describe the sequence of events that we believe occurs within the leg during a single pulse cycle. Then, following a brief accounting of the unsteady aspects and their presumed importance, the model will be developed in detail.

The nomenclature used is as in Figure 18. With no transport gas input the overall pressure drop, (P_3-P_4), which is determined by the bed pressure balance, is easily sealed by the packed solids in the horizontal and vertical sections. Gas flows between vessels at a low rate estimated from the Ergun equation for packed-bed pressure drop (expressed in terms of relative interstitial gas-solids velocity):

$$\frac{(P_3 - P_4)}{(L_S + L_H)} g_c = 150 \frac{\mu U_r}{d_p^2}\left(\frac{1 - \varepsilon_p}{\varepsilon_p}\right)^2 + 1.75 \frac{\rho_g U_r^2}{d_p} \frac{1 - \varepsilon_p}{\varepsilon_p} \qquad (1)$$

where ε_p is the voidage in the leg; U_r the relative velocity; and μ, d_p, and ρ_g the gas viscosity, average particle size, and gas density, respectively. Assuming the fluid-bed vessels to be operating at approximately equal fluidizing velocities, the imposed pressure drop will be:

$$P_3 - P_4 = \rho_{FB}\, g\, L_v/g_c \quad , \qquad (2)$$

where ρ_{FB} is the fluid-bed density.

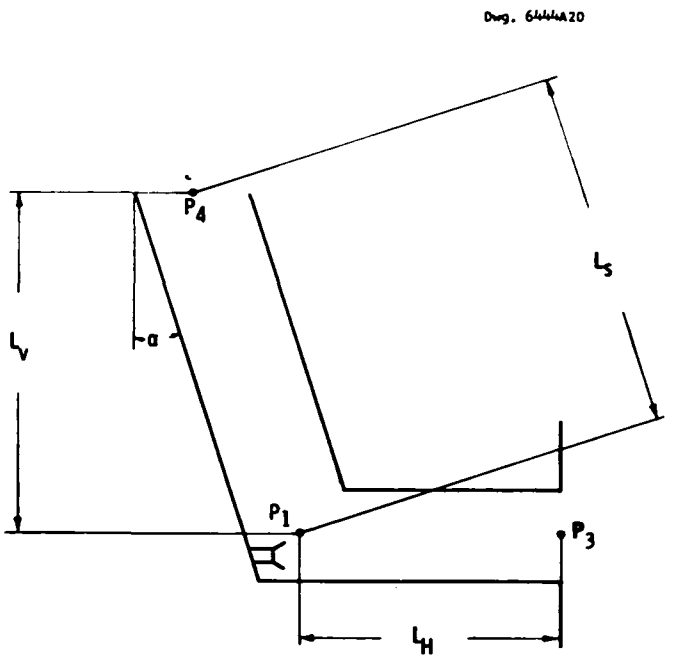

Figure 18. Nomenclature for Transport Model

With the introduction of pulse air, solids flow begins, and the pressure P_1 jumps to a level larger than P_3. The pressure drop now imposed upon the vertical leg section will now be

$$P_1 - P_4 = (P_1 - P_3) + \rho_{FB}\, g\, L_v/g_c \quad . \tag{3}$$

If the imposed pressure gradient is greater than the density of the vertical leg solids, in other words,

$$\frac{P_1 - P_4}{L_s} > \rho_p \frac{(1 - \varepsilon_p)g}{g_c} \quad , \tag{4}$$

then the state is unstable and the leg will fluidize to relieve the excess pressure, liberating pulse gas in the upward direction and causing loss (or reversal) of solids flow. In practice, the fluidization of the downcomer is inevitable unless ρ_{FB} is rather low.

The fact that a short time interval is needed for the fluidization to occur is what makes the pulse system work, and makes it indeed necessary. Estimation of the fluidizing time will be discussed later. The important point is that, once fluidization is complete, further pulse gas is wasted. The transport gas input must be halted for a sufficient time to allow defluidization.

7.1.2 Steady State Assumptions

Solids flow was modeled assuming a steady state flow pattern during the effective portion of each pulse - in other words, before fluidization has occurred. In this first detailed examination of the fluid mechanics of this system it has been necessary to neglect several unsteady aspects of the momentum exchange process. These include the following:

- A finite time is required for jet formation and decay. This "hollowing-out" of the horizontal portion of the leg would require unsteady terms in the gas and solids mass balances and in the momentum balance. The much greater model complexity entailed did not seem appropriate at this time, so we retained the steady state assumption. Jet formation did appear rapid in the experiments, and it seems that solids pushed out when the void is formed are replaced from the same (horizontal) direction.
- Depending on the specific piping arrangement, the velocity of gas issuing from the pulse nozzles may not be constant during a pulse. In this study an average flow during the pulse was derived and used in the analysis. The results suggest that the order of proportionality between solids and gas flow is not a strong function of gas velocity except at low values. These instances, corresponding to very long on-times and low flow rates, are inefficient and, hence, not of practical interest.

- The system pressure balances may change somewhat with time if unequal transfer of material in the two directions occurs (see 6.3.2 above). This will effect both the fluidizing time and the gas bypass rate. The steady state assumption depends on roughly constant bed levels. We circumvented this potential problem by taking data at the point of equal bed depth in each run.
- It was initially assumed that the vertical solids voidage was constant at the packed bed value during the entire effective pulse time. This was found to be a poor assumption for short off-times, when defluidization and/or repacking are not complete. The assumption of packed bed voidage had to be relaxed for these cases which are very poor operating points, although the constancy assumption remains. Relaxation of this assumption would require more knowledge of the unsteady behavior of fluidized systems than is now available and would greatly complicate the model solution.

7.1.3 Mass Balances

On the basis of experimental observations, the flow configuration of Figure 19 was used for the steady state portion of the model. The control volume is represented by the dotted boundary. Gas enters the system at the nozzle, generating a jet which entrains and carries solids to the receiving vessel in dilute phase transport above a region of stagnant solids. The mass balance for the pulse gas is then

$$\underset{\text{(A)}}{v_2 S_2 \rho_2} + \underset{\text{(B)}}{v_1 \varepsilon_1 S_1 \rho_1} = \underset{\text{(C)}}{v_3 \varepsilon_3 S_3 \rho_3} + \underset{\text{(D)}}{v_{RH} \varepsilon_p (S_1 - S_3) \rho_1} \quad . \tag{5}$$

In the above equation the terms represent:

(A) Gas in at nozzle,

(B) Gas in from above with solids (for the present application v_1 will usually be negative)

Dwg. 6444A24

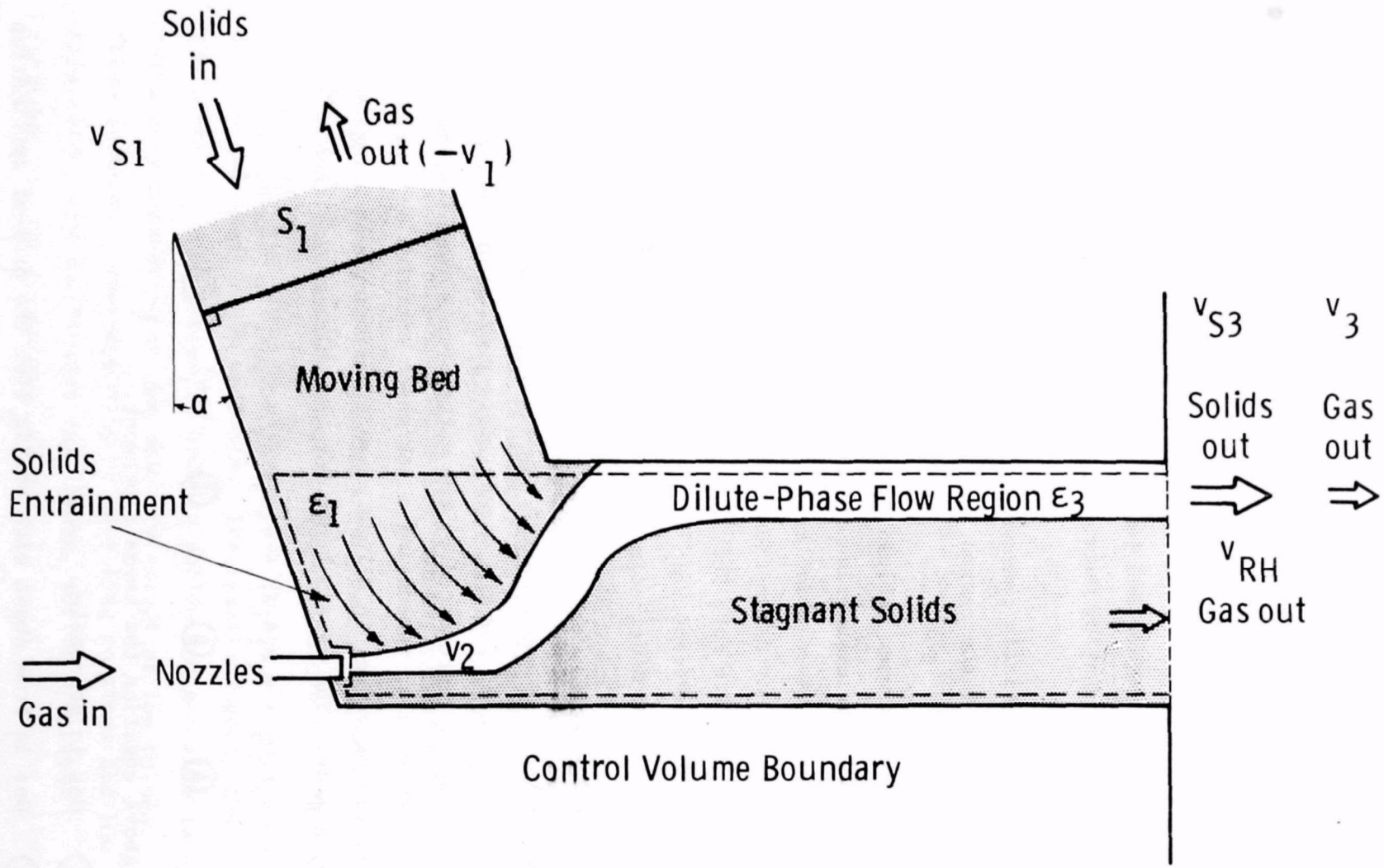

Figure 19. Solids Transport Model Flow Profile

Ⓒ Gas out in dilute phase

Ⓓ Gas out through the stagnant solids.

For solids the mass balance is

$$v_{s1}S_1\rho_p(1 - \varepsilon_1) = v_{s3}S_3\rho_p(1 - \varepsilon_3) \quad , \tag{6}$$

where the left-hand term represents the solids entering from above, and the right-hand term is the efflux of solids in the lean phase.

Defining

$$k \equiv v_{s3}/v_3 \tag{7}$$

and

$$v_R \equiv v_{s1} - v_1 \quad , \tag{8}$$

equation 6 may be written:

$$(v_1 + v_R)(1 - \varepsilon_1)S_1 = kv_3(1 - \varepsilon_3)S_3 \quad . \tag{9}$$

Note that v_1 and v_{s1} are positive downward, while v_R is positive upward. All velocities are actual (i.e. not superficial).

7.1.4 Momentum Balance

A momentum-force balance for the horizontal direction was developed. Note that because of the angle of the vertical section, solids enter the control volume with a finite, though small, horizontal momentum. The overall balance is

$$\underset{\text{Ⓐ}}{-P_1(S_1 - S_2)g_c} = \underset{\text{Ⓑ}}{v_2^2\rho_2S_2} - \underset{\text{Ⓒ}}{v_3^2\rho_3\varepsilon_3S_3} - \underset{\text{Ⓓ}}{k^2v_3^2\rho_p(1 - \varepsilon_3)S_3}$$

$$\underset{\text{Ⓔ}}{-P_3S_1g_c} + \underset{\text{Ⓕ}}{P_2S_2g_c} - \underset{\text{Ⓖ}}{v_1^2\rho_1(\sin\alpha)\varepsilon_1S_1} + \underset{\text{Ⓗ}}{(v_1 + v_R)^2\rho_p(\sin\alpha)(1 - \varepsilon_1)S_1} \tag{10}$$

where the various terms are:

- (A) Force of gas on projected area to rear of leg
- (B) Gas momentum in at nozzle
- (C) Gas momentum out in dilute phase to receiving vessel
- (D) Solids momentum out in dilute phase to receiving vessel
- (E) Pressure of outlet stream (assumed constant over the entire cross-section)
- (F) Pressure of gas in at nozzle. (Note that the control surface crossed by the gas in the vertical section has no vertical component.)
- (G) Gas momentum out via vertical section. If the net flow of gas in the vertical section is downward, the sign of this term is reversed.
- (H) Solids momentum in from above.

In this balance the viscous fluid-wall effect and the momentum of the gas leaking through the stagnant solids have been neglected.

7.1.5 Horizontal Pressure Drop

The vertical and horizontal relative velocities can be estimated from the Ergun equation (equation 1) using pressure gradients of $(P_1 - P_4)/L_S$ and $(P_1 - P_3)/L_H$, respectively. The jet pressure, P_2, is assumed equal to P_1. P_3 and P_4 (Figure 18) must be estimated from system pressure balances.

The pressure drop $(P_1 - P_3)$ in the horizontal dilute phase was modeled by the correlation of Wen and Simons:[12]

$$\left(\frac{P_1 - P_3}{L_H}\right) = \frac{41.82\ U_S^{0.45}\rho_{DS}}{(D_t/d_p)^{0.25}} \quad , \tag{11}$$

where

$(P_1 - P_3)/L_H$ is the pressure gradient	(N/m^3)
d_p is the particle size	(m)
D_t is four times the mean hydraulic radius	(m)

ρ_{DS} is the average dispersed solids density in the horizontal section (kg/m^3)

U_S is the superficial solids velocity in the entire horizontal area. (m/s)

The parameter ρ_{DS} is defined as

$$\rho_{DS} = \rho_p \left(\frac{2(1 - \varepsilon_3)S_3 + (1 - \varepsilon_1)(S_1 - S_3)}{S_1} \right), \tag{12}$$

where the average dilute phase density is approximated as twice the final density due to acceleration. The superficial velocity U_S is then

$$U_S = \frac{kv_3 S_3 (1 - \varepsilon_3)\rho_p}{2\ S_1 \rho_{DS}} \tag{13}$$

7.1.6 Dilute Phase Flow Area

Referring to Figure 19, the areas S_1 and S_2 will be known in any application, but S_3 must be estimated. For this model we estimate this dilute phase flow area by assuming that the similarity of jet expansion is valid for the heterogeneous system. The final flow area will, therefore, be a function of leg geometry only.

The jet model is illustrated in Figure 20. The individual gas jet at each nozzle expands as a circular jet until interference from neighboring jets is encountered. Beyond this point expansion is as a plane jet. No further jet expansion is assumed to occur once the jet passes beneath the lip of the horizontal section. From this point dilute phase horizontal transport occurs to the exit of the transfer leg. In practice, the dilute phase exists at the top of the horizontal section because of buoyancy. The actual mechanics must be very complex. The vertical position of the dilute phase has no influence in the model.

The distance from the nozzle outlet to the transition from circular jets to a plane jet is

$$x_1 = \frac{x_n - d_o}{2 \tan \theta}, \tag{14}$$

Dwg. 6444A11

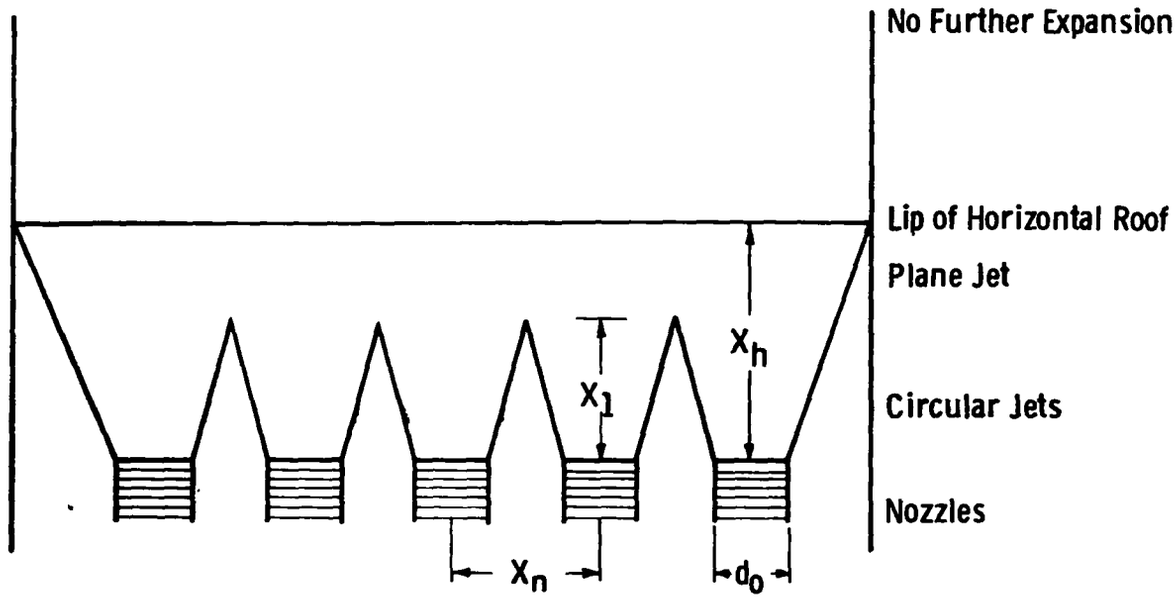

Figure 20a. Top View of Jet Expansion Model

Dwg. 6444A12

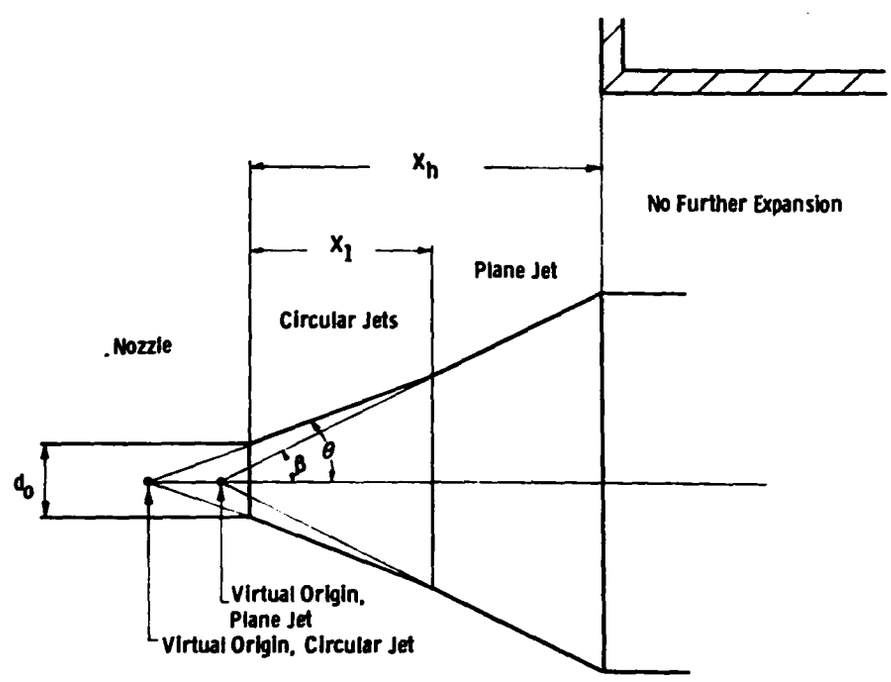

Figure 20b. Side View of Jet Expansion Model

where

x_n is the distance between nozzle centers

d_o is the nozzle diameter and

Θ is the circular jet half-angle.

If

$x_1 \geq x_h$, the final area S_3 is given by

$$S_3 = \frac{\pi}{4} N(2\ x_h \tan \Theta + d_o)^2, \tag{15}$$

where

x_h is the distance from the nozzle to horizontal ceiling

and

N is the number of nozzles.

If

$x_1 < x_h$,

$$S_3 = W[x_n + (d_o - x_n)(\frac{\tan \beta}{\tan \Theta}) + 2\ x_h \tan \beta], \tag{16}$$

where

W is the channel width

and

β is the plane jet half-angle.

In the model β was taken as 7.64° and Θ as 6.35°. Development of these equations and half angle estimates are in Appendix C1. Equation 15 applied to our data. It was assumed that the dilute phase flow region was a rectangular channel of this area. Confirmation of this approach at other geometries is needed before extrapolation to variant cases.

7.1.7 Fluidizing Time

No unrestrained bed of solids can seal a pressure gradient in excess of the bed density. The process of fluidizing the vertical leg requires a short amount of time (<0.4 s), during which a virtual seal exists, allowing solids flow in the proper direction.

The time required to fluidize a leg when a pressure drop in excess of the bulk density of the material in the leg is imposed is approximated by

$$t_M = \sqrt{\frac{2\ L_s^{\ 2}\ \rho_p(1 - \varepsilon_1)}{\Delta P\ g_c}}\ . \tag{17}$$

The derivation of equation 17 is given in Appendix C2.

For

$$\frac{\Delta P}{L_v} \simeq \rho_p(1 - \varepsilon_1)\ g/g_c$$

and

$$L_S = L_V,$$

Equation 17 reduces to

$$t_M = \sqrt{\frac{2\ L_s}{g}}\ . \tag{18}$$

If

$$L_s > L_v,$$

then

$$t_M = \sqrt{\frac{2\ L_s}{g}\ (\frac{L_s}{L_v})},$$

which yields improved flow. In the model solids flow was assumed to stop completely during a pulse at t_M given by equation 17 with $\Delta P = (P_1 - P_4)$ as defined in Figure 18.

7.1.8 Vertical Section Voidage

The vertical void fraction, ε_1, was assumed to be constant during any given pulse. The valve of ε_1 can, however, be significantly greater than the normal packed density if sufficient defluidizing time is not allowed. Experimentally, we observed that at least 1.5 s defluidizing time is required for complete repacking (i.e. insensitivity of transfer efficiency to off-time) when the pulse on-time exceeded t_M. Proportionately less time is needed for shorter on-times because only partial

expansion of the vertical leg section solids occurs. The voidage ε_1 will thus be a function of the pulse on-off times. Its importance is in determining the optimum on-time, t_M (requiring an iterative procedure), and the amount of pulse gas that escapes vertically upward during each pulse. As the off-time is reduced, ε_1 will approach unity, and bypassing of pulse gas will be complete.

In the model, semiempirical relationships were used to reflect this behavior. The rationale behind these is discussed in Appendix C3.
For $t_{ON} \geq t_M$

$$\varepsilon_1 = 1 - (1 - \varepsilon_p)\left(\frac{t_{OFF} - 0.54}{0.87}\right) \tag{19}$$

and for $t_{ON} < t_M$

$$\varepsilon_1 = 1 - (1 - \varepsilon_p)\left(\frac{t_{OFF} - 0.54}{0.87}\right)\left(\frac{t_M}{t_{ON}}\right)^{1/2} \tag{20}$$

In either case ε_1 cannot be less than ε_p or greater than unity.

7.1.9 Dilute Phase Voidage

It was necessary to estimate the voidage in the dilute phase at plane three in Figure 19 (or to estimate the degree of particle acceleration). Depending on the degree of acceleration achieved, the voidage will be somewhere between ε_1 and $\sim$0.95. The degree of acceleration will depend on particle properties, system geometry, the nozzle gas characteristics, and the transport gas waveform.

On the basis of our data, an empirical relationship was derived to estimate the dilute phase voidage, ε_3. The ratio of dispersed density to initial settled density was presumed to be dependent upon the particle Reynolds number at the nozzle and the on-, off-, and fluidizing times. The dependence on periodicity is presumably needed to account for the development and degeneration of the jet and dilute phase during the pulse cycle.

For $t_{ON} \geq t_M$

$$\left(\frac{1 - \varepsilon_3}{1 - \varepsilon_1}\right) = 0.0376\left(\frac{t_M}{t_{OFF}}\right)^{-1.44}\left(\frac{\rho_2 v_2 d_p}{\mu}\right)^{-0.042} \tag{21}$$

For $t_{ON} < t_M$

$$\left(\frac{1 - \varepsilon_3}{1 - \varepsilon_1}\right) = 0.217\left(\frac{t_{ON}}{t_{OFF}}\right)^{-0.543}\left(\frac{\rho_2 v_2 d_p}{\mu}\right)^{-0.045} \tag{22}$$

One can see from these equations that the final void fraction is not strongly dependent on the nozzle velocity. This is compatible with the jet similarity formulation. The voidage varies strongly with the shape of the pulse curve around a median of about 0.85 because of end effects.

The void fraction ε_3 will also probably depend upon the relative entrainment area available which would be

$$A_r = \left(\frac{x_h W}{S_3}\right), \tag{23}$$

where x_h is the distance from nozzle to horizontal overhang, and W is the leg width. These were not varied in our experiments and so no effect of this group is included in equations 21 or 22. The extension of the model to conditions of significantly different x_h is not recommended at this stage.

7.1.10 Model Summary and Procedure

Solution of the model for the overall average solids flow rate at any set of conditions requires the simultaneous solutions of the above equations. Table 5 lists the independent and dependent variables covered by the model. A flow sheet for the solution of these equations is given in Figure 21. A listing of a computer program to solve these equations will be found in Appendix D.

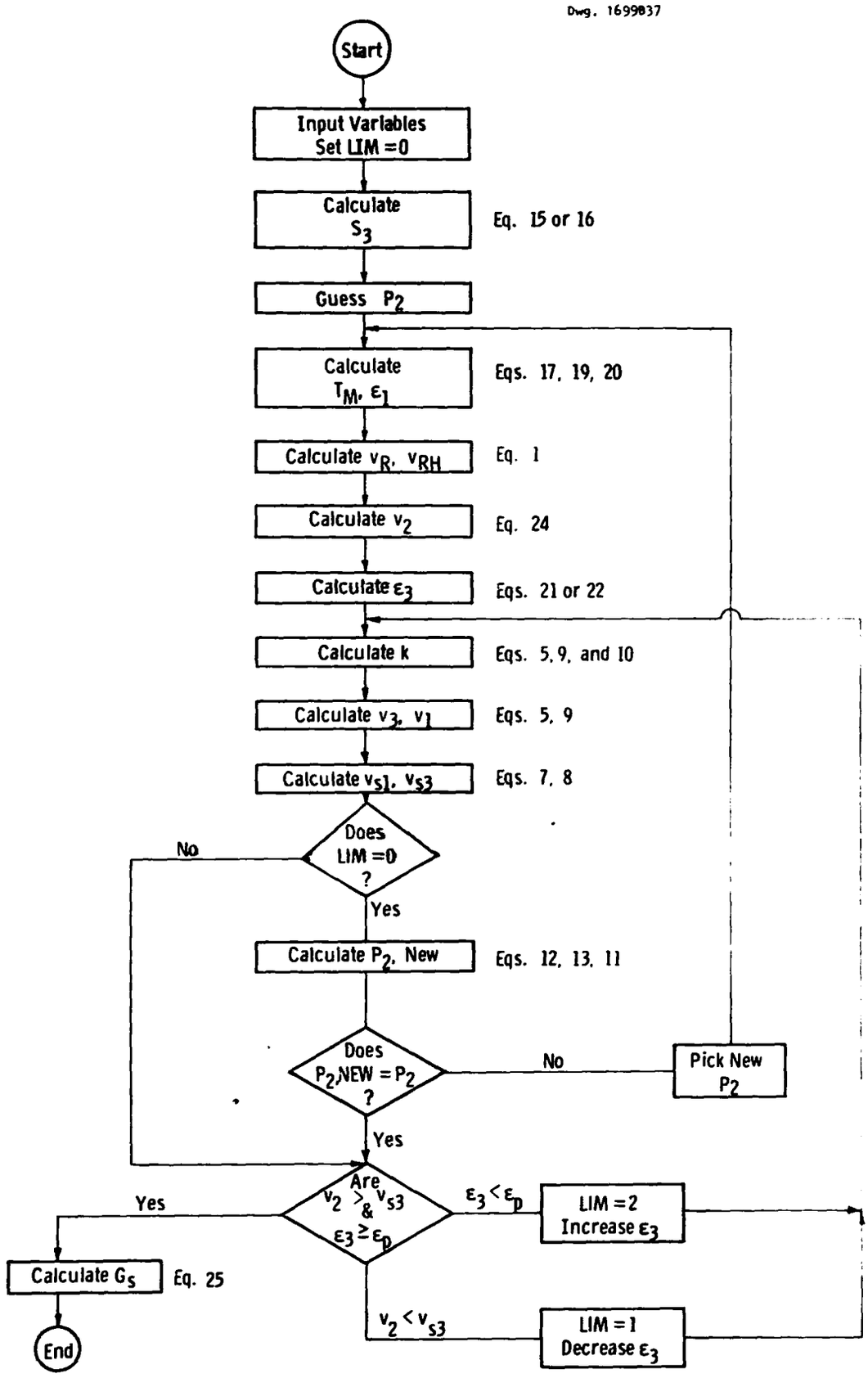

Figure 21. Transfer Leg Model Flow Sheet

TABLE 5

TRANSFER LEG MODEL - VARIABLES

A. INDEPENDENT (INPUT) VARIABLES

Transfer Leg Geometry

α	Angle of vertical section
L_S	Length of vertical section
L_H	Length of horizontal section
S_1	Cross-sectional area of leg
S_2	Nozzle outlet area (total)
D_T	4 times the mean hydraulic radius of leg cross section
d_0	Nozzle diameter
x_h	Distance from nozzle to overhang
x_n	Distance between nozzle centers
W	Leg width
N	Number of nozzles

Particulate Properties

ϵ_p	Loose bulk density
ρ_p	Particle (aerodynamic) density
d_p	Average particle size (projected surface area mean)

Pulse Gas Properties

T	Temperature
M	Molecular weight
μ	Viscosity

System Properties

P_3	Pressure at leg discharge
$\Delta P^\circ = (P_3 - P_4)$	Total pressure drop cross leg
G_A	Overall pulse gas average mass flow
t_{on}	Pulse duration
t_{off}	Time between pulses

B. DEPENDENT VARIABLES

S_3	Dilute phase flow area
v_1	Downward interstitial gas velocity
v_2	Pulse gas nozzle velocity
v_3	Interstitial velocity of gas in dilute phase at exit
v_R	Upward interstitial gas velocity relative to solids
v_{RH}	Horizontal interstitial gas velocity in stagnant solids
v_{s1}	Downward moving bed solids velocity
v_{s3}	Dilute phase exit solids velocity
$P_1 = P_2$	Pressure at bend of transfer slot
ϵ_1	Moving bed voidage in vertical section
ϵ_3	Dilute phase exit voidage
t_M	Fluidizing time
G_s	Overall solids flow rate
W_p	Transport air rate during pulse
W_H	Horizontal air rate during pulse
T.R.	Transport ratio (mass)

Referring to Figure 19, the area S_3 is first calculated from either equation 15 or 16. An initial guess for P_2 ($=P_1$) must then be made to begin the iterative procedure. A reasonable first guess would be 3 kPa in excess of P_3.

The fluidizing time and vertical section voidage are then determined from the simultaneous solution of equations 17 and either 19 or 20, depending on the pulse duration. The relative gas velocities upward and horizontally through the stagnant solids below the transfer region are calculated from the Ergun equation (equation 1) using voidages ε_1 and ε_p, and pressure gradients $(P_1 - P_4)/L_s$ and $(P_1 - P_3)/L_H$, respectively. The jet velocity is

$$v_2 = \frac{G_A}{\rho_2 S_2} \left(\frac{t_{ON} + t_{OFF}}{t_{ON}}\right), \tag{24}$$

where G_A is the <u>overall</u> average mass flow rate of air. At this point the voidage ε_3 can be determined from the appropriate equation (21 or 22).

If v_1 and v_3 are eliminated from the momentum balance (equation 10) by using the mass balances (equations 5 and 9), a direct solution for the ratio, k, of solids to gas velocity at the transfer leg outlet can be obtained. Then all velocities, v_1, v_3, v_{S1}, and v_{S2}, can be obtained from equations 5, 9, 7, and 8. A new value of P_2 is now calculated by successively applying equations 12, 13, and 11. The procedure is repeated until the calculated value of P_2 agrees with the guessed value. The overall solids flow rate is

$$G_S = v_{S3} S_3 (1 - \varepsilon_3) \rho_p \left(\frac{t_s}{t_{ON} + t_{OFF}}\right) \tag{25}$$

where t_s is the minimum of t_{ON} and t_M.

7.2 MODEL PERFORMANCE

Tabulated predictions compared to experimental values obtained with the final configuration are presented in Appendix E, together with predicted values of other parameters. The average error was 0.67 kg/s, which

is about the reproducibility of the experimental data at the highest flow rates obtained. The worst performance occurs for very short off-time runs, which feature incomplete defluidization between pulses and are unstable and not optimum. In general, if the model predicts $\varepsilon_1 > \varepsilon_p$, the off-time is too short for safe operation.

A significant source of error in the modeling work is the assumption of a square-wave pulse curve, as discussed previously. The solids flow measurement was also limited to an accuracy of ±20 percent. The activated alumina material used in the study proved to be attrition-prone and was difficult to characterize as to particle density and, hence, voidage. In light of these limitations and the large number of assumptions required in the model development, performance is good.

To test the model, we applied it to the conditions of the tests conducted by FW on the three-tube sparger transfer slot selected for the demonstration plant design.[11] The geometry of the transfer leg is shown in Figure 22. The bulk specific gravity of the material was given as 1.43. In addition, the following conditions were assumed or gleaned from the FW report:

- The effective void fraction was 0.45.
- The leg discharge pressure (P_3) was 112 kPa (absolute).
- The imposed pressure differential ($P_3 - P_4$) was ∿2.4 kPa.
- The operating temperature was 310 K.
- The fluidizing velocities were sufficiently high that fluidization of the downcomer solids did not occur. Solids therefore would be transferred during the entire on-time.
- The average particle size was 750 μm
- The flared inlet to the leg was assumed only to affect the ability of the bed to keep the leg full of solids.

Table 6 compares FW's test results with the predictions of the model for a single leg. The experimental results and model predictions support one another well. The surmised relative freedom of the FW tests

from downcomer fluidization or voidage variation, allow these data points to fall into the range of conditions that is most easily and accurately modeled. These stable operating points result from the high fluidizing velocities and, hence, high bed expansion characteristic of that study. Note that our experimental system and that of FW have equivalent values of x_h. Application of the model to variations in this parameter has not been tested and is not recommended.

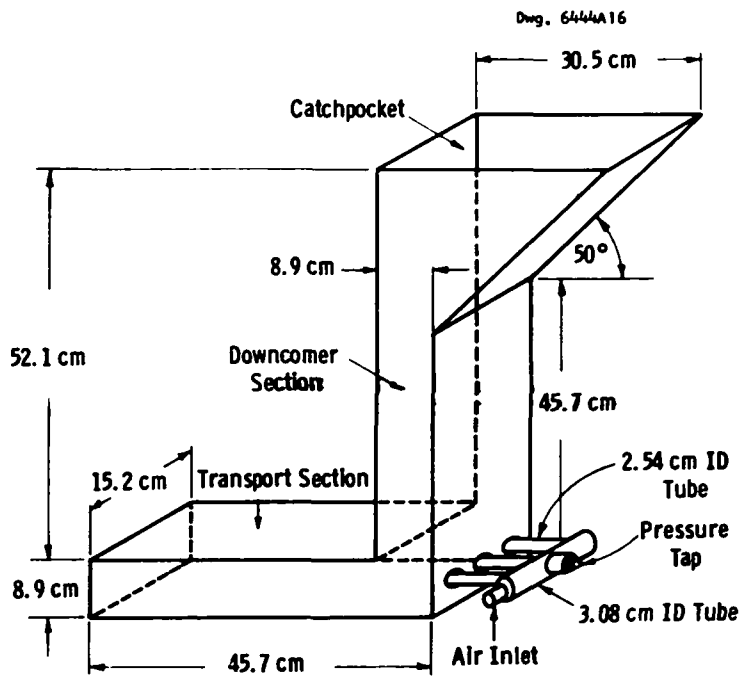

Figure 22. CAFB Demonstration Plant Transport Leg Design[11]

TABLE 6

COMPARISON OF FWEC FINAL DESIGN DATA* AND MODEL PREDICTIONS

FW Run No.	On-Time, s	Off-Time, s	Average airflow rate, kg/s	Actual solids rate, kg/s	Predicted solids rate, kg/s
LS-1	0.5	7.5	0.0120	1.34	1.26
-2	0.7	9.2	0.0110	1.21	1.33
-3	0.5	12.0	0.0086	0.86	0.98
-4	0.5	2.6	0.0300	2.38	2.17
-4R	0.5	2.6	0.0277	2.47	2.15
-5	0.5	4.0	0.0221	2.03	1.78
-5R	0.5	4.0	0.0207	1.99	1.76
-6	0.5	7.0	0.0149	1.64	1.34

* See Reference 11.

8.0 DEMONSTRATION PLANT PERFORMANCE PROJECTIONS

The use of the model was extrapolated to conditions expected or possible in the CAFB demonstration plant. In the experimental portion of this work it was often not possible or feasible to change only one variable at a time. The model allows us to explore the effects of each variable individually. Tables 7 through 17 present the results of this investigation. The base conditions used are as follows, with any changes listed in the appropriate table:

Leg geometry - as per Figure 22 (per leg)
Particle size - 1500 μm
Packed bed voidage - 0.45
Particle density - 1800 kg/m^3
Gas - air at 500 K
Pressure at leg discharge - 128 kPa abs
Imposed ΔP° on leg $(P_3 - P_4)$ - 4 kPa.

8.1 Total Transport Gas Flow Rate

Table 7 shows that increasing the transport gas rate while holding all other parameters constant will result in increased solids transfer but lower efficiency (T.R.). If the demonstration plant requires 3.2 kg/s solids flow in each direction, then two legs, each with a transport gas flow rate of about 0.04 kg/s, will be needed at this set of conditions. The efficiency is rather low; the reasons for this will be seen later.

8.2 Pulse Gas On- and Off-Times

Table 8 shows the effect of the transport gas waveform at constant total pulse gas input. Points 13 through 19 in this table predict that solids flow and transport efficiency both will be maximized at about 0.2 s on-time with the time between pulses at 1.5 s. As the

TABLE 7

EFFECT OF TOTAL GAS FLOW RATE

Point	t_{ON},	t_{OFF},	t_M,	G_A,	W_P,	W_H,	ε_1	ε_3	(P_2-P_3),	T.R.,	G_S,
-	s	s	s	kg/s	kg/s	kg/s	-	-	kPa	kg/kg	kg/s
1	0.3	1.5	0.29	0.007	0.04	0.0324	0.45	0.84	3.6	193	1.35
2	0.3	1.5	0.29	0.010	0.06	0.0504	0.45	0.84	3.6	135	1.35
3	0.3	1.5	0.29	0.015	0.09	0.0804	0.45	0.84	3.6	91	1.37
4	0.3	1.5	0.29	0.020	0.12	0.1105	0.45	0.84	3.6	70	1.40
5	0.3	1.5	0.29	0.025	0.15	0.1406	0.45	0.84	3.7	58	1.45
6	0.3	1.5	0.28	0.030	0.18	0.1707	0.45	0.84	3.8	50	1.51
7	0.3	1.5	0.28	0.035	0.21	0.2008	0.45	0.84	3.8	45	1.57
8	0.3	1.5	0.28	0.040	0.24	0.2309	0.45	0.84	3.9	41	1.64
9	0.3	1.5	0.28	0.050	0.30	0.2911	0.45	0.84	4.1	36	1.79
10	0.3	1.5	0.27	0.070	0.42	0.4118	0.45	0.84	4.4	30	2.13
11	0.3	1.5	0.26	0.100	0.60	0.5929	0.45	0.83	5.0	27	2.66
12	0.3	1.5	0.24	0.200	1.20	1.1977	0.45	0.82	6.5	23	4.50

TABLE 8

EFFECT OF ON- AND OFF-TIMES AT CONSTANT TOTAL GAS FLOW RATE

Point	t_{ON},	t_{OFF},	t_M,	G_A,	W_P,	W_H,	ε_1	ε_3	(P_2-P_3),	T.R.,	G_S,
-	s	s	s	kg/s	kg/s	kg/s	-	-	kPa	kg/kg	kg/s
13	0.1	1.5	0.25	0.03	0.480	0.4734	0.45	0.67	6.2	46	1.39
14	0.2	1.5	0.27	0.03	0.255	0.2464	0.45	0.76	4.6	54	1.61
15	0.3	1.5	0.28	0.03	0.180	0.1707	0.45	0.84	3.8	50	1.51
16	0.4	1.5	0.29	0.03	0.142	0.1331	0.45	0.84	3.7	45	1.36
17	0.5	1.5	0.29	0.03	0.120	0.1105	0.45	0.84	3.6	42	1.26
18	1.0	1.5	0.29	0.03	0.075	0.0654	0.45	0.84	3.6	33	0.98
19	1.5	1.5	0.29	0.03	0.060	0.0504	0.45	0.84	3.6	27	0.81
20	0.3	1.0	0.24	0.03	0.130	0.0967	0.70	0.84	1.7	26	0.78
21	0.3	1.5	0.28	0.03	0.180	0.1707	0.45	0.84	3.8	50	1.51
22	0.3	2.0	0.27	0.03	0.230	0.2214	0.45	0.74	4.7	54	1.63
23	0.3	2.5	0.25	0.03	0.280	0.2723	0.45	0.61	5.9	57	1.72
24	0.3	3.0	0.24	0.03	0.330	0.3232	0.45	0.46	7.2	58	1.73

on-time is increased the amount of time available for solids flow increases up to a point (t_M), but the dilute phase voidage increases. These effects cause opposite changes in solids flow rate. Points 20 to 24 show that both flow rate and efficiency increase regularly with off-time. This is because more time is allowed for repacking between pulses, allowing ε_3 to become lower. Note that for $t_{ON} = 0.3$ and $t_{OFF} = 1.0$ the vertical voidage is predicted to be 0.70 with a resulting high ε_3 and the loss of approximately half the transport gas upward (compare horizontal and total gas input rates during pulse, W_H and W_P). This point should be avoided.

Table 9 lists the expected flows at the same on- and off-times as Table 8, but at constant transport gas flow rate during the pulse. This is perhaps a better way to look at this effect because nozzle velocity is constant. The trends are similar to the previous case with efficiencies varying more and solids flow rates less, as might be expected from Table 7.

8.3 Process Related Parameters

Certain variables influencing leg operation will be determined by the overall process specifications and pressure balance. Table 10 shows the predicted operation at various temperatures. An overall temperature is used in the model for gas at any point. Solids temperature does not enter into the calculation. Operation will apparently not depend strongly on the precise temperature so consideration of temperature profiles and heat transfer effects will not be necessary. Because no gas is entrained from either vessel during a pulse (i.e. $W_P > W_H$, some pulse gas going upward and some horizontally) the very hot reactor gases will not significantly mix with transport gas in the legs except at the entrance and exit. Gas temperatures in the leg should therefore all be in the 400 to 600 K range, assuming an input gas temperature of about 400 K. The main effect of temperature, according to the models, is in determining gas loss upward during the early part of the pulse, using the Ergun equation.

TABLE 9

EFFECT OF ON- AND OFF-TIMES AT CONSTANT GAS FLOW RATE DURING PULSE

Point -	t_{ON}, s	t_{OFF}, s	t_M, s	G_A, kg/s	W_P, kg/s	W_H, kg/s	ε_1, -	ε_3, -	(P_2-P_3), kPa	T.R., kg/kg	G_S, kg/s
44	0.1	1.5	0.26	0.0156	0.25	0.2420	0.45	0.66	5.5	69	1.08
45	0.2	1.5	0.27	0.0294	0.25	0.2414	0.45	0.76	4.6	54	1.60
46	0.3	1.5	0.28	0.0417	0.25	0.2409	0.45	0.84	3.9	40	1.67
47	0.4	1.5	0.28	0.0526	0.25	0.2409	0.45	0.84	3.9	30	1.57
48	0.5	1.5	0.28	0.0625	0.25	0.2409	0.45	0.84	3.9	24	1.50
49	1.0	1.5	0.28	0.1000	0.25	0.2409	0.45	0.84	3.9	12	1.20
50	1.5	1.5	0.28	0.1250	0.25	0.2409	0.45	0.84	3.9	8	1.00
51	0.3	1.0	0.24	0.0577	0.25	0.2175	0.70	0.94	2.0	18	1.03
52	0.3	1.5	0.28	0.0417	0.25	0.2409	0.45	0.84	3.9	40	1.67
53	0.3	2.0	0.27	0.0326	0.25	0.2415	0.45	0.74	4.8	51	1.67
54	0.3	2.5	0.25	0.0268	0.25	0.2422	0.45	0.61	5.9	62	1.67
55	0.3	3.0	0.24	0.0227	0.25	0.2428	0.45	0.45	7.0	73	1.66

TABLE 10

EFFECT OF TEMPERATURE

Point -	t_{ON}, s	t_{OFF}, s	t_M, s	G_A, kg/s	W_P, kg/s	W_H, kg/s	ε_1 -	ε_3 -	(P_2-P_3), kPa	T.R., kg/kg	G_S, kg/s	T, K
38	0.3	1.5	0.29	0.03	0.18	0.1689	0.45	0.84	3.7	49	1.46	400
39	0.3	1.5	0.28	0.03	0.18	0.1712	0.45	0.84	3.8	50	1.51	500
40	0.3	1.5	0.28	0.03	0.18	0.1721	0.45	0.84	3.8	52	1.55	600
41	0.3	1.5	0.28	0.03	0.18	0.1740	0.45	0.84	3.9	54	1.63	800
42	0.3	1.5	0.28	0.03	0.18	0.1754	0.45	0.84	4.0	57	1.70	1000
43	0.3	1.5	0.28	0.03	0.18	0.1774	0.45	0.83	4.2	62	1.87	1500

The pressure at the discharge end of the leg will have little if any effect on operation, provided the overall imposed pressure drop is constant. This is demonstrated in Table 11 where P_3 varies from 102 to 180 kPa absolute, and $(P_3 - P_4)$ is maintained at 4 kPa as in the other tables. The reason for the slight dependence lies again in the Ergun equation pressure dependence.

If the two fluid beds are operated at different pressures, bed levels, and/or fluidizing velocities, the pressure drop across each leg may be different, necessitating operation of the pulse system at different conditions to maintain equal and opposite transfer rates. The effect of the imposed pressure difference is illustrated in Table 12, where $P_3 - P_4$ is varied from 0 to 20 kPa. At no pressure difference $P_2 - P_4 = P_2 - P_3$ and no tendency to fluidize occurs. At $P_3 - P_4 = 2$ kPa fluidization is now possible but takes more time than the pulse (at this on-time). A sharp drop in both flow rate and efficiency occurs with a further increase in $\Delta P°$. Thus the imposed pressure drop simply determines in which of two regimes the system will operate, fluidizing on nonfluidizing. Within either category operation is nearly independent of the pressure drop. The designer should expect that $\Delta P°$ will be, in practice, sufficiently large that the leg will fluidize with enough on-time.

8.4 PARTICULATE PROPERTIES

As particle size increases, upward gas loss will increase, according to the Ergun equation. In addition, the horizontal pressure loss will increase (according to the Wen and Simons[12] correlation used in the model $(P_2 - P_3) \propto d_p^{0.25}$). A look at the momentum balance shows the factors have opposite effects on solids flow rate. Table 13 shows that the transfer rate and efficiency do go through minima as particle size increases. The effect is small, however, as might be expected.

On the other hand, particle density is seen to be of paramount importance. Comparison of points 63 and 66 in Table 14 clearly indicates this. These predictions show why the tests performed at FW were so

TABLE 11

EFFECT OF RECEIVING VESSEL ABSOLUTE PRESSURE

Point	t_{ON},	t_{OFF},	t_M,	G_A,	W_P,	W_H,	ε_1	ε_3	(P_2P_3),	T.R.,	G_S,	P_3,
-	s	s	kg/s	kg/s	kg/s	kg/s	-	-	kPa	kg/kg	kg/s	kPa, abs
25	0.3	1.5	0.28	0.03	0.18	0.1717	0.45	0.84	3.8	52	1.56	102
26	0.3	1.5	0.28	0.03	0.18	0.1715	0.45	0.84	3.8	51	1.54	108
27	0.3	1.5	0.28	0.03	0.18	0.1710	0.45	0.84	3.8	51	1.52	120
28	0.3	1.5	0.29	0.03	0.18	0.1702	0.45	0.84	3.7	50	1.49	140
29	0.3	1.5	0.29	0.03	0.18	0.1695	0.45	0.84	3.7	49	1.47	160
30	0.3	1.5	0.29	0.03	0.18	0.1689	0.45	0.84	3.7	48	1.45	180

TABLE 12

EFFECT OF PRESSURE GRADIENT ACROSS TRANSFER LEG

Point	t_{ON},	t_{OFF},	t_M,	G_A,	W_P,	W_H,	ε_1	ε_3	(P_2-P_3),	T.R.,	G_S,	ΔP^o (P_3-P_4)
-	s	s	s	kg/s	kg/s	kg/s	-	-	kPa	kg/kg	kg/s	kPa
31	0.3	1.5	****	0.03	0.18	0.1759	0.45	0.81	4.1	61	1.82	0
32	0.3	1.5	0.32	0.03	0.18	0.1733	0.45	0.81	4.1	61	1.83	2
33	0.3	1.5	0.28	0.03	0.18	0.1710	0.45	0.84	3.8	51	1.52	4
34	0.3	1.5	0.25	0.03	0.18	0.1691	0.45	0.81	4.1	50	1.51	6
35	0.3	1.5	0.22	0.03	0.18	0.1674	0.45	0.78	4.4	50	1.51	8
36	0.3	1.5	0.21	0.03	0.18	0.1660	0.45	0.75	4.5	50	1.49	10
37	0.3	1.5	0.16	0.03	0.18	0.1559	0.45	0.63	5.6	50	1.49	20

TABLE 13

EFFECT OF AVERAGE PARTICLE SIZE

Point	t_{ON},	t_{OFF},	t_M,	G_A,	W_P,	W_H,	ε_1	ε_3	(P_2-P_3),	T.R.,	G_S,	d_p,
-	s	s	s	kg/s	kg/s	kg/s	-	-	kPa	kg/kg	kg/s	μm
56	0.30	1.5	0.30	0.03	0.18	0.1813	0.45	0.80	2.9	54	1.62	500
57	0.30	1.5	0.30	0.03	0.18	0.1782	0.45	0.85	3.0	47	1.42	750
58	0.30	1.5	0.29	0.03	0.18	0.1755	0.45	0.85	3.3	48	1.45	1000
59	0.30	1.5	0.28	0.03	0.18	0.1707	0.45	0.84	3.8	50	1.51	1500
60	0.30	1.5	0.28	0.03	0.18	0.1666	0.45	0.84	4.1	52	1.55	2000
61	0.30	1.5	0.27	0.03	0.18	0.1631	0.45	0.84	4.5	53	1.58	2500

TABLE 14

EFFECT OF PARTICLE DENSITY

Point	t_{ON},	t_{OFF},	t_M,	G_A,	W_P,	W_H,	ε_1	ε_3	(P_2-P_3),	T.R.,	G_S,	ρ_p
-	s	s	s	kg/s	kg/s	kg/s	-	-	kPa	kg/kg	kg/s	kg/m^3
62	0.3	1.5	0.27	0.03	0.18	0.1716	0.45	0.83	3.2	43	1.28	1500
63	0.3	1.5	0.28	0.03	0.18	0.1707	0.45	0.84	3.8	50	1.51	1800
64	0.3	1.5	0.30	0.03	0.18	0.1702	0.45	0.85	4.0	55	1.64	2000
65	0.3	1.5	0.30	0.03	0.18	0.1691	0.45	0.81	5.5	80	2.40	2500
66	0.3	1.5	0.32	0.03	0.18	0.1680	0.45	0.81	6.5	94	2.82	3000

much more efficient than can be expected in the demonstration plant. FW's particle density was (bulk specific gravity 1.43, $\varepsilon = 0.45$) at least 2900 kg/m^3, whereas, if the plant material has a bulk specific gravity of 1.0, the particle density will be 1800 kg/m^3. The effect of particle density is difficult to separate from the intricate momentum balance. Higher particle density results in a higher horizontal pressure drop (equations 11 to 13) and, hence, higher P_1 and P_2. One would also expect the particles to be less completely accelerated so kv_3 is lower. A look at the momentum balance (equation 10) shows that

$$G_S = kv_3\rho_p(1 - \varepsilon_3)S_3 \propto P_1, P_2, \rho_p, (\frac{1}{kv_3}), \qquad (26)$$

all of which factors are increased. This particle density dependence might also be suspected if entrainment is expected to be on a volume-for-volume basis as is common with homogeneous jets.

8.5 LEG GEOMETRY VARIATION

In Table 15 the horizontal channel height is varied from its normal 0.089 m, with all other leg dimensions remaining constant. This variation essentially allows variation in the stagnant solids inventory in the horizontal line. Solid flows are given both on an absolute and per unit area basis for comparison. Thinner slots are both less efficient (T.R. column) and of lower capacity. As expected, they are much more efficient on a per unit area basis simply because proportionately less area is devoted to stagnant solids. Thus, transport gas is saved by going to the deeper channel, but the probability for agglomerate formation in the stagnant region might increase. The model predicts solids flow to be proportional to channel width, if the number of nozzles is increased accordingly.

At some point it might be desired to operate the transport leg between deeper fluid beds. The vertical height could thus be greater, but the imposed pressure drop would be correspondingly larger, $\Delta P/L$, remaining about the same. Table 16 shows the effect of vertical height at constant pressure gradient. A deeper packed vertical bed will require

TABLE 15

EFFECT OF HORIZONTAL SLOT HEIGHT

Point -	t_{ON}, s	t_{OFF}, s	t_M, s	G_A, kg/s	W_P, kg/s	W_H, kg/s	ε_1 -	ε_3 -	(P_2-P_3), kPa	T.R., kg/kg	G_S/S_1, kg/s/m^2	H_h, m	G_S, kg/s
67	0.3	1.50	0.29	0.03	0.18	0.1626	0.45	0.85	3.3	60	78	0.1530	1.81
68	0.3	1.50	0.29	0.03	0.18	0.1657	0.45	0.85	3.6	58	89	0.1274	1.73
69	0.3	1.50	0.28	0.03	0.18	0.1688	0.45	0.84	4.0	54	105	0.1020	1.63
70	0.3	1.50	0.28	0.03	0.18	0.1704	0.45	0.84	4.3	52	116	0.0892	1.57
71	0.3	1.50	0.27	0.03	0.18	0.1719	0.45	0.83	4.6	50	130	0.0764	1.51

TABLE 16

EFFECT OF VERTICAL HEIGHT AT CONSTANT $\Delta P/L$

Point -	t_{ON}, s	t_{OFF}, s	t_M, s	G_A, kg/s	W_P, kg/s	W_H, kg/s	ε_1 -	ε_3 -	(P_2-P_3), kPa	T.R., kg/kg	G_S, kg/s	L_v, m
72	0.3	1.5	0.35	0.03	0.18	0.1720	0.45	0.81	4.5	63	1.88	0.800
73	0.3	1.5	0.32	0.03	0.18	0.1715	0.45	0.81	4.5	63	1.88	0.700
74	0.3	1.5	0.29	0.03	0.18	0.1705	0.45	0.85	4.2	53	1.58	0.600
75	0.3	1.5	0.28	0.03	0.18	0.1704	0.45	0.84	4.3	52	1.57	0.564
76	0.3	1.5	0.25	0.03	0.18	0.1699	0.45	0.81	4.5	52	1.55	0.500
77	0.3	1.5	0.20	0.03	0.18	0.1688	0.45	0.73	5.2	52	1.55	0.400

more time to fluidize (equation 17) and, in this case, the transition from fluidizing to nonfluidizing flow occurs, with a corresponding increase in solids flows and efficiency. Whether this transition occurs will, of course, depend on the pressure drop and on-time.

Horizontal length is important because it effects the pressure at the transport slot elbow. The dependence is shown in Table 17. The increased pressure effect is evidently more important than the decreased solids flow time, at least for this selection of variables.

Use of the model for other values of the distance between the nozzles and the horizontal ceiling is not recommended until equations 21 and 22 can be corrected for this variable, as discussed at the end of Section 7.1.9. This distance could be altered by nozzle insertion or reduction of vertical slot width. Reduction of this distance will probably yield sharply lower solids flow rates because of the reduction in entrainment area. Confirmation of the effect of other nozzle diameters and spacings would also be useful.

The model suggests that an increase in the angle of tilt of the downcomer from the vertical will yield slightly improved performance at low angles. Part of the improvement will be due to the additional solids horizontal momentum existing upon entering the jet entrainment area. The main effect, however, is in allowing the use of a longer downcomer at equivalent vertical spacing of leg hopper and discharge. Referring back to Figure 18, L_s increases as L_v remains constant. The effect should be negligible at small angles.

It was noted above that gas bubbles tend to rise along the upper face of a sloped downcomer. Intuitively it may be felt that a completely vertical section will offer more resistance to flow, the bulk solids presumably being more resistant than the solids/wall boundary. An intuitive case can also be made for the opposite view. The sloped wall may exert a downward reaction force component on the solids and/or gas bubble. This issue has not been resolved in this study, the model not accounting for such a mechanism, and is left for future study. The widened hopper for ensuring a full downcomer in the CAFB design appears to be a good idea and is recommended.

TABLE 17

EFFECT OF HORIZONTAL LENGTH

Point	t_{ON},	t_{OFF},	t_M,	G_a,	W_P,	W_H,	ε_1	ε_3	(P_2-P_3),	T.R.,	G_S,	L_H,
-	s	s	s	kg/s	kg/s	kg/s	-	-	kPa	kg/kg	kg/s	m
78	0.3	1.5	****	0.03	0.18	0.1732	0.45	0.81	0.7	36	1.08	0.100
79	0.3	1.5	0.34	0.03	0.18	0.1727	0.45	0.81	1.5	43	1.29	0.200
80	0.3	1.5	0.30	0.03	0.18	0.1710	0.45	0.85	3.2	48	1.43	0.400
81	0.3	1.5	0.28	0.03	0.18	0.1704	0.45	0.84	4.3	52	1.57	0.503
82	0.3	1.5	0.26	0.03	0.18	0.1697	0.45	0.82	5.5	57	1.70	0.600
83	0.3	1.5	0.22	0.03	0.18	0.1684	0.45	0.78	8.6	66	1.98	0.800

9.0 ASSESSMENT

A model has been developed that enables projection of the solids flow rates which will result from a given combination of control variables Because the model is largely theoretical, extrapolation to other conditions should be reasonably reliable. The main uncertain effect is that of nozzle insertion (or distance of nozzle from horizontal slot lip). Other candidates for additional confirming research effort would include nozzle diameter and spacing, overall leg dimensions, and particle density, the latter effort needed to confirm the great significance of this variable as suggested by the model.

In the preceding section a discussion of the effects of changes in key parameters was given, based upon use of the transport model. With the current leg design it will be difficult to achieve the required solids flow rate and transport efficiency if the material density is as low as expected. An optimum pulse length of just less than the fluidizing time ($\sim$0.3 s) is very desirable. In the event this is not possible, this limit should be exceeded by as little as possible. An off-time of 1.5 to 2.0 s shoulb be used depending on the on-time. Each leg will then in all likelihood require 0.04 to 0.05 kg/s transport gas. Gas storage capacity between pulse control elements, and the legs should be minimized so the pulse wave form will be as desired. Delivery pressure is important only in that good gas distribution between the nozzles will be needed. The beds should be operated so as to keep their operating pressures as nearly equal as possible. Within process constraints, fluidizing velocities large enough to cause considerable bed expansion will allow longer on-times and easier, more efficient operation of the transport system. Higher density material will transport more easily and efficiently. There may be a trade-off between material activity and regenerability based upon its density. Certainly further study of the particle density effect is warranted.

Great transport efficiency improvement can probably be made by using more leg width (wider legs or more legs) and a proportionate increase in number of injection nozzles. Table 7 illustrates this point. Using three times the leg width and a gas flow (point 2 in the table) of 0.01 kg/s per three nozzles would require 0.03 kg/s of gas to move 4.08 kg/s of solids at a transfer ratio of 136. To achieve this flow with the current design would require at least 0.10 kg/s total air to move 3.66 kg/s at an efficiency of 37. Smaller increases in capacity and efficiency should result from increased leg depth or length in any direction (Tables 15-17).

The vessels will exchange gas at a low rate in response to the pressure drop imposed across each leg full of packed bed solids between pulses. During the pulses, transport gas will partition and flow upward in addition to horizontally, so that little if any reactor gas should be entrained with the transported solids. If, however, the pulses are long enough to fluidize the transport leg vertical solids, there may be a significant backsurge of gas, especially while pulse air remains on. This will be particularly true for gas going from the high-pressure bed to the other. Every effort should be made to reduce the pulse on-time to below the fluidizing time to maintain the transient virtual seal. The use of two solenoid valves in series, with phases staggered by a fraction of a second, to control pulses may be a means to accomplish this.

Agglomeration and/or plugging will most likely occur in the region of stagnant solids at the bottom of the horizontal leg. Use of a narrower section would reduce this potential problem at a cost in transport efficiency. If the dilute phase flow area could be increased, by using more or wider nozzles as suggested by the jet expansion model, or by the use of a long, narrow sparger slot so as to form a plane jet, the dimensions of this stagnant region could be reduced. Continued experimental studies of such alternative geometries is, therefore, encouraged.

It is possible that the nature of this transport mode could exclude materials of small particle size from exchange between vessels. This would result in the buildup of an inactive bed component with time in either bed. Careful monitoring of this possibility, such as by

periodically analyzing samples of cyclone fines, should be performed. A possible solution would be to recycle fines to opposite beds, if possible within overall system constraints and pressure balances.

10. REFERENCES

1. Archer, D. H., D. L. Keairns, J. R. Hamm, R. A. Newby, W.-C. Yang, L. M. Handman, and L. Elikan, Evaluation of the Fluidized Bed Combustion Process, Vols. I, II, and III. Report to EPA, Westinghouse Research and Development Center, Pittsburgh, PA, November 1971, OAP Contract 70-9, NTIS PB 211-494, 212-916, and 213-152.

2. Keairns, D. L., D. H. Archer, R. A. Newby, E. P. O'Neill, E. J. Vidt, Evaluation of the Fluidized-Bed Combustion Process, Vol. IV, Fluidized-Bed Oil Gasification/Desulfurization. Report to EPA, Westinghouse Research and Development Center, Pittsburgh, PA, December 1973, EPA-650/2-73-048d, NTIS PB 233-101.

3. Keairns, D. L., R. A. Newby, E. J. Vidt, E. P. O'Neill, C. H. Peterson, C. C. Sun, C. D. Busaglia, and D. H. Archer, Fluidized Bed Combustion Process Evaluation - Residual Oil Gasification/Desulfurization Demonstration at Atomospheric Pressure. Report to EPA, Westinghouse Research and Development Center, Pittsburgh, PA, March 1975, EPA-650/2-75-027 a&b, NTIS PB 241-834 and PB 241-835.

4. Rakes, S. L., A Synoptic Review of the EPA Chemically Active Fluid Bed Program, EPA, Research Triangle Park, NC, November 1977.

5. Sulfur Oxide Control System for the Chemically Active Fluid-Bed Process, Westinghouse report to EPA. To be issued.

6. O'Neill, E. P., D. L. Keairns, and M. A. Alvin, Sorbent Selection for the CAFB Residual Oil Gasification Demonstration Plant. Report to EPA, Westinghouse Research and Development Center, Pittsburgh, PA, March 1977, EPA-600/7-77-029, NTIS PB 266-827.

7. Engineering Evaluation of the Chemically Active Fluid Bed Process, Westinghouse report to EPA. To be issued.

8. Craig, J. W. T., G. L. Johnes, G. Moss, J. H. Taylor, Study of Chemically Active Fluid Bed Gasifier for Reduction of Sulfur Oxide Emissions. Report to EPA, Esso Research Centre, Abingdon, UK, APCO Contract CPA 70-46, February 1971.

9. Chemically Active Fluid Bed (CAFB) Process Preliminary Process Design Manual, Foster Wheeler Energy Corp., prepared for EPA, Contract No. 68-02-2106.

10. Newby, R. A., S. Katta, and D. L. Keairns, Calcium-Based Sorbent Regeneration for Fluidized-Bed Combustion: Engineering Evaluation. Report to EPA, Westinghouse Research Laboratories, Pittsburgh, PA, March 1978, EPA-600/7-78-039.

11. Bazan, J. A., Chemically Active Fluid Bed (CAFB) Process Solids-Transport Studies. Report to EPA, Foster Wheeler Energy Corporation, Livingston, NJ, EPA-600/7-77-114, October 1977.

12. Wen, C. Y., and H. P. Simons, Flow Characteristics in Horizontal Fluidized Solids Transport, A.I.Ch.E. Jour., 5 (2): 263-267; June 1959.

APPENDIX A.1

SOLIDS TRANSPORT TEST FACILITY PHOTOGRAPHS AND ENGINEERING DRAWINGS

NOTES

1. Photographs include:
   - Overall view
   - Blower/baghouse
   - Control panel
2. The drawings were prepared before the institution of the current requirement for use of Standard International Units. Significant dimensions are given in the proper units in the body of the test.

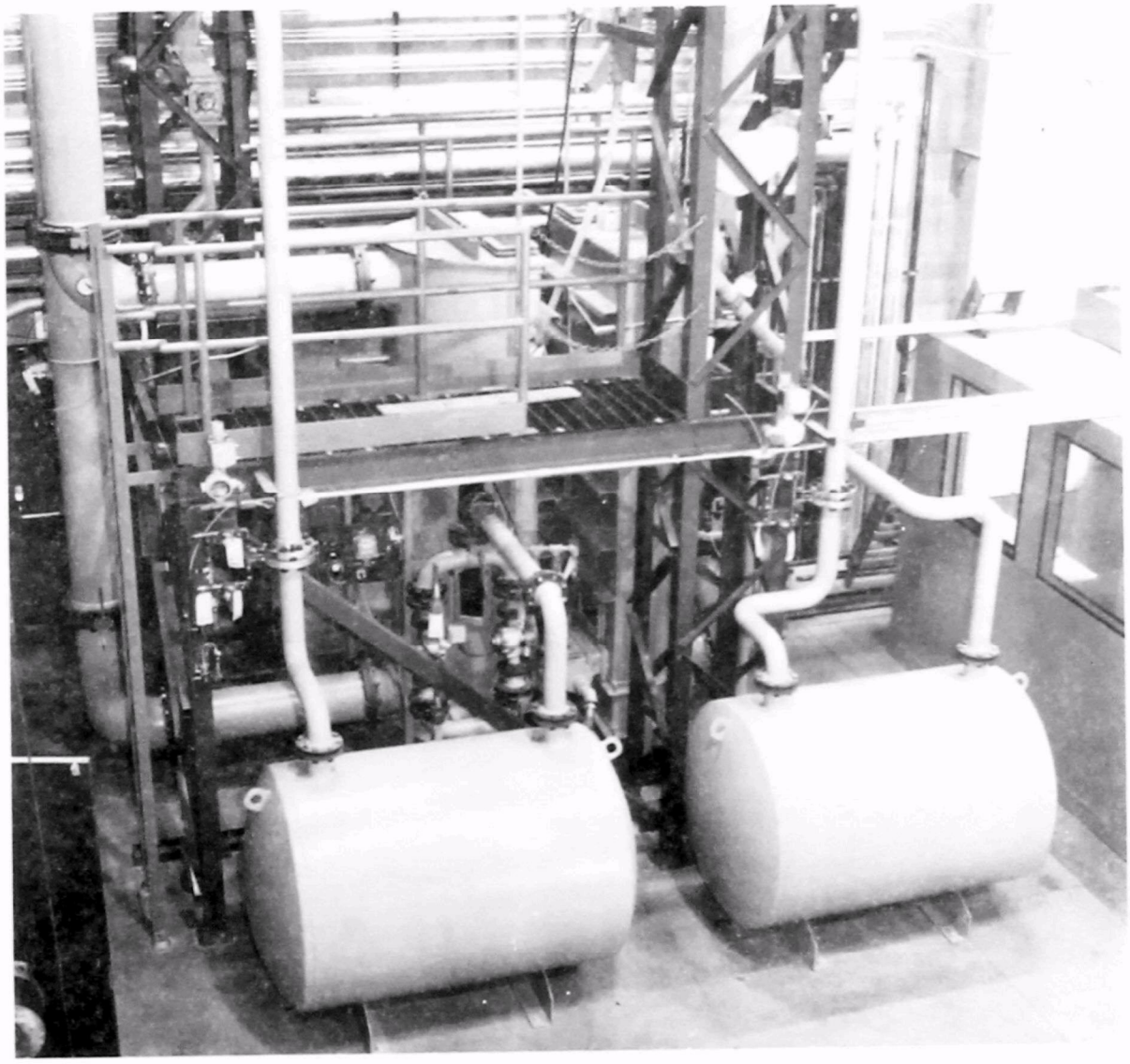

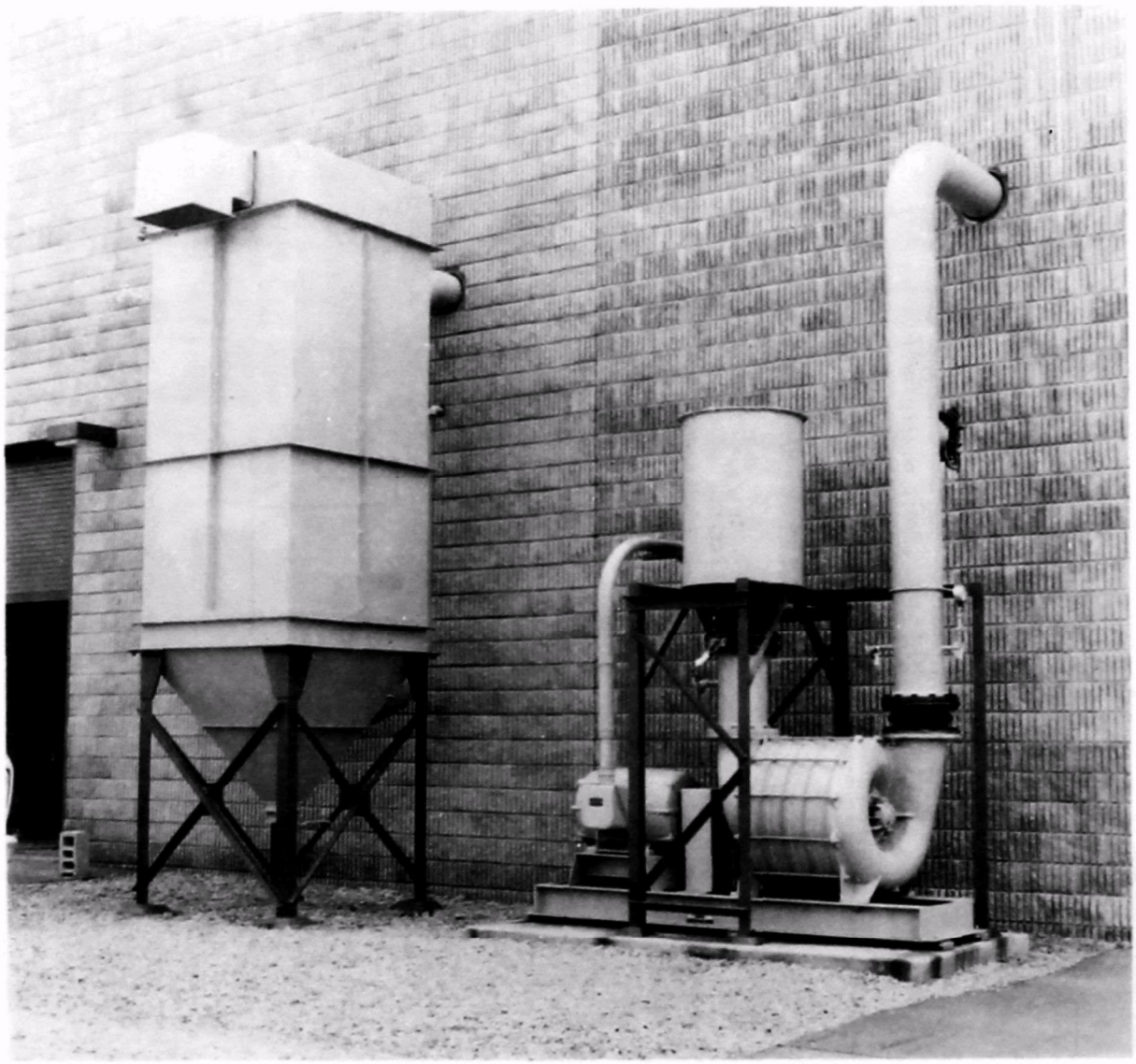

RM-78262

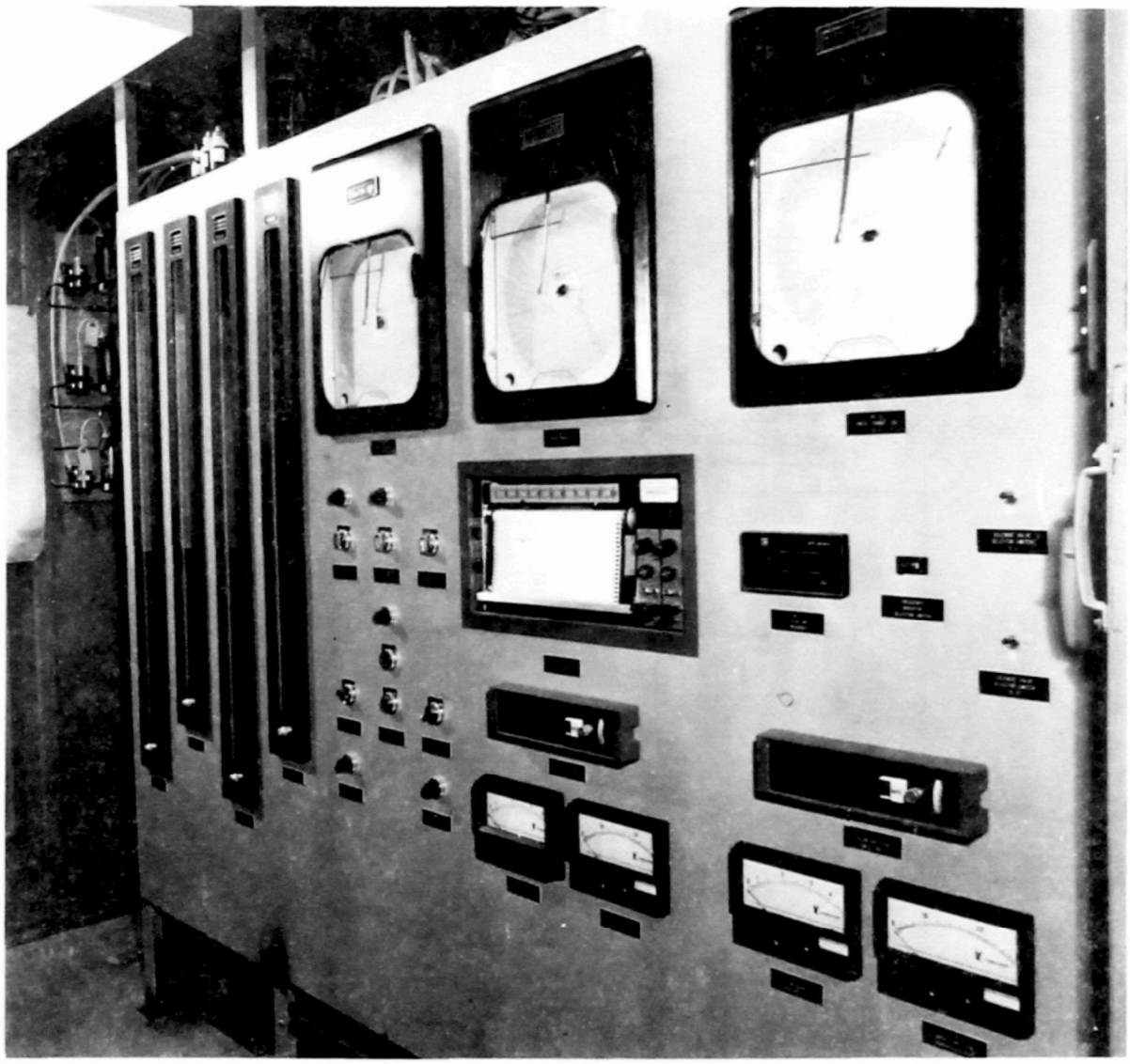

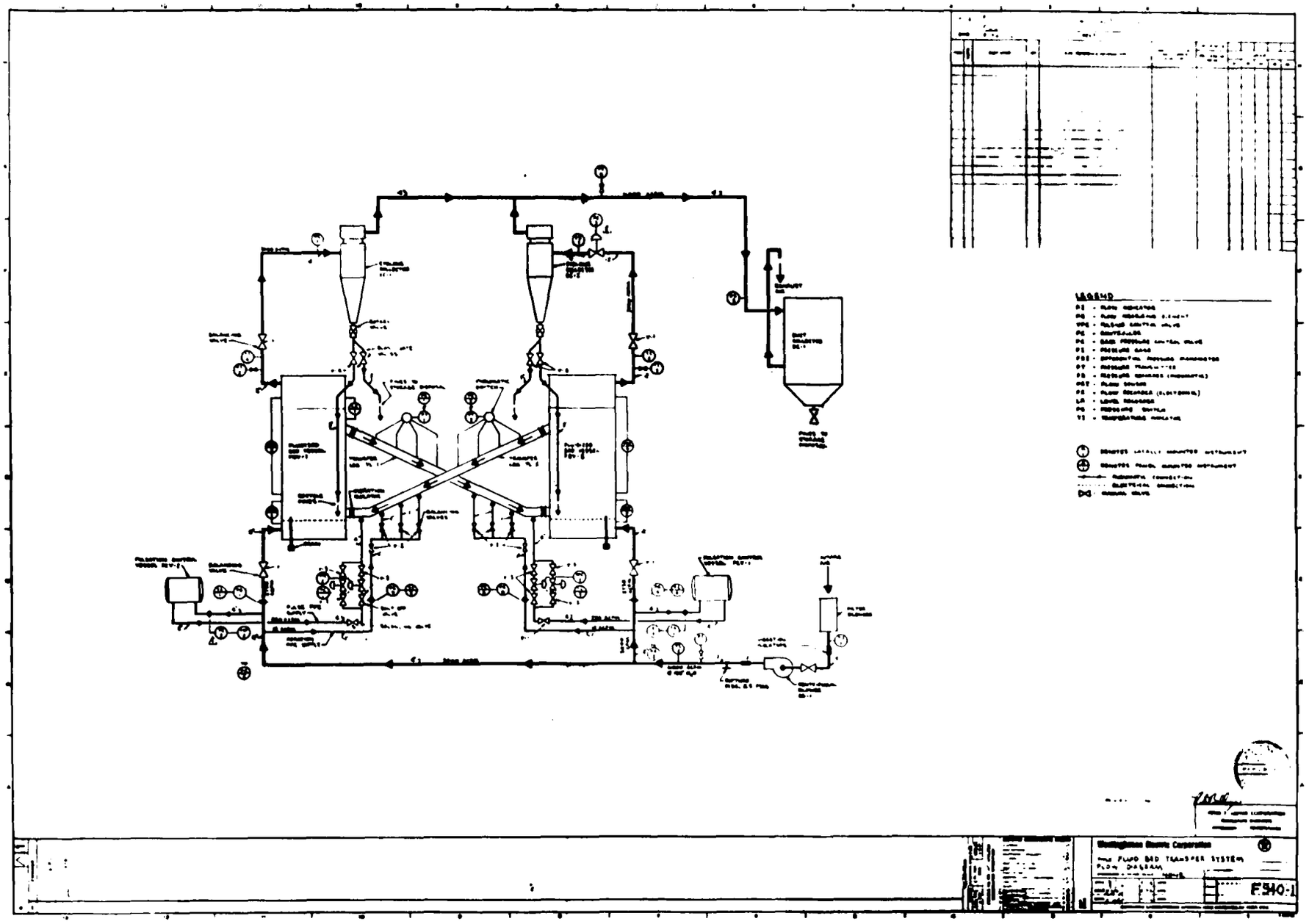
LEGEND
Westinghouse Electric Corporation
F.540-1

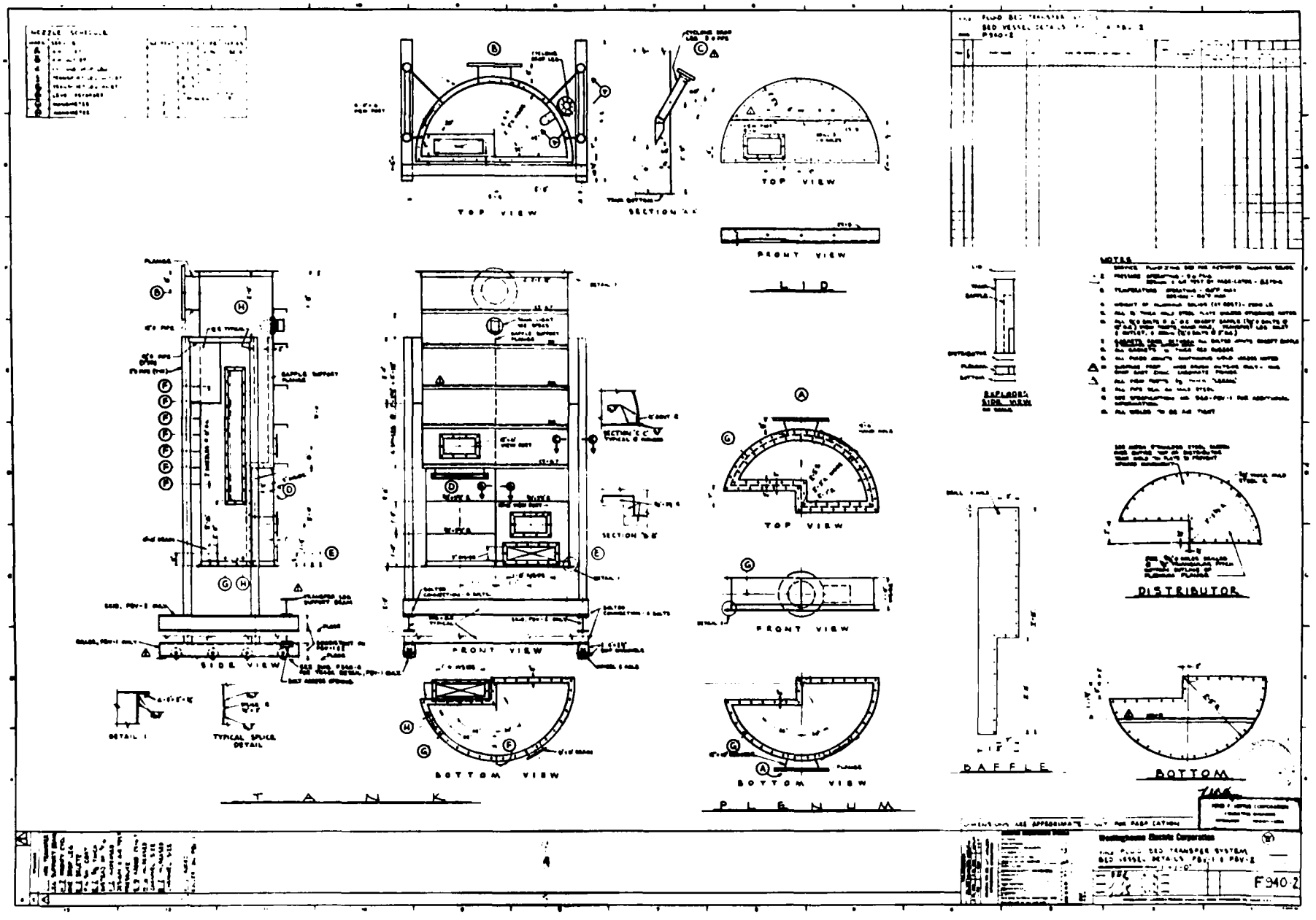
TOP VIEW
SECTION A-A
TOP VIEW
FRONT VIEW
LID
EXPLODED VIEW
SECTION C-C
SECTION D-D
SIDE VIEW
FRONT VIEW
DETAIL 1
TYPICAL SPLICE DETAIL
BOTTOM VIEW
TANK
TOP VIEW
FRONT VIEW
BOTTOM VIEW
PLENUM
BAFFLE
DISTRIBUTOR
BOTTOM
Westinghouse Electric Corporation
F940-2

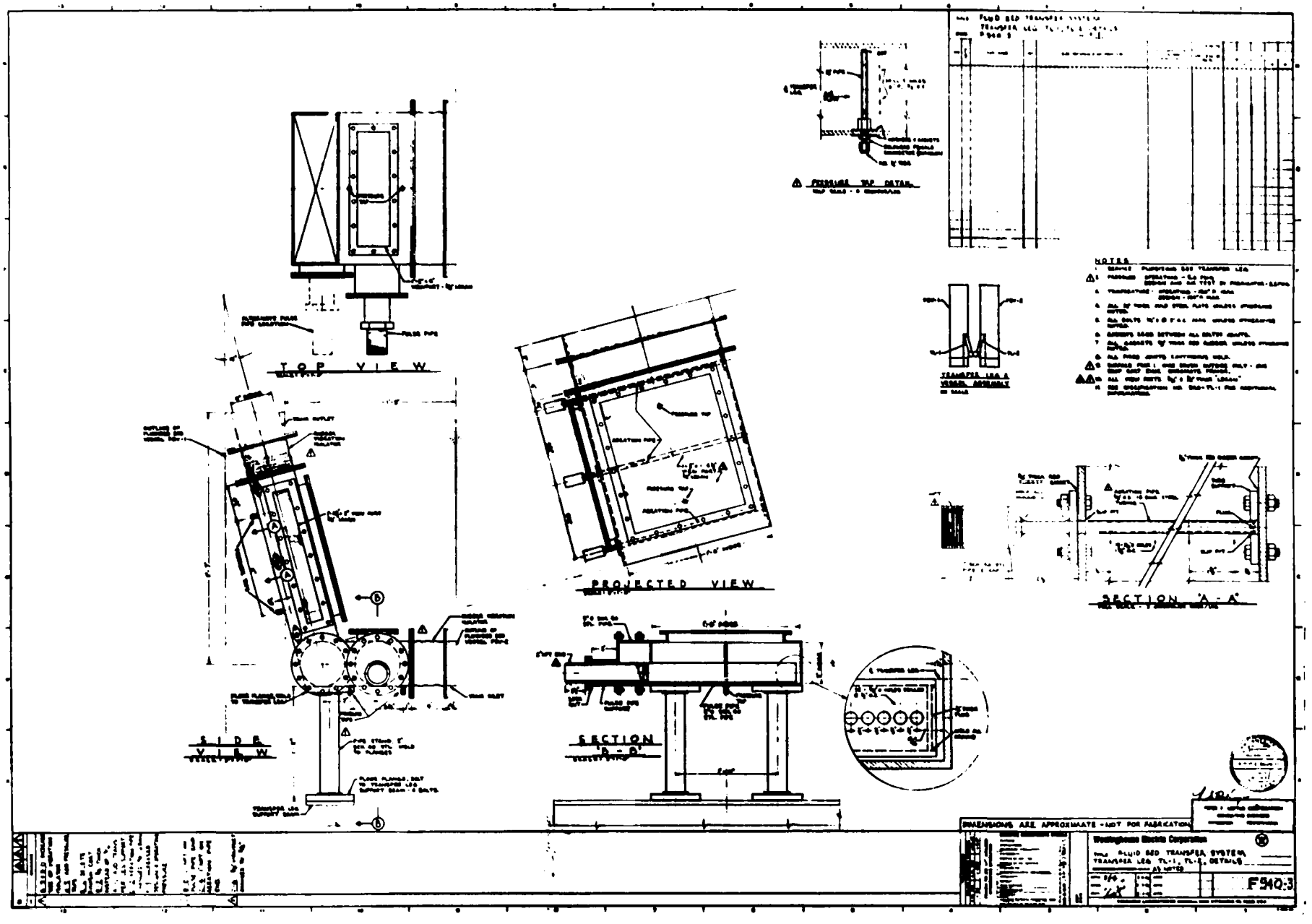
TOP VIEW
SIDE VIEW
PROJECTED VIEW
SECTION B-B'
SECTION A-A'
PRESSURE TAP DETAIL
NOTES
DIMENSIONS ARE APPROXIMATE - NOT FOR FABRICATION
Westinghouse Electric Corporation
FLUID BED TRANSFER SYSTEM
F940-3

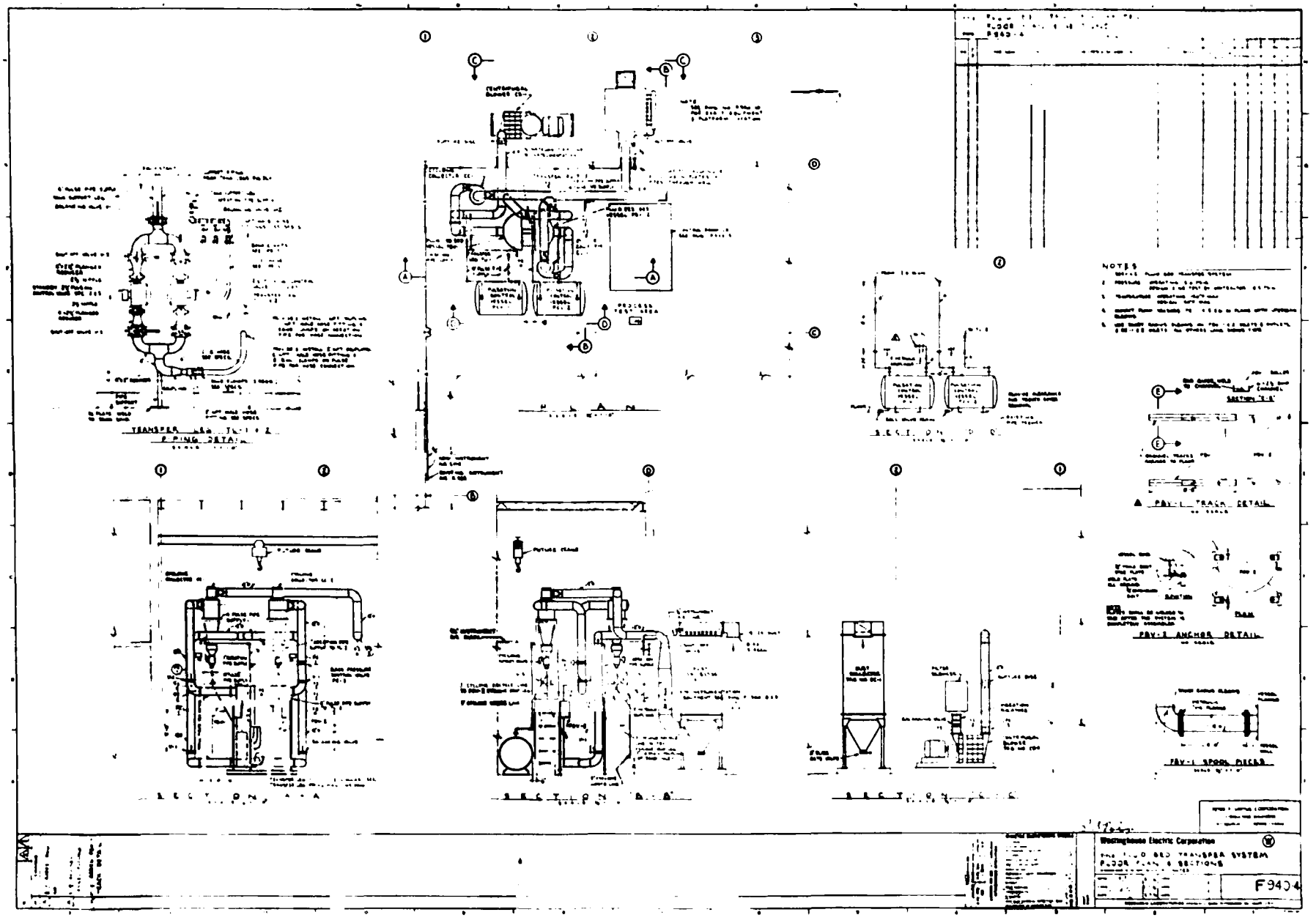
NOTES
PAV-1 TRACK DETAIL
PAV-1 ANCHOR DETAIL
PAV-1 SPOOL PIECES
Westinghouse Electric Corporation
F9404

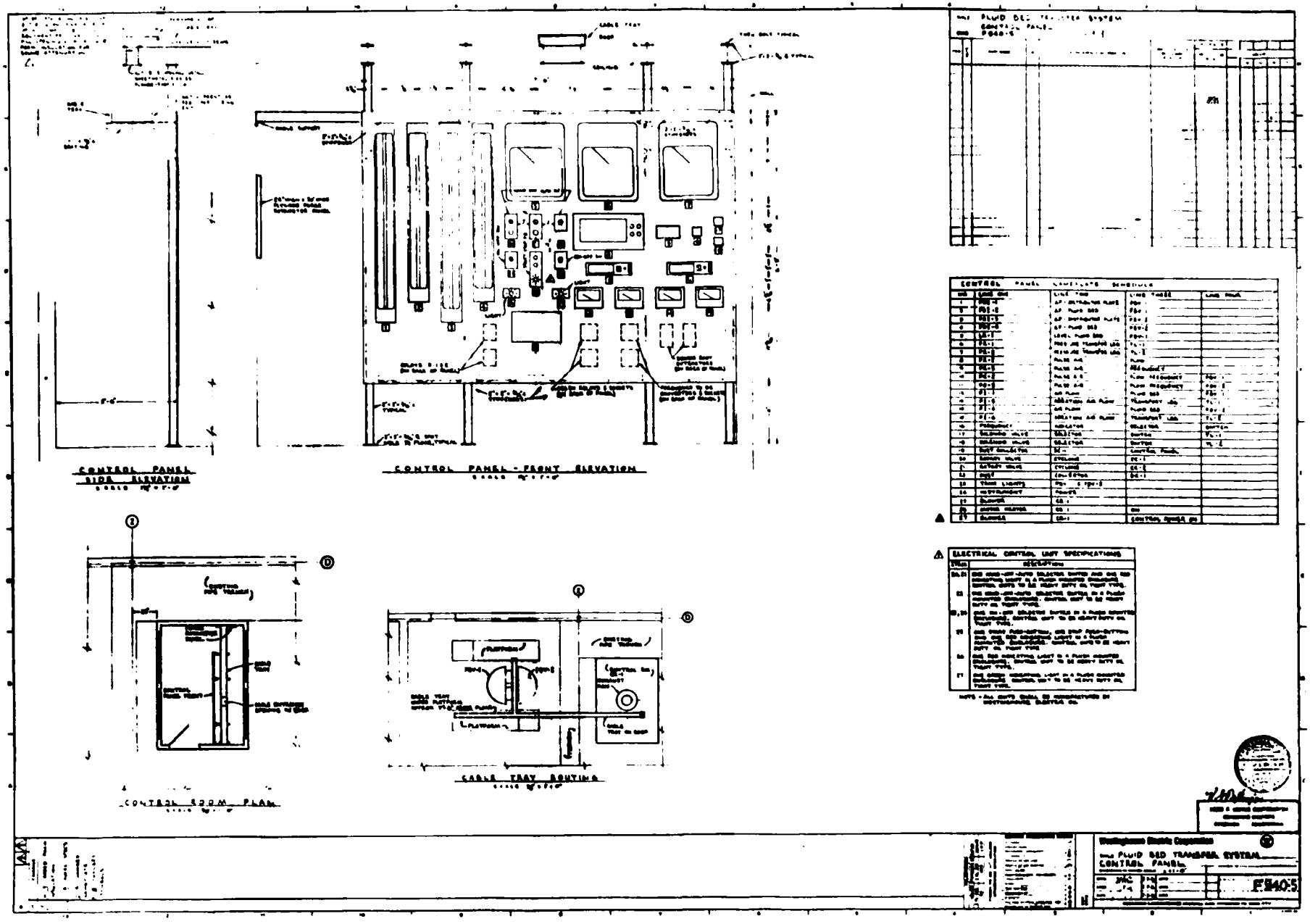
CONTROL PANEL SIDE ELEVATION
CONTROL PANEL - FRONT ELEVATION
CONTROL ROOM PLAN
CABLE TRAY ROUTING
ELECTRICAL CONTROL UNIT SPECIFICATIONS
Westinghouse Electric Corporation
FLUID BED TRANSFER SYSTEM
CONTROL PANEL
FS40-5

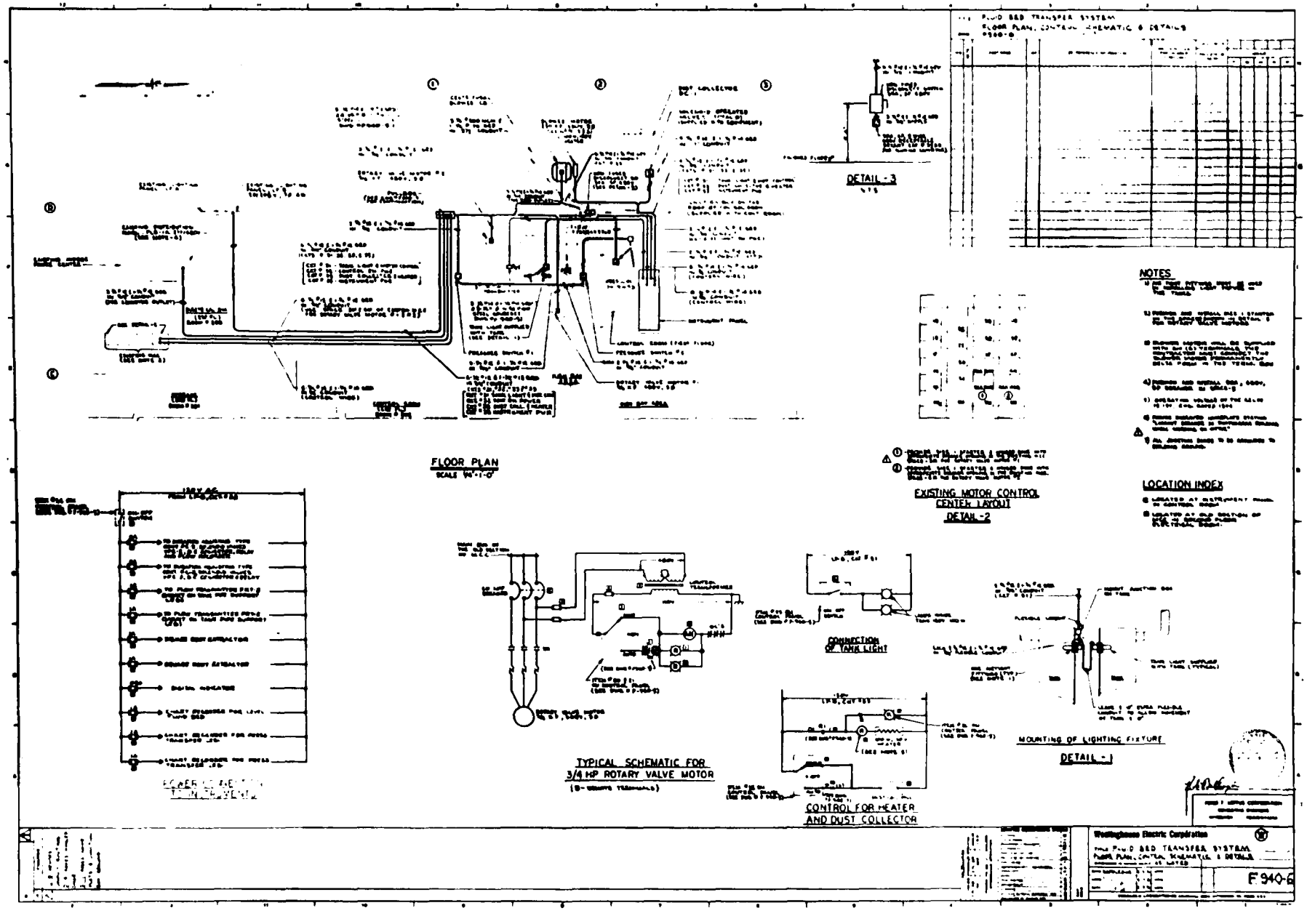
FLOOR PLAN
DETAIL - 3
EXISTING MOTOR CONTROL CENTER LAYOUT
DETAIL - 2
NOTES
LOCATION INDEX
TYPICAL SCHEMATIC FOR 3/4 HP ROTARY VALVE MOTOR
CONNECTION OF TANK LIGHT
MOUNTING OF LIGHTING FIXTURE
DETAIL - 1
CONTROL FOR HEATER AND DUST COLLECTOR
Westinghouse Electric Corporation
F 940-6

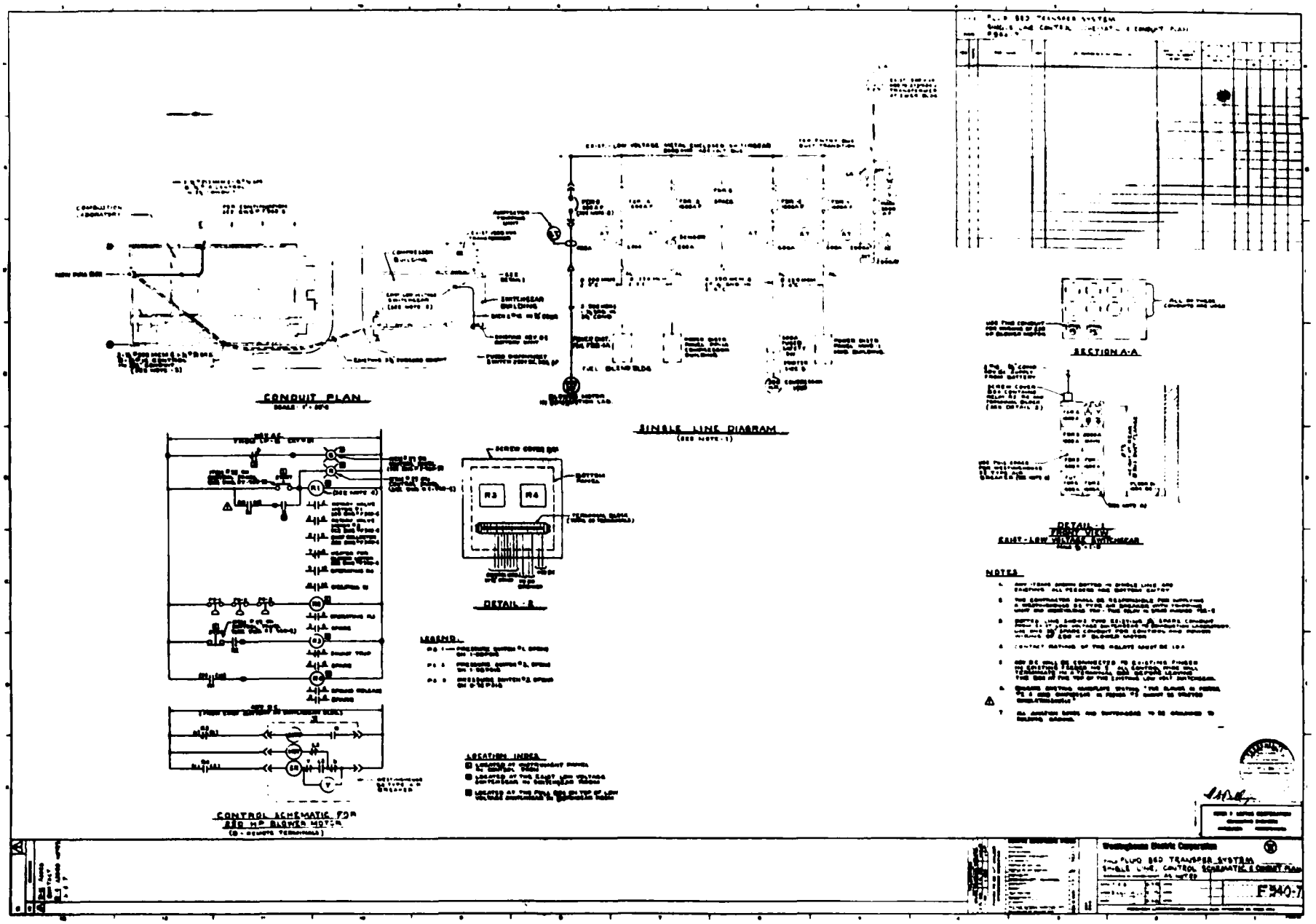
CONDUIT PLAN
SINGLE LINE DIAGRAM
SECTION A-A
DETAIL - A
DETAIL - B
FRONT VIEW
EAST - LOW VOLTAGE SWITCHGEAR
NOTES
LEGEND
LOCATION INDEX
CONTROL SCHEMATIC FOR
FLUID BED TRANSFER SYSTEM
F340-7

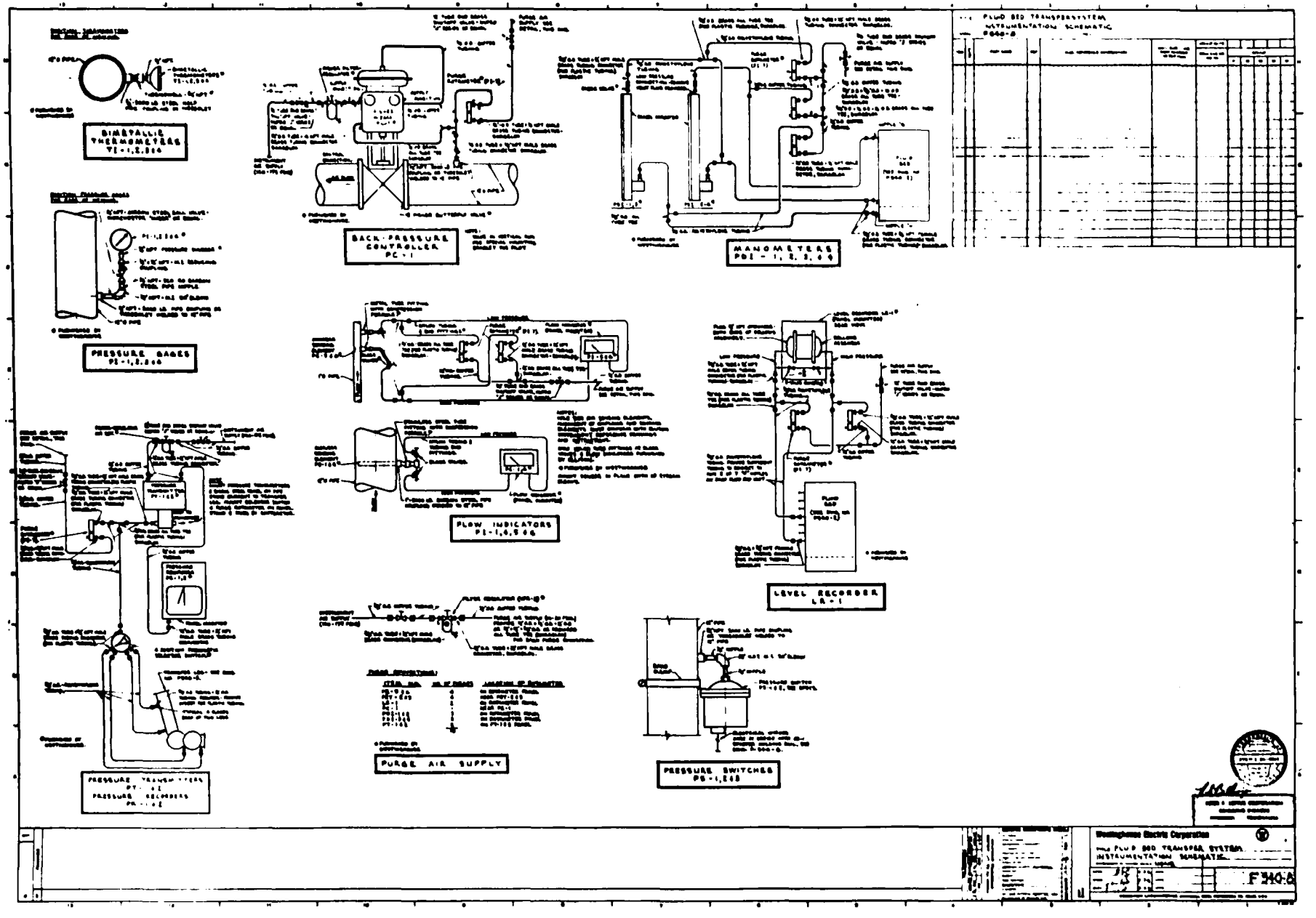
BIMETALLIC THERMOMETERS
BACK-PRESSURE CONTROLLER PC-1
MANOMETERS
PRESSURE GAGES
FLOW INDICATORS
LEVEL RECORDER LR-1
PRESSURE TRANSMITTERS
PRESSURE RECORDERS
PURGE AIR SUPPLY
PRESSURE SWITCHES
Westinghouse Electric Corporation
INSTRUMENTATION SCHEMATIC
F310-6

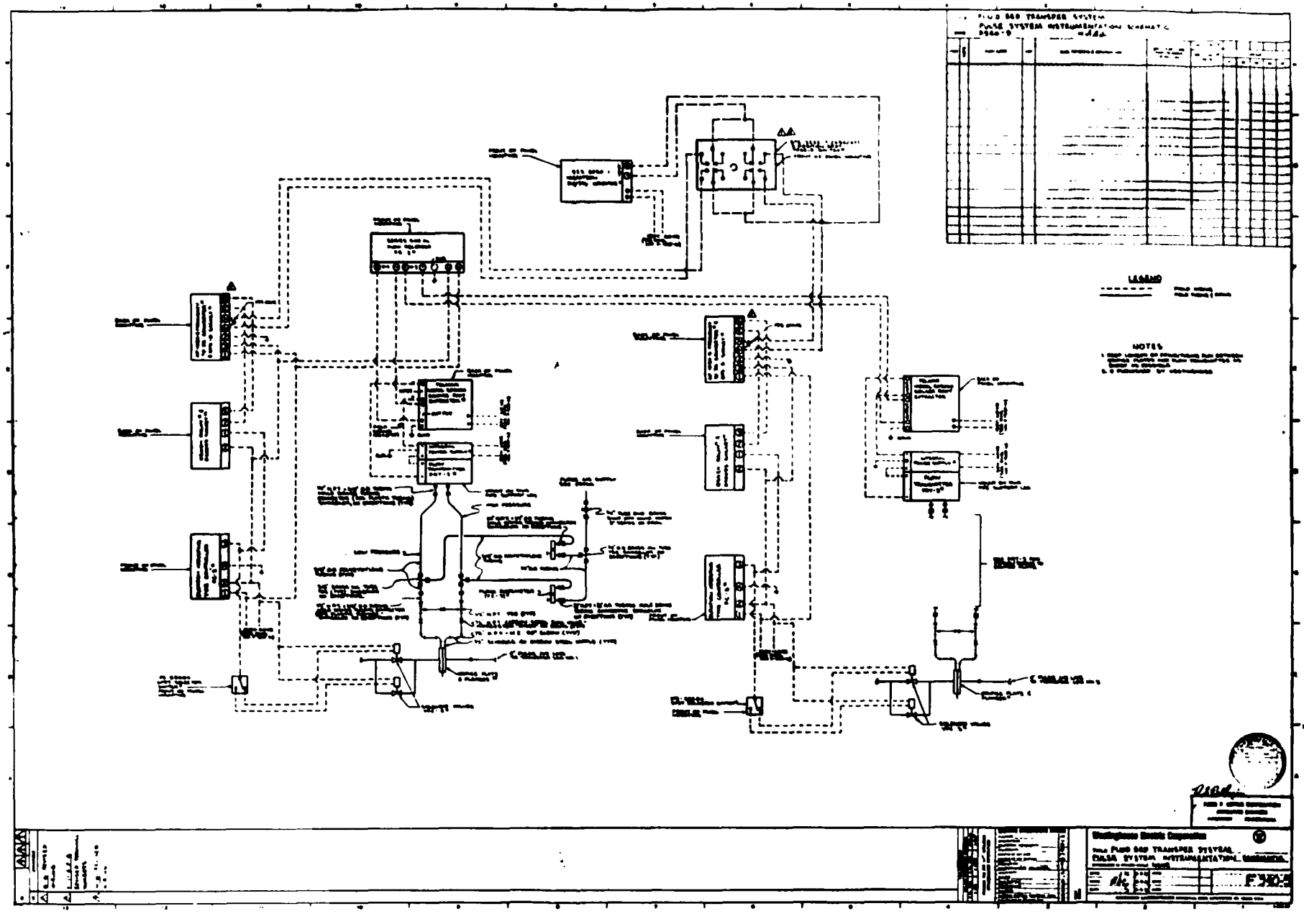
LEGEND
NOTES

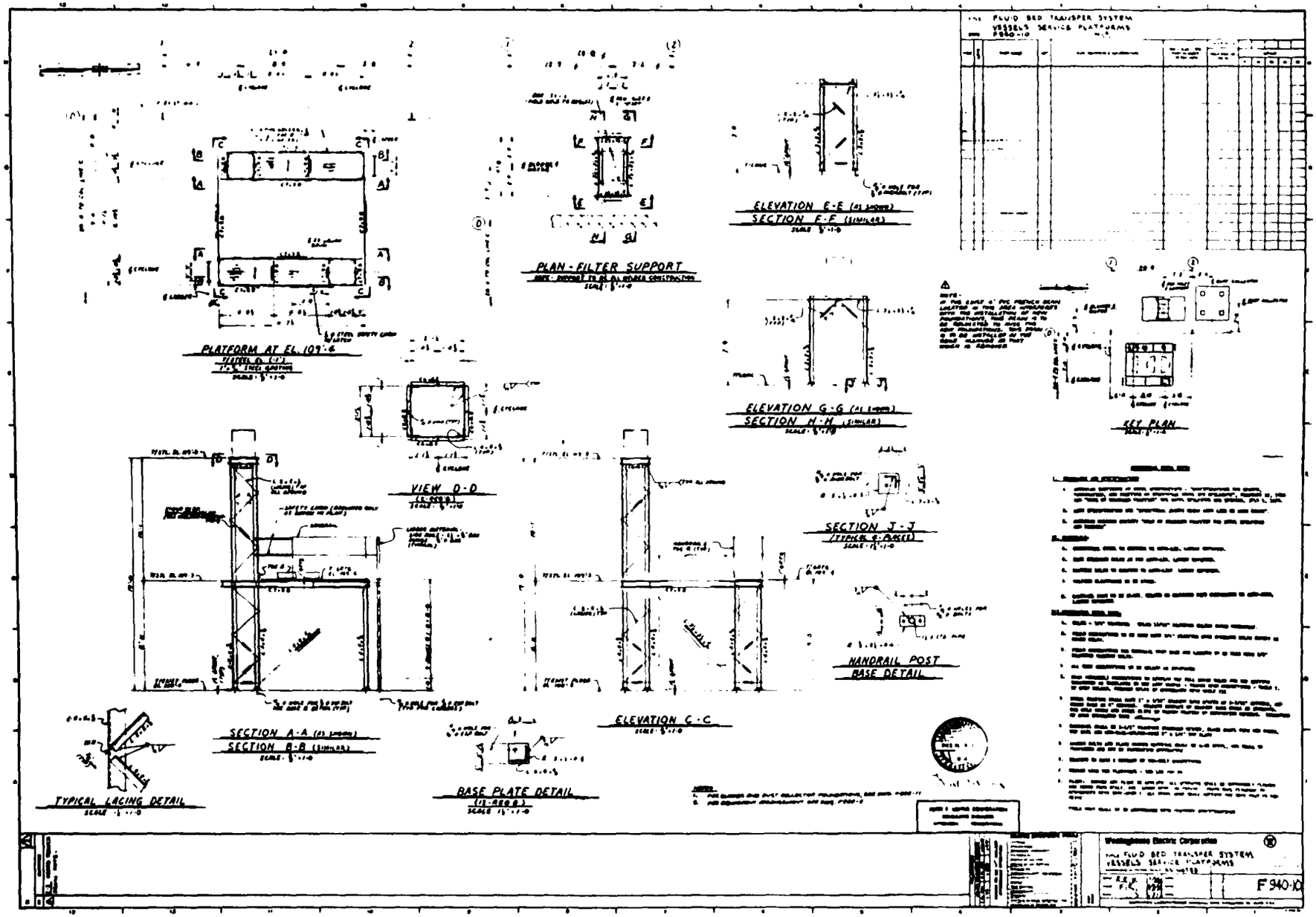
PLATFORM AT EL. 109'-6
PLAN - FILTER SUPPORT
ELEVATION E-E
SECTION F-F
ELEVATION G-G
SECTION H-H
KEY PLAN
VIEW D-D
SECTION J-J
HANDRAIL POST BASE DETAIL
SECTION A-A
SECTION B-B
ELEVATION C-C
TYPICAL LACING DETAIL
BASE PLATE DETAIL
Westinghouse Electric Corporation
F 940-10

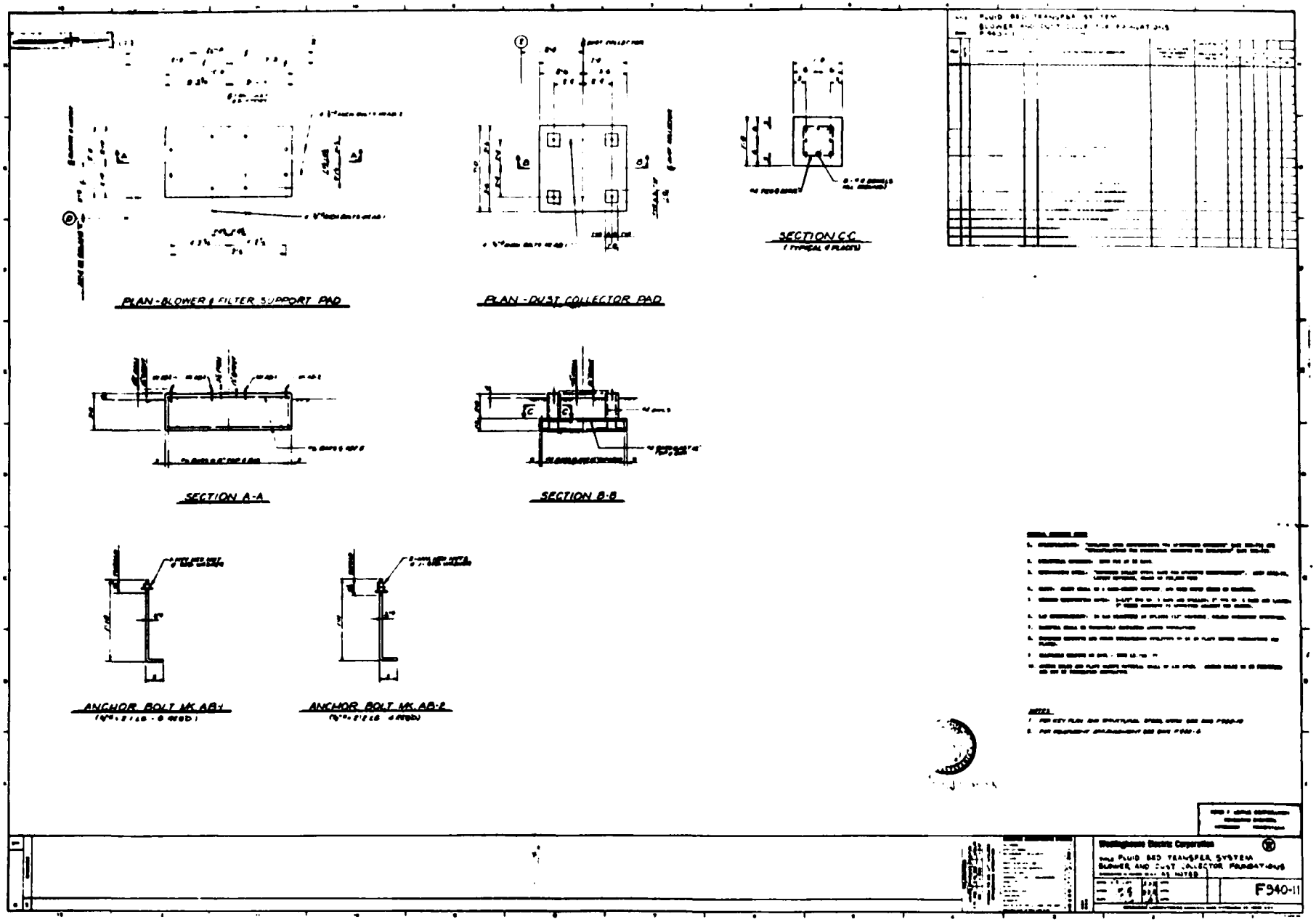
PLAN - BLOWER & FILTER SUPPORT PAD
PLAN - DUST COLLECTOR PAD
SECTION C-C
SECTION A-A
SECTION B-B
ANCHOR BOLT MK AB-1
ANCHOR BOLT MK AB-2
Westinghouse Electric Corporation
FLUID BED TRANSFER SYSTEM
BLOWER AND DUST COLLECTOR FOUNDATIONS
F940-11

APPENDIX A.2

SOLIDS TRANSPORT TEST FACILITY
INSTRUMENT AND AUXILIARY EQUIPMENT SPECIFICATIONS

A.2.1 INSTRUMENTATION

System	Item No.	Description
Air Pulse Controllers	FC-2, 3	(2) - Leeds & Northrup 10676, Series 80 duration adjusting-type controllers. Impulse rate adjustable from 0.5 to 30 pulses/min. Manual station included. Maximum load current: 5 A RMS, 120 V
		Accessories:
		(2) - Leeds & Northrup No. 023868 capacitors to change impulse rate to 1.5 to 90/min.
		(2) - Leeds & Northrup No. 143-82604 SPDT switches to select one of two solenoid coils
Air Pulse Valves	VFC-2, 3	(2) - ASCO No. 8215A93, solenoid operated valves (plus 2 standby valves), size - 6.4 cm
Bimetallic Thermometers	TI-1, 2, 3, 4	(4) - Ashcroft Model 50 E160E, (060) bimetallic thermometers with 13 cm diameter dials
		Accessories:
		(4) - Ashcroft Model T38S75T (060) thermometer wells, 304 SS

System	Item No.	Description
Flow Indicators	FE-1, 4	(2) - Ellison Instrument Type 75, 316 SS, schedule 40 Annubar sensors
	FI-1, 4	(2) - Ellison Instrument Model 77B-12, Eagle Eye flow meters
	FE-5, 6	(2) - Ellison Instrument Type 71, 316 SS Schedule 40 pipe nipple Annubar flow sensors
	FI-5, 6	(2) - Ellison Instrument Model 77B-1 Eagle Eye flow meters
Flow Sensors and Recorders	FRT-2, 3	(2) - ITT Barton Model 752 electronic differential pressure transmitters complete with Model 297 single channel power supply, integrally mounted. Range: 7.5 kPa gauge, adjustable 20 to 100% of calibrated span. Bellows material: SS, complete with molecular bonded strain gauge transducer assembly. Solid state electronics weatherproof unit. Output Signal: 4 to 20 mA dc. Power Requirement: 115 V,ac 60 Hz
		(2) - Telmar Model 509000 square root extractor transmitters. Input: 4-20 mA dc into 100 Ohms Output: 1-5 V dc Accuracy: ± 0.1% to full scale Power Requirement: 115 V,ac, 60 Hz

System	Item No.	Description
Flow Sensors and Recorders (Cont)	FRT-2, 3	Accessories: (2) - Paddle-type orifice plates for 10 cm-schedule 40 pipe. To develop 3.74 kPa differential at flow of 0.118 m^3/s. (Tagged FE-2 and 3) Orifice diameter - 5.71 cm (2) - Paddle-type orifice plates for 10 cm-schedule 40 pipe. To develop 3.74 kPa W. C. differential at flow of 0.59 m^3/s. (Tagged FE-2 and 3) Orifice diameter - 4.13 cm (2) - Pairs-orifice flanges, weld-neck type, for 10 cm-schedule 40 pipe. Flange top locations.
	FR-2	(1) - Leeds & Northrup No. 602-61-61-000-000-3089-3089-6-58-656-291XL extended performance two-pen recorder. Both ranges: AZAR, continuously adjustable-100 mV to 100 V. Span stop response time: 1/3 s Chart speed: selectable in 20 steps from 0.0071 to 0.423 mm/s. Power requirement: 115 V, ac, 60 Hz. (1) - Leeds & Northrup No. 923-2030-1 Numatron digital indicator. Range: ± 3900 mV Accessories: (2) - Action AP-1020-S frequency to dc converters.

System	Item No.	Description
Flow Sensors and Recorders (Cont)		(2) - Leeds & Northrup No. 036211 relays to supply pulse signals to frequency/dc converters.
		(2) - Leeds & Northrup No. P.R.-195-M-0.1-A-0.5 195 Ohm dropping resistors to condition signal to Numatron indicator.
		(2) - Leeds & Northrup Std. 3232-7 (032047) toggle switches to select one of two signals to Numatron indicator.
Level Recorder	LR-1	(1) - ITT Barton Model 202A differential pressure circular chart recorder, single pen-case material: die-cast aluminum. Chart size: 30.5 cm circular. Range: 0-5 kPa Sensing element: Barton Model 199 forged steel with 6900 kPa rating. Chart drive: 240 s Movement power: 120 V,ac 60 Hz.
		Accessories: (1) - Model 254-3A, 3-valve manifold.
Manometers	PDI-1, 3	(2) - Meriam Model 30 EB25 FF 102 cm well-type manometers. Wetted parts: SS Range: 0-10 kPa Indicating fluid: 295 red fluid unity (S. G. 2.95)
	PDI-2, 4	(2) - Meriam Model 30 EB25 FF 90 cm well-type manometers Wetted SS Range: 0-26 kPa Indicating fluid: 295 red fluid (S. G. 2.95)

System	Item No.	Description
Pneumatic Transmitters	PT-1, 2	(2) - ITT Barton Model 273A indicating pneumatic pressure transmitters Input: 0-45 kPa Dial Size: 15 cm Output: 21 to 103 kPa, gauge Accessories: (2) - Fairchild Hiller Model 65332 pressure regulators with drip-well filter and 6.4 cm output gauge. (2) - Honeywell Model No. SP470A1018 four-position manual selector switches.
Pressure Controller	PC-3	(1) - Fisher Controls No. 4162R-7810, 30.5 cm medium pattern butterfly valve, 860 kPa nominal, ASA connections, iron body and disc, 17-4PH shaft and pins, with Fisher 656 size 40 power actuator. (1) - Fisher Controls No. 416ZR Wizard Pilot, yoke mounting. Accessories: (1) - Fisher Controls 67 FR-221 air set.
Pressure Gauges	PI-1	(1) - Ashcroft Model 1009 general service pressure gauges Range: 0-103 kPa
	PI-2, 3	(2) - Ashcroft Model 1188P low-pressure gauges. Range: 0-10 kPa
	PI-4	(1) - Ashcroft Model 1188P low-pressure gauge Range: 0-5 kPa

System	Item No.	Description
Pressure Gauges (Cont)		Accessories: (4) - Ashcroft Model 1/4-112E SS pressure snubbers.
Pressure Recorders	PR-1, 2	(2) - ITT Barton Model 242A pressure recorder receivers Case material: die cast Aluminum with black epoxy. Input signal: 21 to 103 kPa, gauge. Chart range: 0-100 linear, Circular, 30.5 cm diameter Single pen. Chart drive: 24 hr/ revolution and 30 min/ revolution Power requirement: 120 V,ac, 60 Hz.
Purge Air Supply Regulator	VPR-3	(1) - ITT Hammel Dahl Conoflow Model No. FH-60XT-KG1 Airpak filter regulator with integral 5 cm diameter output pressure gauge.
Purge Rotameters	FI-7	(19) - Fischer & Porter Type 10A3135N-53R2110 purge rotameters with differential pressure regulators and integral inlet needle valves.

A.2.2 AUXILIARY EQUIPMENT

Item	Item No.	Description
Control Room	CR-1	Noise Control Products Corp. prefabricated and assembled room with inside dimensions of 2.1 m wide by 3.0 m long by 2 m clear ceiling height. Room provides housing for control panel, purge rotameter manifold assembly, and operating personnel.
Balacning Valve	V-1	Mosser Industries, Inc. (Model AW) manually operated butterfly valve, 1030 kPa line pressure, 172 kPa differential pressure, ductile iron body and blade, TFE-asbestos packing, TFE/glass bearings, SS shaft, and clearance-type seat.
Balancing Valve	V-2	Mosser Industries, Inc. (Model AT) manually operated butterfly valve, 1030 kPa line pressure, 140 kPa differential pressure, cast-iron body, steel blade, steel shaft, and Buna-"N" O-ring seals.
Shutoff Valve	V-3	Center Line Inc., (Series A) - manually operated butterfly valve designed for bubble-tight shutoff at 1030 kPa and 356 K. Valve has a cast-iron body, bronze disc, Buna-"N" O-ring and sleeve, SS stem and disc pin.
Blast Gage Valve	V-4	Mosser Industries, Inc. (Model GT) - Threaded gate valve rated for 140 kPa differential pressure and capable of an uninterrupted flow of solids through the line in the full open position.
Rupture Disc	-	Fike Metal Products Corp. (assembly G) - SS bolted-type and flanged with the capacity to discharge 2.93 m^2/s air at 340 K with a bursting pressure of 59 kPa, gauge.

Item	Item No.	Description
Pressure Switches	PS-1, 2, and 3	Delaval Turbine, Inc., Barksdale Controls Division (Model D1H) - diaphram operated, differential pressure-type to withstand a maximum temperature of 350 K and 69 kPa, gauge, 10 psig maximum pressure on either side of the diaphram. PS-1 and PS-2 will shut down blower (CB-1) when the line pressure reaches 7.45 kPa, gauge. Pressure switch PS-3 will shut down blower (CB-1) when the line pressure reaches 5.0 kPa, gauge.

APPENDIX B

SUPPLEMENTAL DATA

NOTES:

1. These data pertain to the second series of tests (with the rear-wall nozzle sparger).
2. The bed height given is the average settled height of the two beds.
3. Bed pressure drops for runs 1-23 are from a point 7.6 cm above the distributor to the freeboard. Bed pressure drops for subsequent runs were taken from a point level with the leg discharge into that bed to a point level with the leg top leading from that leg (total length 79 cm).
4. Distributor pressure drops include the lower 7.6 cm of fluid bed.
5. Two leg pressures could be recorded at a time. Switch positions in Table B2 are illustrated in Figure B1.

Dwg. 6444A22

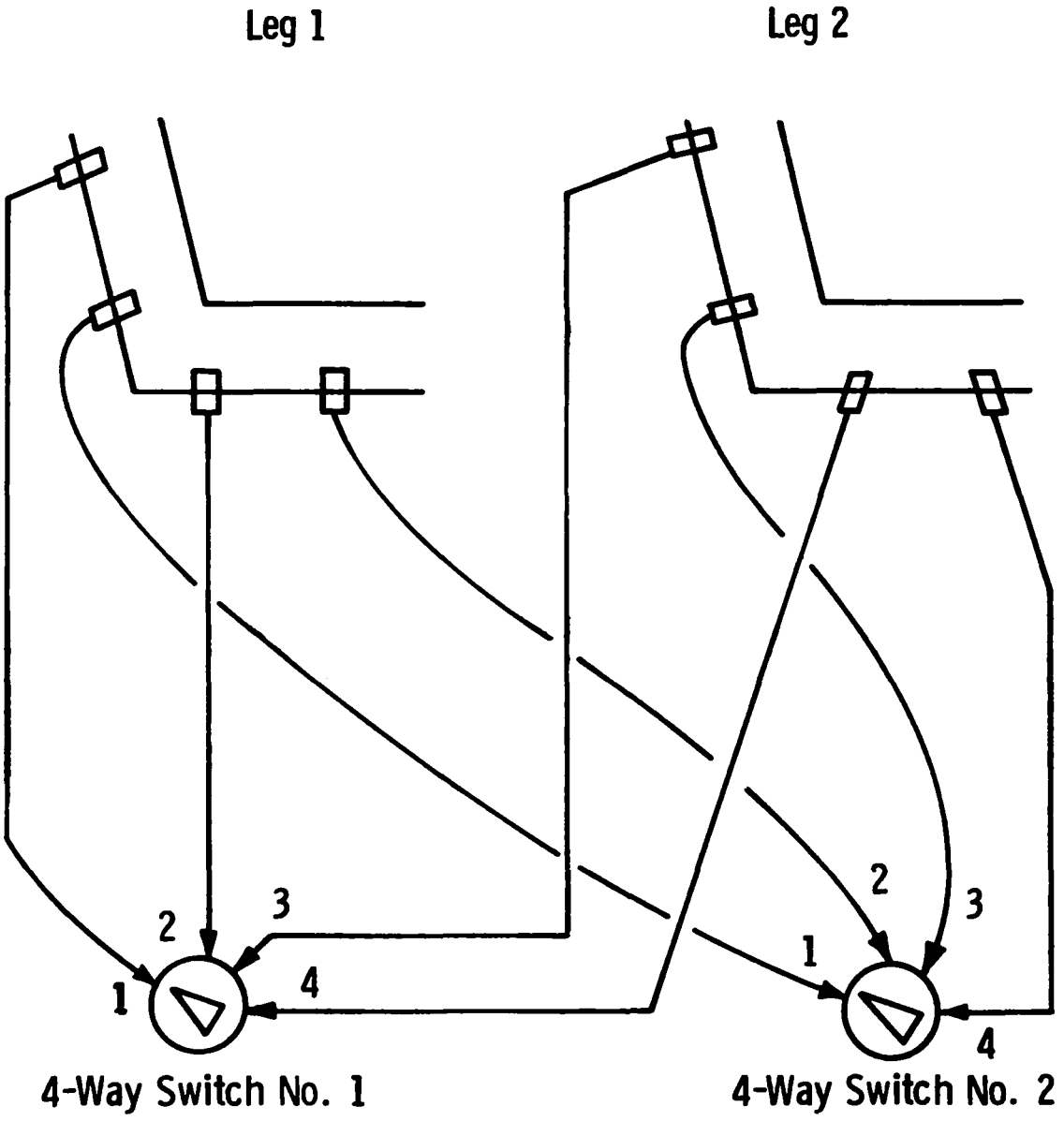

Figure B1. Leg Pressure Recorder Switch Locations

TABLE B1

SUPPLEMENTAL DATA

RUN	BED HEIGHT	FLUIDIZING VELOCITIES BED ONE	TWO	TEMPERATURES BLOWER IN	BLOWER OUT	BEDS
	M	M/S	M/S	K	K	K
1	.81	1.10	1.13	269.	322.	309.
2	.81	1.08	1.08	269.	329.	314.
3	.89	1.01	1.02	274.	336.	316.
4	.88	1.03	1.03	277.	338.	319.
6	.87	1.04	1.04	278.	339.	322.
7	.86	1.04	1.04	279.	339.	323.
8	.85	1.04	1.04	280.	339.	324.
9	.84	1.04	1.04	281.	340.	326.
10	.84	1.04	1.04	281.	341.	327.
11	.83	1.04	1.04	281.	341.	327.
12	.82	1.05	1.05	280.	340.	328.
13	.82	1.05	1.05	280.	340.	328.
14	.81	1.05	1.05	279.	339.	328.
15	.80	1.05	1.05	279.	339.	328.
16	1.26	1.02	1.07	262.	322.	297.
17	1.25	1.06	1.10	262.	322.	306.
18	1.25	1.07	1.11	263.	322.	310.
19	1.24	1.07	1.12	263.	322.	311.
20	1.23	1.08	1.12	263.	322.	312.
21	1.22	1.08	1.12	262.	323.	313.
22	1.21	1.08	1.13	262.	323.	314.
23	1.13	1.07	1.12	262.	330.	317.
29	1.12	.98	1.07	272.	331.	318.
30	1.12	1.03	1.07	272.	332.	318.
31	1.11	1.03	1.07	272.	332.	319.
32	1.11	.99	1.07	271.	331.	319.
33	1.10	1.01	1.05	271.	331.	319.
34	1.10	1.03	1.03	271.	331.	319.
35	1.09	1.03	1.03	271.	331.	319.
36	1.09	.98	1.08	271.	331.	319.
37	1.08	.98	1.08	271.	331.	319.
38	1.08	.98	1.08	271.	331.	319.
39	1.07	.98	1.08	271.	331.	319.
40	1.07	.98	1.02	269.	324.	299.
41	1.06	.99	1.03	269.	326.	303.
42	1.06	1.00	1.04	269.	329.	307.
43	1.06	1.00	1.05	269.	329.	309.
44	1.06	1.01	1.05	270.	330.	312.
45	1.06	1.02	1.06	270.	330.	314.
46	1.06	1.02	1.07	270.	330.	316.
47	1.06	1.02	1.07	270.	330.	316.
48	1.06	1.03	1.07	271.	330.	317.
49	1.06	1.03	1.08	271.	331.	319.
50	1.06	1.04	1.08	271.	331.	321.
51	1.06	1.04	1.09	271.	331.	322.
52	1.05	1.05	1.09	272.	332.	324.
53	1.05	1.04	1.09	272.	332.	323.
54	1.05	1.04	1.08	272.	332.	322.
55	1.05	1.03	1.08	272.	332.	320.
56	1.05	1.03	1.07	276.	333.	319.
57	1.05	1.03	1.07	276.	333.	319.
58	1.05	1.03	1.07	276.	333.	319.

TABLE B1 (Cont)

RUN	BED HEIGHT	FLUIDIZING VELOCITIES BED ONE	TWO	TEMPERATURES BLOWER IN	BLOWER OUT	BEDS
	M	M/S	M/S	K	K	K
59	1.05	1.03	1.07	276.	333.	319.
60	1.05	.99	1.03	272.	331.	305.
61	1.04	1.01	1.05	273.	333.	311.
62	1.04	1.02	1.07	274.	334.	317.
63	1.04	1.02	1.07	274.	334.	317.
64	1.03	1.03	1.07	274.	334.	318.
65	1.03	1.03	1.07	274.	334.	319.
66	1.02	1.03	1.08	274.	334.	321.
67	1.02	1.04	1.08	274.	334.	321.
68	1.02	1.04	1.08	274.	334.	322.
69	1.01	1.04	1.08	274.	336.	322.
70	1.01	1.04	1.08	274.	336.	322.
71	1.01	1.03	1.08	274.	337.	322.
72	1.00	1.03	1.08	277.	337.	322.
73	1.00	1.03	1.08	277.	337.	322.
74	1.00	1.03	1.08	277.	337.	322.
75	.99	1.03	1.08	277.	337.	322.
76	1.09	.92	.93	281.	336.	302.
77	1.08	.94	.94	281.	338.	309.
78	1.07	.96	.96	281.	341.	315.
79	1.06	.96	.96	281.	341.	317.
80	1.05	.97	.97	282.	342.	319.
81	1.04	.97	.98	282.	342.	320.
82	1.03	.97	.98	282.	342.	321.
83	1.02	.98	.98	282.	342.	322.
84	1.01	.98	.98	282.	342.	322.
85	1.00	.98	.98	282.	342.	322.
86	1.08	.97	1.02	286.	343.	314.
87	1.08	.99	1.03	286.	344.	318.
88	1.08	1.00	1.04	287.	344.	321.
89	1.08	1.00	1.04	287.	344.	322.
90	1.07	1.00	1.05	268.	343.	322.
91	1.07	1.00	1.04	288.	342.	320.
92	1.07	.99	1.04	289.	341.	318.
93	1.07	.99	1.04	289.	344.	320.
94	1.07	.99	1.04	290.	347.	322.
95	1.07	1.00	1.04	290.	347.	323.
96	1.07	1.00	1.04	290.	348.	324.
97	1.07	1.00	1.05	290.	346.	325.
98	1.07	1.00	1.05	291.	349.	326.
99	1.07	1.01	1.05	292.	349.	327.
100	1.06	1.01	1.05	292.	349.	327.
101	1.06	1.01	1.06	293.	349.	328.
102	1.06	1.01	1.06	293.	349.	328.
103	1.06	1.01	1.06	293.	349.	329.
104	1.06	1.01	1.06	293.	350.	329.
105	1.06	1.01	1.06	293.	351.	330.
106	1.06	1.01	1.06	293.	351.	330.
107	1.06	1.01	1.06	293.	351.	330.
108	1.06	1.01	1.06	293.	351.	330.
109	1.06	1.01	1.06	293.	351.	330.
110	1.06	1.01	1.06	293.	351.	330.
111	1.05	1.01	1.11	293.	351.	330.
112	1.05	.94	1.03	268.	342.	302.
113	1.05	.96	1.04	288.	344.	308.
114	1.04	.97	1.06	288.	345.	312.
115	1.04	.98	1.07	288.	346.	317.

TABLE B1 (Cont)

RUN	BED HEIGHT	FLUIDIZING VELOCITIES BED ONE	TWO	TEMPERATURES BLOWER IN	BLOWER OUT	BEDS
	M	M/S	M/S	K	K	K
116	1.04	.99	1.08	288.	347.	321.
117	1.03	1.00	1.09	289.	347.	322.
118	1.03	1.00	1.09	289.	347.	323.
119	1.02	1.00	1.09	269.	347.	324.
120	1.02	1.00	1.09	290.	347.	325.
121	1.02	1.00	1.10	290.	348.	326.
122	1.01	1.01	1.10	290.	348.	326.
123	1.01	1.01	1.10	290.	348.	327.
124	1.00	1.01	1.10	291.	348.	327.
125	1.00	1.01	1.10	291.	348.	327.
126	1.00	1.01	1.10	291.	348.	327.
127	.99	1.01	1.10	291.	348.	327.
128	.99	.95	1.03	283.	329.	299.
129	.99	.96	1.05	283.	333.	304.
130	.99	.97	1.06	283.	336.	309.
131	.99	.98	1.07	283.	339.	314.
132	.99	.99	1.08	284.	342.	318.
133	.99	.99	1.08	284.	342.	319.
134	.99	1.00	1.09	283.	342.	321.
135	.99	1.00	1.09	283.	342.	322.
136	.99	1.00	1.09	283.	342.	322.
137	.99	1.00	1.09	283.	342.	322.
138	.99	1.00	1.09	283.	342.	322.
139	1.00	1.00	1.05	288.	346.	311.
140	1.00	1.01	1.06	288.	346.	314.
141	1.00	1.02	1.06	288.	346.	317.
142	1.00	1.03	1.07	289.	346.	320.
143	1.00	1.04	1.08	289.	347.	323.
144	1.00	1.04	1.09	289.	347.	323.
145	1.00	1.04	1.09	289.	347.	324.
146	1.00	1.05	1.09	289.	347.	325.
147	1.00	1.05	1.09	269.	347.	326.
148	1.00	1.05	1.09	289.	347.	326.
149	1.00	1.05	1.09	289.	348.	327.
150	1.00	1.05	1.09	289.	348.	327.
151	1.00	1.05	1.05	290.	348.	327.
152	.99	1.05	1.05	290.	348.	327.
153	.99	1.05	1.05	290.	348.	328.
154	.99	1.05	1.05	290.	348.	328.
155	.99	1.05	1.05	291.	348.	328.
156	.99	1.05	1.05	291.	346.	328.
157	.99	1.06	1.06	292.	348.	329.
158	.99	1.06	1.06	292.	346.	329.
159	.99	1.06	1.06	292.	349.	329.
160	.99	1.06	1.06	292.	349.	329.
161	.99	1.06	1.06	292.	349.	329.
162	.99	1.06	1.06	292.	349.	329.
163	.99	1.06	1.06	292.	349.	329.
164	.99	1.06	1.06	292.	349.	329.
165	.99	1.06	1.06	292.	349.	329.
167	.98	1.06	1.06	291.	349.	330.
166	.98	1.06	1.06	291.	349.	330.
170	.98	1.06	1.06	291.	349.	330.
171	.98	1.06	1.06	291.	349.	330.
172	.98	1.06	1.06	291.	349.	330.
173	.98	1.06	1.06	291.	349.	330.

TABLE B1 (Cont)

RUN	BED HEIGHT	FLUIDIZING VELOCITIES BED ONE	TWO	TEMPERATURES BLOWER IN	BLOWER OUT	BEDS
	M	M/S	M/S	K	K	K
174	.98	1.06	1.06	291.	349.	330.
175	.98	.95	.99	276.	318.	293.
176	.98	.95	.99	276.	320.	296.
177	.97	.96	1.00	276.	322.	298.
178	.97	.96	1.00	276.	324.	301.
179	.97	.96	1.01	276.	327.	303.
180	.97	.97	1.01	276.	329.	305.
181	.97	.97	1.02	276.	331.	307.
182	.97	.98	1.02	276.	333.	309.
183	.97	.98	1.02	276.	336.	312.
184	.96	.98	1.03	276.	336.	313.
185	.96	.99	1.03	277.	336.	315.
186	.96	.99	1.04	277.	336.	317.
187	.96	1.00	1.05	277.	335.	318.
188	.96	1.00	1.05	277.	335.	319.
189	.96	1.00	1.05	277.	335.	319.
190	.95	1.01	1.05	277.	334.	320.
191	.95	1.01	1.05	278.	334.	320.
192	.95	1.01	1.05	278.	334.	320.
193	.95	1.01	1.05	278.	334.	320.
194	.95	1.01	1.06	278.	334.	321.
195	.94	1.01	1.06	278.	334.	321.
196	.94	1.01	1.06	278.	333.	321.
197	.94	1.01	1.06	278.	333.	321.
198	.94	1.01	1.06	278.	333.	322.
199	.94	1.02	1.06	278.	333.	322.
200	.94	1.02	1.06	278.	333.	322.
201	.93	1.02	1.06	278.	333.	322.
202	.93	1.02	1.06	278.	333.	322.
203	.93	1.02	1.06	278.	333.	322.
204	.93	1.02	1.06	278.	333.	322.
205	.93	1.02	1.06	278.	333.	322.
206	.93	1.02	1.06	278.	333.	322.
207	1.02	.32	.36	278.	336.	303.
208	1.01	.32	.36	278.	338.	306.
209	1.01	.75	.83	279.	341.	308.
210	1.01	.76	.84	279.	341.	311.
211	1.01	.50	.59	280.	341.	314.
212	1.01	.51	.59	280.	342.	315.
213	1.01	.51	.59	281.	342.	316.
214	1.01	.51	.59	281.	342.	317.
215	1.01	.51	.60	281.	343.	318.
216	1.01	.51	.60	281.	343.	319.
217	1.01	.51	.60	282.	343.	321.
218	1.01	.51	.60	282.	343.	321.
219	1.00	.51	.60	282.	344.	322.
220	1.00	.51	.60	283.	344.	322.
221	1.00	.51	.60	284.	344.	323.
222	1.00	.52	.60	286.	344.	323.

TABLE B1 (Cont)

RUN	BED HEIGHT	FLUIDIZING VELOCITIES BED ONE	TWO	TEMPERATURES BLOWER IN	BLOWER OUT	BEDS
	M	M/S	M/S	K	K	K
223	1.00	.52	.60	288.	344.	323.
224	1.00	.52	.60	287.	344.	323.
225	1.00	.52	.60	286.	345.	324.
226	1.00	.52	.60	284.	345.	324.
227	1.00	.52	.60	284.	346.	324.
228	1.00	.52	.60	284.	346.	324.
229	1.00	.52	.60	284.	346.	324.
230	.99	.52	.60	284.	346.	324.
231	.99	.52	.60	284.	346.	324.
232	.99	.52	.60	284.	346.	324.
233	.99	.52	.60	284.	346.	324.
234	.99	.52	.60	284.	346.	324.
235	.99	.52	.60	284.	346.	324.
236	.99	.52	.60	284.	346.	324.
237	.99	.52	.60	284.	346.	324.
238	.99	.52	.60	284.	346.	324.
239	.99	.52	.60	284.	346.	324.
240	.99	.52	.60	284.	346.	324.
241	1.02	.32	.40	284.	342.	306.
242	1.02	.33	.41	285.	344.	309.
243	1.02	.33	.41	285.	346.	311.
244	1.02	.33	.41	286.	347.	314.
245	1.02	.33	.42	286.	348.	317.
246	1.02	.33	.42	286.	348.	318.
247	1.01	.33	.42	286.	348.	319.
248	1.01	.34	.42	286.	348.	321.
249	1.01	.34	.42	287.	349.	322.
250	1.01	.34	.42	287.	349.	322.
251	1.01	.34	.42	287.	349.	322.
252	1.01	.34	.42	287.	349.	323.
253	1.01	.34	.42	287.	349.	323.
254	1.01	.34	.42	287.	349.	323.
255	1.01	.34	.42	287.	349.	324.
256	1.01	.34	.42	287.	349.	324.
257	1.01	.34	.42	287.	349.	324.
258	1.01	.34	.42	287.	349.	324.
259	1.01	.34	.42	287.	349.	324.
260	1.01	.34	.42	287.	349.	324.
261	1.01	.34	.42	287.	349.	324.
262	1.01	.34	.42	287.	349.	324.
263	1.01	.34	.42	287.	349.	324.
264	1.01	.34	.42	287.	349.	324.
265	1.01	.34	.42	287.	349.	324.
266	1.01	.34	.42	287.	349.	324.
267	1.01	.34	.42	287.	349.	324.
268	1.01	.34	.42	287.	349.	324.
269	1.01	.34	.42	287.	349.	324.
270	1.01	.34	.42	287.	349.	324.
271	1.01	.34	.42	287.	349.	324.
272	1.01	.34	.42	287.	349.	324.

TABLE B2

SUPPLEMENTAL DATA

ALL UNITS KILOPASCALS EXCEPT SWITCH POSITIONS

RUN	GAUGE PRESSURES			PRESSURE DROPS				LEG PRESSURES-GAUGE			
	BLOWER	BED ONE	BED TWO	BED ONE	BED TWO	DIST ONE	DIST TWO	SWITCH POS	1 P	SWITCH POS	2 P
1	49.	1.7	1.6	7.8	7.8	4.3	3.7				
2	49.	3.2	3.1	6.4	8.5	4.6	3.5				
3	42.	2.0	1.7	9.0	7.2	4.3	2.9	1	6.7	2	9.0
4	42.	1.7	1.7	7.2	8.7	4.2	2.9	3	6.3	3	9.9
6	43.	1.7	1.7	6.6	9.2	4.0	2.9	4	8.1	4	4.9
7	42.	1.7	1.7	8.8	7.1	4.0	3.3			2	9.9
8	42.	1.7	1.6	6.6	9.2	4.0	3.1	3	8.5	4	8.5
9	41.	1.7	1.7	9.2	6.6	3.8	3.3	1	5.4	2	8.5
10	41.	1.7	1.7	6.9	9.4	4.4	3.3	1	5.4	2	6.7
11	41.	1.7	1.7	9.0	6.9	4.0	3.2	1	5.8	2	8.5
12	42.	1.7	1.7	6.4	9.2	4.4	2.9	3	8.5	4	8.5
13	42.	1.7	1.7	8.7	7.2	4.3	3.2	1	6.3	2	8.5
14	42.	1.9	1.7	5.8	9.5	4.3	2.9				
15	42.	1.9	1.7	8.7	7.1	4.2	2.9	1	6.3	2	8.5
16	44.	1.9	1.7	13.6	11.6	3.8	3.3				
17	44.	1.9	1.7	10.4	13.9	4.2	2.7	3	13.0	4	12.1
18	44.	2.0	2.0	13.9	10.1	3.8	2.9	1	7.6	2	12.1
19	44.	2.0	2.0	10.7	13.6	4.3	3.1	3	13.4	4	12.5
20	44.	2.0	2.0	13.9	11.0	4.0	3.3				
21	44.	2.0	2.0	10.7	13.9	4.0	2.8	3	6.7	4	9.9
22	44.	2.0	2.0	14.2	10.4	3.9	3.5				
23	41.	2.0	2.0	10.4	13.6	4.2	2.9				
29	41.	1.9	1.7	7.8	7.9	4.0	3.3	3	9.4	4	11.2
30	41.	2.0	1.9	7.7	8.2	4.1	3.4	3	8.5	4	11.2
31	41.	2.0	1.9	7.5	8.1	3.9	3.3	1	8.5	2	11.2
32	41.	1.9	2.0	7.7	7.8	3.7	3.5	1	8.5	2	10.8
33	41.	1.9	2.0	7.9	8.1	4.0	3.3	3	9.0	4	10.3
34	41.	1.9	2.0	7.7	8.2	3.5	2.9	3	8.5	4	11.2
35	41.	1.9	2.0					1	8.5	2	10.8
36	41.	2.0	1.9	7.7	7.8	3.7	3.7	1	8.5	2	10.8
37	41.	2.0	1.9					3	9.0	4	11.2
38	41.	2.0	1.9					3	9.4	4	11.2
39	41.	2.0	1.9					1	9.0	2	10.8

TABLE B2 (Cont)

RUN	GAUGE PRESSURES			PRESSURE DROPS				LEG PRESSURES-GAUGE			
	BLOWER	BED ONE	BED TWO	BED ONE	BED TWO	DIST ONE	DIST TWO	SWITCH POS	1 P	SWITCH POS	2 P
40	41.	1.9	1.7	7.9	8.1	3.8	3.3	1	8.5	2	11.2
41	41.	1.9	1.9	8.1	8.4	4.8	3.5	3	9.0	4	10.8
42	41.	1.9	1.7	7.9	8.1	4.0	3.4	3	8.5	4	11.2
43	41.	1.9	1.7	8.1	7.9	4.0	3.7	1	9.0	2	11.2
44	41.	1.9	1.9	8.1	8.1	3.7	3.0	1	9.0	2	11.2
45	41.	1.9	1.9					3	8.5	4	11.2
46	41.	1.9	1.9	7.9	8.1	4.0	3.5	3	9.0	4	10.8
47	41.	1.9	1.9					1	9.4	2	11.2
48	41.	1.9	1.9	7.9	7.9	4.0	3.3	1	8.5	2	10.8
49	41.	1.9	1.9					3	9.0	4	11.2
50	41.	1.9	1.9					3	8.5	4	11.2
51	41.	1.9	1.9					1	9.0	2	11.2
52	41.	1.9	1.9	8.1	8.1	3.8	3.3	1	9.0	2	10.8
53	41.	1.9	1.9					3	9.0	4	11.2
54	41.	1.9	1.9					3	9.0	4	11.2
55	41.	1.9	1.9					1	9.0	2	11.2
56	41.	1.9	1.9	7.7	7.8	4.1	2.9	1	8.5	2	11.2
57	41.	1.9	1.9					3	8.5	4	11.2
58	41.	1.9	1.9					3	9.4	4	11.2
59	41.	1.9	1.9					1	9.0	2	10.8
60	42.	1.7	1.7	8.2	7.7	3.7	3.3	1	8.5	2	10.8
61	42.	1.7	1.7	7.5	8.2	4.0	2.9	3	8.5	4	10.8
62	42.	1.7	1.9	7.8	7.9	4.2	3.2	3	8.5	4	10.8
63	42.	1.7	1.9	7.8	7.9	4.0	3.3	1	9.0	2	10.8
64	42.	1.7	1.9	7.9	8.1	4.0	3.3	1	8.5	2	10.8
65	42.	1.7	1.9					3	8.5	4	10.8
66	42.	1.7	1.9					3	9.0	4	11.2
67	42.	1.7	1.9					1	8.5	2	10.8
68	42.	2.0	2.0	7.9	8.1	4.0	3.3	1	8.5	2	11.2
69	42.	2.0	2.0					3	8.5	4	10.8
70	42.	2.0	2.0					3	9.0	4	10.8
71	42.	2.0	2.0					1	9.0	2	11.2
72	42.	2.0	2.0	8.1	8.1	3.7	2.9	1	8.1	2	11.2

TABLE B2 (Cont)

RUN	GAUGE PRESSURES			PRESSURE DROPS				LEG PRESSURES-GAUGE			
	BLOWER	BED ONE	BED TWO	BED ONE	BED TWO	DIST ONE	DIST TWO	SWITCH POS	1 P	SWITCH POS	2 P
73	42.	2.0	2.0					3	8.5	4	10.8
74	42.	2.0	2.0					3	8.1	4	10.8
75	42.	2.0	2.0					1	9.0		
76	40.	1.9	1.5	8.8	7.7	3.8	3.3	2	10.3		
77	40.	1.9	1.5					4	10.8	3	9.9
78	40.	1.9	1.5	7.8	8.7	4.0	2.9	4	10.8	3	10.3
79	40.	1.9	1.5					2	10.8	1	9.4
80	41.	1.9	1.4					2	10.3	1	9.9
81	41.	1.9	1.4	8.1	8.1	4.0	2.9	4	10.8	3	9.9
82	41.	1.9	1.4					4	10.8	3	10.3
83	41.	1.9	1.4					2	10.8	1	9.4
84	41.	1.9	1.4					2	10.8	1	9.9
85	41.	1.9	1.4					4	10.8	3	10.3
86	48.	2.0	2.0	7.5	8.1	4.4	3.7	2	11.2	1	9.9
87	48.	2.0	2.0					4	10.8	3	9.4
88	48.	2.0	2.1	7.8	8.4	4.8	3.3	4	10.8	3	9.4
89	48.	2.0	2.1					2	11.2	1	9.9
90	48.	2.0	2.0					2	11.6	1	9.9
91	48.	2.0	2.0					4	11.2	3	9.4
92	48.	2.0	2.0	8.1	8.1	4.4	3.3	4	10.8	3	9.0
93	48.	2.1	2.0					2	11.2	1	9.4
94	48.	2.2	2.0	6.9	8.1	4.4	3.3	2	10.8	1	9.9
95	48.	2.2	2.0					4	11.2	3	9.4
96	48.	2.1	2.0					4	11.2	3	9.4
97	48.	2.0	2.0					2	11.2	1	9.9
98	48.	2.0	2.0	7.5	8.1	4.4	3.7	2	11.2	1	10.3
99	48.	2.0	2.0					4	10.8	3	9.4
100	48.	2.1	2.0					4	11.6	3	9.9
101	48.	2.2	2.0					2	12.1	1	10.8
102	48.	2.2	2.0	7.5	8.1	4.4	3.3	2	11.2	1	11.2
103	48.	2.2	2.0					4	11.6	3	10.8
104	48.	2.2	2.0					4	11.6	3	10.8
105	48.	2.2	2.0					2	12.1	1	11.2

TABLE B2 (Cont)

RUN	GAUGE PRESSURES			PRESSURE DROPS				LEG PRESSURES-GAUGE			
	BLOWER	BED ONE	BED TWO	BED ONE	BED TWO	DIST ONE	DIST TWO	SWITCH POS	1 P	SWITCH POS	2 P
106	48.	2.2	2.0					2	11.6	1	9.9
107	48.	2.2	2.0					4	12.1	3	10.8
108	48.	2.2	2.0					4	11.6	3	10.3
109	48.	2.2	2.0					2	12.1	1	10.8
110	48.	2.2	2.0					2	11.6	1	11.2
111	48.	2.2	2.0					4	11.2	3	10.8
112	48.	2.0	1.9	7.9	8.4	4.8	3.7	1	6.7	1	10.3
113	48.	2.0	1.9					3	6.7	3	10.8
114	48.	2.0	1.9					3	6.7	3	10.8
115	48.	2.0	2.0					1	6.7	1	10.3
116	48.	2.0	2.0	7.8	8.1	4.4	3.7	1	6.7	1	9.4
117	48.	2.0	2.0					3	7.2	3	10.8
118	48.	2.0	2.0					3	7.6	3	11.2
119	48.	2.0	2.0					1	6.7	1	9.9
120	48.	2.0	2.0	7.8	8.4	4.4	3.7	1	6.7	1	10.3
121	48.	2.0	2.0					3	7.2	3	10.8
122	48.	2.0	2.0					3	7.2	3	10.8
123	48.	2.0	2.0					1	6.7	1	9.9
124	48.	2.0	2.0					1	6.7	1	9.9
125	48.	2.0	2.0					3	7.2	3	10.8
126	48.	2.0	2.0					3	7.2	3	10.3
127	48.	2.0	2.0					1	6.7	1	9.9
128	48.	2.0	2.0	7.5	8.4	4.8	3.7				
129	48.	2.0	2.0								
130	48.	2.0	2.0								
131	48.	2.0	2.0								
132	48.	2.0	2.0								
133	48.	2.0	2.0								
134	48.	2.0	2.0								
135	48.	2.0	2.0								
136	48.	2.0	2.0								
137	48.	2.0	2.0								
138	48.	2.0	2.0								

TABLE B2 (Cont)

RUN	GAUGE PRESSURES			PRESSURE DROPS				LEG PRESSURES-GAUGE			
	BLOWER	BED ONE	BED TWO	BED ONE	BED TWO	DIST ONE	DIST TWO	SWITCH 1 POS	P	SWITCH 2 POS	P
139	47.	2.0	2.0	7.8	8.1	4.4	3.3	2	8.1		
140	47.	2.0	2.0					4	8.1		
141	47.	2.0	2.0					4	7.6	3	10.3
142	47.	2.0	2.0					2	8.5	1	10.8
143	47.	2.0	2.0	7.2	8.7	4.4	3.7	2	7.6	1	9.4
144	47.	2.0	2.0					4	7.6	3	9.0
145	47.	2.0	2.0					4	7.2	3	9.0
146	47.	2.0	2.0					2	7.6	1	9.0
147	47.	2.0	2.0					2	7.6	1	9.0
148	47.	2.0	2.0					4	8.1	3	9.9
149	47.	2.0	2.0					4	8.1	3	8.5
150	47.	2.0	2.0					2	8.1	1	9.0
151	47.	2.0	2.0					2	8.1	1	9.0
152	47.	2.0	2.0					4	8.1	3	10.8
153	47.	2.0	2.0					4	7.6	3	9.4
154	47.	2.0	2.0					2	8.5	1	9.9
155	47.	2.0	2.0					2	8.5	1	9.4
156	47.	2.0	2.0					4	8.1	3	9.9
157	47.	2.0	2.0					4	8.1	3	9.9
158	47.	2.0	2.0					2	9.0	1	9.9
159	47.	2.0	2.0					2	8.5	1	9.9
160	47.	2.0	2.0					4	8.5		
161	47.	2.0	2.0					4	7.2	3	9.0
162	47.	2.0	2.0					2	7.6		
163	47.	2.0	2.0					2	7.6	1	9.0
164	47.	2.0	2.0					4	7.6	3	9.4
165	47.	2.0	2.0					4	7.6	3	9.4
167	47.	2.0	2.0					2	7.2	1	8.5
168	47.	2.0	2.0					4	7.2	3	8.1
170	47.	2.0	2.0								
171	47.	2.0	2.0								
172	47.	2.0	2.0								
173	47.	2.0	2.0								

TABLE B2 (Cont)

RUN	GAUGE PRESSURES			PRESSURE DROPS				LEG PRESSURES-GAUGE			
	BLOWER	BED ONE	BED TWO	BED ONE	BED TWO	DIST ONE	DIST TWO	SWITCH POS	1 P	SWITCH POS	2 P
174	47.	2.0	2.0								
175	48.	2.0	2.0	7.5	7.8	4.4	3.7				
176	48.	2.0	2.0								
177	48.	2.0	2.0								
178	48.	2.0	2.0								
179	48.	2.0	2.0								
180	48.	2.0	2.0								
181	48.	2.0	2.0								
182	48.	2.0	2.0								
183	48.	2.0	2.0								
184	48.	2.0	2.0								
185	48.	2.0	2.0								
186	48.	2.0	2.0								
187	48.	2.0	2.0								
188	48.	2.0	2.0								
189	48.	2.0	2.0								
190	48.	2.0	2.0								
191	48.	2.0	2.0								
192	48.	2.0	2.0								
193	48.	2.0	2.0								
194	48.	2.0	2.0								
195	48.	2.0	2.0								
196	48.	2.0	2.0								
197	48.	2.0	2.0								
198	48.	2.0	2.0								
199	48.	2.0	2.0								
200	48.	2.0	2.0								
201	48.	2.0	2.0								
202	48.	2.0	2.0								
203	48.	2.0	2.0								
204	48.	2.0	2.0								
205	48.	2.0	2.0								
206	48.	2.0	2.0								

TABLE B2 (Cont)

RUN	GAUGE PRESSURES			PRESSURE DROPS				LEG PRESSURES-GAUGE			
	BLOWER	BED ONE	BED TWO	BED ONE	BED TWO	DIST ONE	DIST TWO	SWITCH 1 POS	P	SWITCH 2 POS	P
207	27.	1.2	1.2	8.1	8.1	2.7	2.2	2	11.2		
208	27.	1.2	1.2					2	8.5		
209	34.	1.7	1.7	8.1	7.8	3.3	2.9	2	11.2		
210	34.	1.7	1.7					2	9.4		
211	31.	1.5	1.2	7.8	8.1	2.9	2.6	2	11.2		
212	31.	1.5	1.3					2	9.4		
213	31.	1.6	1.3					2	8.5		
214	31.	1.6	1.4					2	11.6		
215	31.	1.6	1.4					2	11.6		
216	31.	1.7	1.4					2	8.5		
217	31.	1.7	1.4					2	9.4		
218	31.	1.7	1.5					2	11.6		
219	31.	1.7	1.5					2	11.6		
220	31.	1.7	1.5					2	9.4		
221	31.	1.7	1.5					2	9.4		
222	31.	1.7	1.5					2	11.6		
223	31.	1.7	1.5								
224	31.	1.7	1.5								
225	31.	1.7	1.5								
226	31.	1.7	1.5								
227	31.	1.7	1.5	8.1	8.4	3.3	2.3				
228	31.	1.7	1.5								
229	31.	1.7	1.5								
230	31.	1.7	1.5								
231	31.	1.7	1.5								
232	31.	1.7	1.5								
233	31.	1.7	1.5								
234	31.	1.7	1.5								
235	31.	1.7	1.5								
236	31.	1.7	1.5								
237	31.	1.7	1.5								
238	31.	1.7	1.5								
239	31.	1.7	1.5								

TABLE B2 (Cont)

RUN	GAUGE PRESSURES			PRESSURE DROPS				LEG PRESSURES-GAUGE			
	BLOWER	BED ONE	BED TWO	BED ONE	BED TWO	DIST ONE	DIST TWO	SWITCH 1 POS	P	SWITCH 2 POS	P
240	31.	1.7	1.5								
241	28.	1.5	1.2	7.9	8.4	2.7	2.2				
242	28.	1.5	1.2								
243	28.	1.5	1.2								
244	28.	1.5	1.2								
245	28.	1.5	1.2								
246	28.	1.5	1.2								
247	28.	1.5	1.2								
248	28.	1.5	1.2								
249	28.	1.5	1.2								
250	28.	1.5	1.2								
251	28.	1.5	1.2								
252	28.	1.5	1.2								
253	28.	1.5	1.2								
254	28.	1.5	1.2								
255	28.	1.5	1.2								
256	28.	1.5	1.2								
257	28.	1.5	1.2								
258	28.	1.5	1.2								
259	28.	1.5	1.2								
260	28.	1.5	1.2								
261	28.	1.5	1.2								
262	28.	1.5	1.2								
263	28.	1.5	1.2								
264	28.	1.5	1.2								
265	28.	1.5	1.2								
266	28.	1.5	1.2								
267	28.	1.5	1.2								
268	28.	1.5	1.2								
269	28.	1.5	1.2								
270	28.	1.5	1.2								
271	28.	1.5	1.2								
272	28.	1.5	1.2								

APPENDIX C

MODEL DEVELOPMENT DETAILS

C.1 JET AREA

It is well known[C1] that homogeneous jets have similar geometries. Application of jet expansion assumptions to predict the dilute phase flow area in this model was achieved by assuming that gas jets into solids also possess similarity. In addition, it was assumed that the relation of a plane jet to a circular jet in a fluidized system was similar to the relation in a homogeneous system.

Figure C-1 illustrates the nomenclature and geometry involved. Circular jets issue from nozzles with a half-angle Θ at the virtual origin. When the jets interfere a plane jet is formed whose half-angle is slightly larger due to the lesser degree of freedom. It is assumed that the jet radius is equal to half the nozzle center-to-center spacing at the transition point. From trigonometry we know that (refer to Figure C-1):

$$\frac{x_n}{2(x_1 + y_2)} = \tan \Theta \qquad \text{(C-1)}$$

and

$$\frac{d_o}{2(y_2)} = \tan \Theta \quad . \qquad \text{(C-2)}$$

From these

$$x_1 = \frac{x_n - d_o}{2 \tan \Theta} \quad . \qquad \text{(C-3) and (14)}$$

Dwg. 6444A10

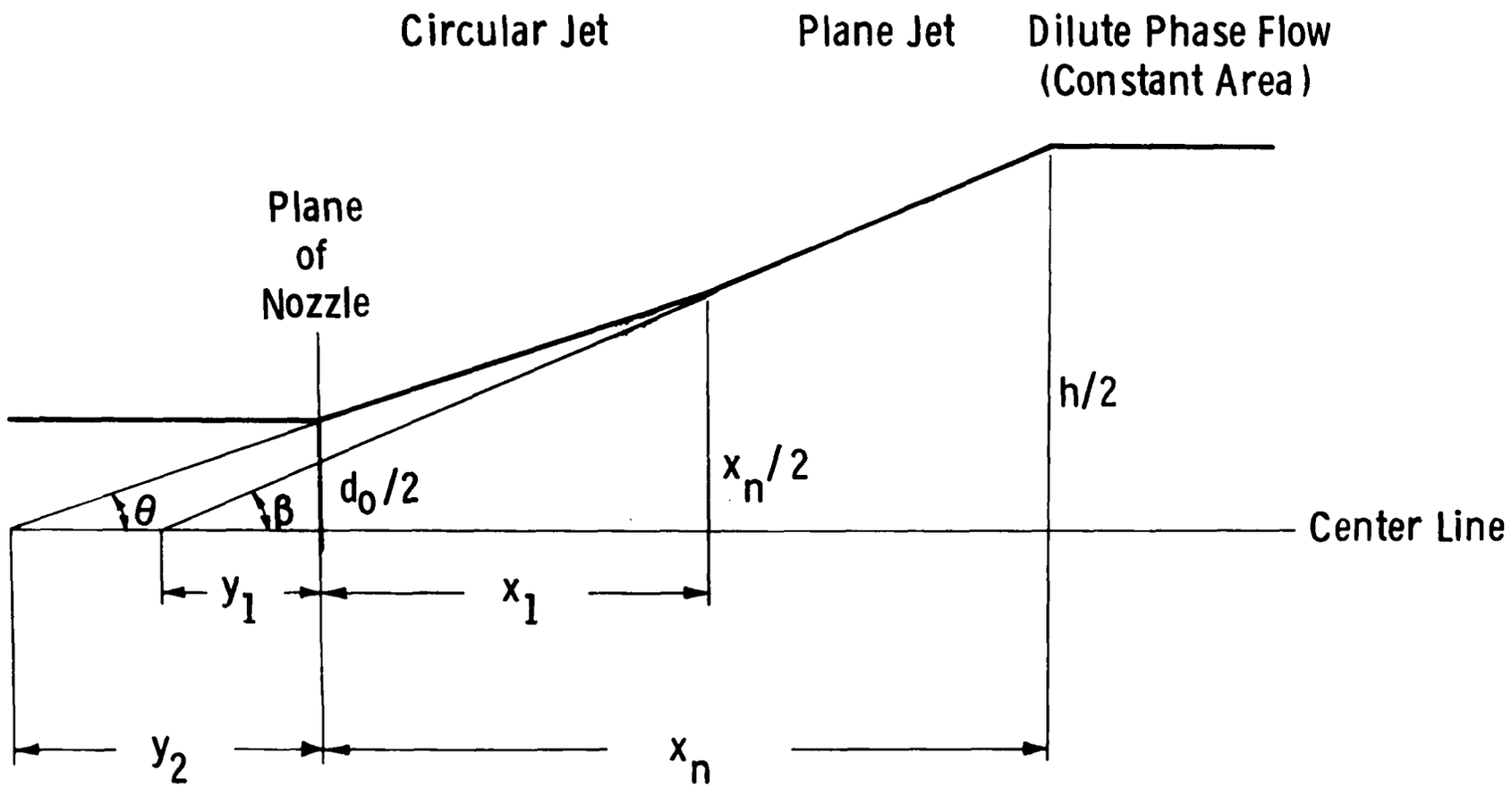

Figure C-1. Geometry and Nomenclature of Jet Expansion

If $x_1 \leq x_h$, then a transition to a plane jet occurs and

$$\frac{h}{2(x_h + y_1)} = \tan \beta \qquad \text{(C-4)}$$

and

$$\frac{x_n}{2(x_1 + y_1)} = \tan \beta \quad . \qquad \text{(C-5)}$$

Combining Equations C-3, 4, 5 yields

$$h = x_n + (d_o - x_n) \left(\frac{\tan \beta}{\tan \Theta}\right) + 2x_h \tan b \quad , \qquad \text{(C-6)}$$

and thus

$$S_3 = h \cdot W = W[x_n + (d_o - x_n) \left(\frac{\tan \beta}{\tan \Theta}\right) + 2x_h \tan \beta] \quad . \text{(C-7) and (16)}$$

If $x_1 > x_h$, then jets are spaced widely enough not to interfere and the radius of a jet at x_h is

$$r = (x_h + y_2) \tan \Theta \quad . \qquad \text{(C-8)}$$

But

$$y_2 = d_o/(2 \tan \Theta) \quad , \qquad \text{(C-9)}$$

so

$$r = x_h \tan \Theta + \frac{d_o}{2} \quad . \qquad \text{(C-10)}$$

Therefore,

$$S_3 = N\pi r^2 = \frac{\pi}{4} N(2\, x_h \tan \Theta + d_o)^2 \quad . \qquad \text{(C-11) and (15)}$$

These estimates of the dilute phase flow require predicting the jet half-angles, Θ and β. Merry[C2] found that for a circular horizontal gas jet into a fluidized bed, Θ was 6.35°. We used this value. Rajaratnam[C1] presents a detailed discussion of both circular and plane turbulent

homogeneous jets. Following his discussion it can be shown that the angle formed between the circular jet centerline and the line consisting of the locus of those points where velocity is half the centerline velocity is about 5.4°. For a plane jet this angle is 6.5°. Similarity requires that the ratio of plane jet to circular jet half-angles (6.5°/5.4° = 1.20) be the same for all homogeneous jets when the half-angles are defined consistently. We have assumed this ratio also applies to consistently define half-angles in the heterogeneous case. Therefore β was taken as 1.2 x 6.35 = 7.64°.

C.2 FLUIDIZING TIME ESTIMATION

The fluidizing time denotes the time required for significant gas bypassing to be achieved once a large pressure gradient is imposed upon a bed of solids. Figure C-2 illustrates the phenomenon. A pressure gradient in excess of bed density has been applied to a bed. Fluidized solids exist above the bed boundary ($z > L_S$). The local pressure gradient ($\Delta P/L_S$) in the bed is assumed to be neither a function of height nor time (the bed is pushed up by the bubble). Voidage is constant at ε_1.

The net force on a thin layer of solids ahead of the bubble is $(\frac{\Delta P}{L_S})$ A (Δz). The mass of the layer is $\rho_p A(\Delta z)\ (1 - \varepsilon_1)$. The acceleration of this slab is then

$$\frac{d^2z}{dt^2} = \frac{\Delta P\ g_c}{L_s \rho_p (1 - \varepsilon_1)} \quad . \tag{C-12}$$

Boundary conditions are that at t = 0

$$z = 0 \tag{C-13}$$

and

$$\frac{dz}{dt} = 0 \tag{C-14}$$

for the last slab close to the air bubble.

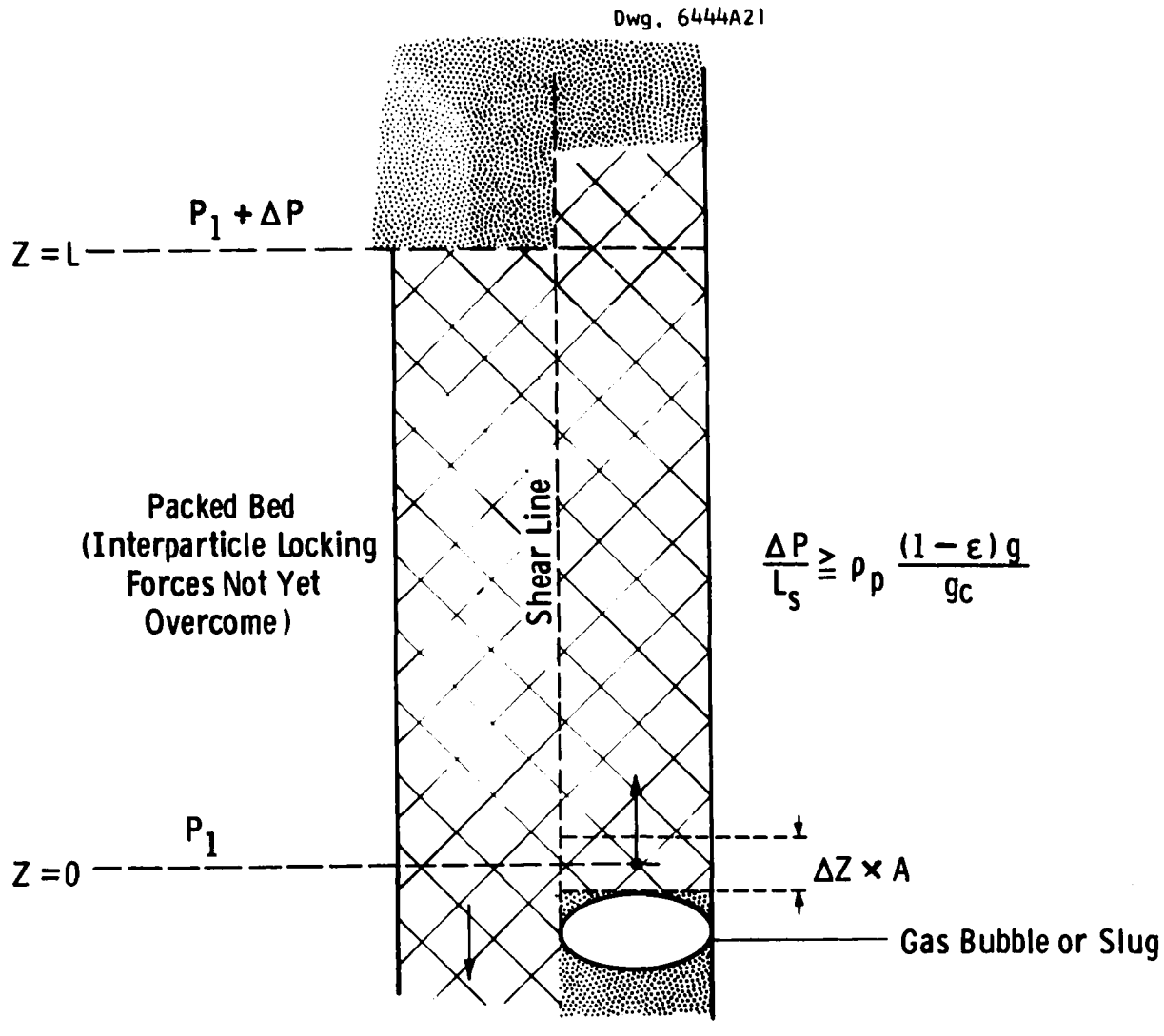

Figure C-2. Fluidizing Dynamics

Solving

$$z = \frac{\Delta P \; g_c}{2L_S\rho_p(1 - \varepsilon_1)} \; t^2 \quad , \qquad \text{(C-15)}$$

the leg will be fluidized (the bubble will have risen, clearing a path for gas bypassing), at time t_M where $z = L_S$.

$$t_M = \sqrt{\frac{2L_S{}^2\rho_p(1 - \varepsilon_1)}{\Delta P \; g_c}} \qquad \text{(C-16) and (17)}$$

After $t = t_M$ all available gas passes upward, clearing the rest of the leg rapidly, until such time as the pressure gradient is reduced to a stable level consistent with the bed density.

An alternative expression can be derived from a force balance on a rising gas slug in a fluid bed. We assume that the bed is initially fluid and that C_D is the drag coefficient of the fluid bed on the slug front. If the slug is approximated by a rising blunt-nosed cylinder starting at $z = 0$, with z the position of its top,

$$\frac{d^2z}{dt^2} = g\left[\frac{\rho_p(1 - \varepsilon_1)}{\rho_g} - 1\right] - \frac{C_D}{2}\left(\frac{\rho_p}{\rho_g}\right) v^2{}_z \; (1 - \varepsilon_1) \qquad \text{(C-17)}$$

is the force balance. Assuming C_D is constant, with the same boundary conditions as before, at $z = L_S$, $t = t_M$;

$$t_M = \sqrt{\frac{2 \; C_D L_S}{g}} \qquad \text{(C-18)}$$

provided also that $\rho_p(1 - \varepsilon_1) >> \rho_g$.

Standard drag coefficient correlations (Perry[C3]) for a disc oriented perpendicularly to flow suggest that for a Reynolds number in excess of about 100, C_D is of the order unity. Thus equation C-18 reduces to

$$t_M = \sqrt{\frac{2 \; L_S}{g}} \qquad \text{(C-19)}$$

which is equation C-16 with

$$(\Delta P/L_S) = \rho_p \ (1 - \varepsilon_1) \ g/g_c \quad . \qquad \text{(C-20)}$$

C3. DEFLUIDIZING BEHAVIOR AND VERTICAL SECTION VOIDAGE ESTIMATION

Equations 19 and 20 (Section 7.1.8) were derived empirically to reflect experimental trends. The density of material in the vertical section will not return to its packed value unless sufficient time is allowed between pulses. To approximate behavior at short off-times we assumed that the density was proportional to the relative time allowed.

$$\left(\frac{1 - \varepsilon_1}{1 - \varepsilon_p}\right) \propto \left(\frac{\text{time allowed for packing}}{\text{time required for complete packing}}\right) \cdot \qquad \text{(C-21)}$$

The data suggest that about the first half-second of off-time does not permit substantial packing. Evidently this is due to the need to allow pulse gas to escape against the direction of solids flow. The little packing that does occur in this time is more than reversed by the next pulse, so each subsequent pulse sees a higher vertical voidage, and a seal is not possible.

The best value of this response time for our data was ∿0.54 s. Therefore, only off-time in excess of this value permits a voidage less than one, and equation C-21 is modified to:

$$\frac{(1 - \varepsilon_1)}{(1 - \varepsilon_p)} = \frac{t_{OFF} - 0.54}{1.41-0.54} = \left(\frac{t_{OFF} - 0.54}{0.87}\right) \qquad \text{(C-22) and (19)}$$

$$= \left(\frac{t_{OFF} - t_R}{t_p}\right) \quad .$$

In this equation 1.4 is the experimental minimum time required for complete repacking at long on-times.

At shorter on-times ($t_{ON} < t_M$) less time is required for repacking. Sutton and Richmond[C4] suggest that bed heights fall exponentially with time, approaching the packed density asymptotically. Packing occurs most rapidly early during deaeration. We have approximated this behavior by

$$t_p = 0.87\sqrt{\frac{t_{ON}}{t_M}}$$

for $t_{ON} < t_M$, yielding Equation 20 in Section 7-1.8.

REFERENCES

C1. Rajaratnam, N., Turbulent Jets, New York: Elsevier Scientific Publishing Company; 1976, Chapters 1 and 2.

C2. Merry, J. M. D., Penetration of a Horizontal Gas Jet into a Fluidized Bed, Trans. Instn. Chem. Engrs. 49: 189-195; 1971.

C3. Perry, J H., ed., Chemical Engineer's Handbook, 4th Edition, New York: McGraw-Hill Book Co.; 1963, Chapter 5, p. 60.

C4. Sutton, H. M., and R. A. Richmond, Improving the storage Conditions of Fine Powders by Aeration, Trans. Instn. Chem. Engrg., 51: 97-104; 1973.

APPENDIX D

SOLIDS TRANSPORT MODEL PROGRAM LISTING

```
C MOMENTUM BALANCE MODEL FOR CAFB SOLIDS TRANSFER SYSTEM
      REAL K,K1,K2,K3,K4,K5,K6,L,MU,NOZ,M
      INTEGER RUN
C   REMEMBER TO USE PROPER I/O DEVICE CODES
      INPUT=5
      IOUT=6
C
C  INPUT VARIABLES
C
C
C GENERAL DATA, PARTICLE PROPERTIES, LEG GEOMETRY
C
C****  N=NUMBER OF DATA POINTS FOR THIS GEOMETRY AND MATERIAL
C**** EP=PACKED BED VOIDAGE, NORMAL LOOSE
C**** DP=AVERAGE PARTICE SIZE, MICROMETERS
C**** RHOP=PARTICLE DENSITY, KILOGRAMS PER CUBIC METER
C**** S1=CROSS-SECTIONAL FLOW AREA OF LEG, SQUARE METERS
C**** S2=CROSS-SECTIONAL FLOW AREA OF NOZZLES (TOTAL), SQUARE METERS
C**** L=VERTICAL LENGTH, METERS
C**** HL=HORIZONTAL LENGTH, METERS
C**** AL=ANGLE OF DOWNCOMER FROM VERTICAL, RADIANS
C**** DT=MEAN HYDRAULIC  DIAMETER OF LEG, METERS
C**** DN=NOZZLE DIAMETER, CENTIMETERS
C**** XH=DISTANCE FROM NOZZLE TO OVERHANG, CENTIMETERS
C**** XN=NOZZLE SEPARATION (CENTER-TO-CENTER), CENTIMETERS
C**** NOZ=NUMBER OF NOZZLES
C**** XW=LEG WIDTH, METERS
C**** M=MOLECULAR WEIGHT OF TRANSPORT GAS
      READ (INPUT,10) N,EP,DP,RHOP
   10 FORMAT (I5,3F10.3)
      READ (INPUT,20) S1,S2,L,HL,AL,DT,DN,XH,XN,NOZ
   20 FORMAT (2F8.6,8F8.4)
      READ (INPUT,21) XW
   21 FORMAT (F10.3)
      READ (INPUT,22) M
   22 FORMAT (F10.5)
      DP=.000001*DP
      DN=.01*DN
      XH=.01*XH
      XN=.01*XN
      WRITE (IOUT,23)
```

```
   23 FORMAT (1H1,///' RUN   TON   TOFF    TM      GA      WP      WH',
     1'     E1     E3     PO   SRAT     GSP'//)
C
C CALCULATION OF DILUTE PHASE FLOW AREA S3, SQUARE METERS
C
      X1=(XN-DN)/.223
      H=.223*XH+DN
      S3=NOZ*.785*H**2
      IF (X1 .GE. XH) GO TO 25
      H=XN+(DN-XN)*1.21+.268*XH
      S3=H*NOZ*XN
   25 CONTINUE
      IF (S3 .GT. S1) S3=S1
      ES=.99
      TP=.87
      DO 1000 J=1,N
C
C INDIVIDUAL POINTS
C
C**** RUN=RUN NUMBER
C**** TON=PULSE DURATION, SECONDS
C**** TOFF=TIME BETWEEN PULSES, SECONDS
C**** GA=OVERALL TRANSPORT GAS FLOW, KG/S
C**** P3=PRESSURE AT LEG DISCHARGE, KILOPASCALS
C**** DELP=NORMAL TOTAL PRESSURE DIFFERENTIAL ACROSS LEG, KILOPASCALS
C**** T=OPERATING TEMPERATURE OF TRANSPORT GAS, KELVIN
C**** MU=TRANSPORT GAS VISCOSITY, KG/M/S
      READ (INPUT,30) RUN,TON,TOFF,GA,P3,DELP,T,MU
   30 FORMAT (I5,5F9.4,F10.1,F9.7)
      P3=P3*1000.
      P3A=P3
      DELP=DELP*1000.
      TNN=TON
      LIM=0
      E3=.85
   50 CONTINUE
C
C   INITIAL GUESS ON PRESSURE AT NOZZLE
C
      PP=P3A+2000.
      NN=0
```

```
C
C    ITERATE ON PRESSURE AT NOZZLE
C
      DO 500 JP=1,100
  100 P3=P3A
      PP=ABS(PP)
      P2=PP
      P1=P2
C***DALP=PRESSURE LOSS OVER VERTICAL
      DALP=DELP+P1-P3
C    E1=VERTICAL SECTION VOIDAGE
C      TM=EFFECTIVE TIME OF PULSE
      E1=ES-(ES-EP)/TP*(TON+TOFF-TNN-.54)
      IF (E1 .GT. ES) E1=ES
      IF (E1 .LT. EP) E1=EP
      TM=100000.
      IF (DALP .LE. 0.) GO TO 150
      TM=SQRT(RHOP*(1.-E1)*L**2/DALP*2.)
      IF (TON .GT. TM) GO TO 150
  145 E1=ES-(ES-EP)/TP*(TON+TOFF-TNN-.54)*SQRT(TM/TON)
      IF (E1 .GT. ES) E1=ES
         IF (E1 .LT. EP) E1=EP
      TM2=SQRT(RHOP*(1.-E1)*L**2/DALP*2.)
      IF (ABS(TM-TM2) .LT. .01) GO TO 150
      TM=TM2
      GO TO 145
  150 CONTINUE
      IF ((DALP/L) .GE. (RHOP*(1.-EP)*9.8)) GO TO 151
      E1=EP
      TM=100000.
  151 CONTINUE
C    GAS DENSITIES
      RHO1=P1/T*M/8.314/1000.
      RHO2=RHO1*P2/P1
      RHO3=RHO1*P3/P1
      A=1.75*(1.-E1)/E1*RHO1/DP
      B=150.*((1.-E1)/E1/DP)**2*MU
      C=-DALP/L
C    UPWARD RELATIVE VELOCITY
      IF (C .GT. 0.) VR=-(SQRT(B**2+4.*A*C)-B)/2./A
      IF (C .LE. 0.) VR=(SQRT(B**2-4.*A*C)-B)/2./A
      TS=TM
      IF (TM .GT. TNN) TS=TNN
```

```
C     NOZZLE VELOCITY
      V2=GA/RHO2/S2*(TON+TOFF)/TNN
      IF (LIM .NE. 0) GO TO 170
C    DILUTE PHASE VOIDAGE CORRELATION
      E3=1.-(1.-E1)*(RHO2*V2*DP/MU)**(-.04224)*(TS/(TON+TOFF-TNN))**
     1(-1.44419)*.03759
      IF (TNN .GE. TM) GO TO 170
      E3=1.-(1.-E1)*(RHO2*V2*DP/MU)**(-.04527)*(TS/(TON+TOFF-TNN))**
     1(-.54258)*.21704
  170 CONTINUE
      A=1.75*(1.-EP)/EP*RHO1/DP
      B=150.*((1.-EP)/EP/DP)**2*MU
      C=(P3-P1)/HL
C    HORIZONTAL GAS VELOCITY IN STAGNANT SOLIDS REGION
      IF (C .LE. 0.) VRH=(SQRT(B**2-4.*A*C)-B)/2./A
      IF (C .GT. 0.) VRH=-(SQRT(B**2+4.*A*C)-B)/2./A
C
C  SOLUTION OF MOMENTUM BALANCE
C
      VEC=1.
      OGSP=0.
  200 CONTINUE
C     GROUPED KNOWNS IN BALANCES
      K1=P3*S1-P1*S1+P1*S2-P2*S2-V2**2*S2*RHO2+VEC*VR**2*S1*E1*RHO1*
     1SIN(AL)
      K2=(S3*(1.-E3)/(1.-E1))**2/S1*SIN(AL)*(RHOP*(1.-E1)-VEC*RHO1*E1)-
     1(1.-E3)*RHOP*S3
      K3=S3*E3*RHO3
      K4=V2*S2*RHO2-VR*E1*RHO1*S1-VRH*EP*(S1-S3)*RHO1
      K5=E1*RHO1*S3*(1.-E3)/(1.-E1)
      K6=-2.*VEC*VR*(1.-E3)/(1.-E1)*S3*E1*RHO1*SIN(AL)
      A=K1*K5**2-K2*K4**2-K4*K5*K6
      B=K3*K4*K6-2.*K1*K3*K5
      C=K1*K3**2+K3*K4**2
      Q=B**2-4.*A*C
      IF (Q .LT. 0.) K=-B/2./A
      IF (Q .LT. 0.) GO TO 500
      ZKP=(-B+SQRT(Q))/2./A
      ZKN=(-B-SQRT(Q))/2./A
      K=ZKP
      IF (ABS(ZKP-.5) .GT. ABS(ZKN-.5)) K=ZKN
C    DILUTE PHASE GAS AND SOLIDS VELOCITIES
  500 V3=K4/(S3*E3*RHO3-K*E1*RHO1*S3*(1.-E3)/(1.-E1))
      VS3=K*V3
```

```
170*            IF (VS3 .LT. 0.) VS3=0.
171*        560 CONTINUE
172*      C   DOWNWARD VELOCITY OF GAS
173*            V1=K*V3*(1.-E3)*S3/(1.-E1)/S1-VR
174*            IF (VEC .LT. 0.) GO TO 502
175*      C   CHECK ASSUMPTION THAT GAS NET FLOW IS UPWARD
176*      C       IF NOT, CORRECT
177*            IF (V1 .LT. 0.) GO TO 502
178*            VEC=-1.
179*            GO TO 200
180*        502 CONTINUE
181*      C   TOTAL AND HORIZONTAL GAS MASS FLOW RATE,DURING PULSE.
182*            WP=GA*(TON+TOFF)/TNN
183*            WH=WP-(VR-VS3*S3*(1.-E3)/(1.-E1)/S1)*E1*RHO1*S1
184*      C   DOWNWARD SOLIDS VELOCITY
185*            VS1=VS3*(1.-E3)*S3/S1/(1.-E1)
186*      C
187*      C PRESSURE FROM WEN AND SIMONS CORRELATION, PASCALS
188*      C
189*            RHOS=(2.*(1.-E3)*S3+(1.-E1)*(S1-S3))*RHOP/S1
190*            US=VS3*S3*(1.-E3)*RHOP/S1/RHOS
191*            US=US/2.
192*            IF (US .LT. 0.) US=0.
193*            P2N=91.82*US**.45*RHOS*HL*(DP/DT)**.25+P3
194*            IF (ABS(P2N-P2) .LE. 100.) GO TO 950
195*      C
196*      C   NEW GUESS FOR NOZZLE PRESSURE:  WEGSTEIN'S METHOD
197*      C
198*            X=P2
199*            FX=P2N
200*            NN=NN+1
201*            IF (NN .EQ. 50) GO TO 1000
202*            IF (NN-1) 1,1,2
203*          2 IF (X-XLAST) 3,1,3
204*          3 SLOPE=(FX-FLAST)/(X-XLAST)
205*            DENOM=SLOPE-1.
206*            IF (DENOM) 4,1,4
207*          4 FACTR=SLOPE/DENOM
208*            PP=FACTR*X+(1.-FACTR)*FX
209*          5 XLAST=X
210*            FLAST=FX
211*            GO TO 504
212*          1 PP=.9*PP+.1*FX
213*            GO TO 5
```

```
  504 CONTINUE
  450 CONTINUE
C     PREDICTED SOLIDS FLOW RATE
      GSP=VS3*S3*(1.-E3)*RHOP*TS/(TON+TOFF)
      IF (LIM .EQ. 2) GO TO 506
C    CHECK TO SEE SOLIDS VELOCITY LESS THAN NOZZLE VELOCITY
  505 IF (VS3 .LT. V2) GO TO 506
      LIM=1
      E3=E3-.01
      IF (E3 .LE. (E1+.01)) GO TO 507
      GO TO 50
C    CHECK DILUTE PHASE VOIDAGE EXCEEDS PACKED VOIDAGE
  506 IF (E3 .GT. EP) GO TO 507
      LIM=2
      E3=E3+.01
      GO TO 50
  507 CONTINUE
      OGSP=GSP
  550 CONTINUE
      GSP=OGSP
      P2=P2/1000.
      P3=P3/1000.
      PD=P2-P3
      SRAT=GSP/GA
C
C  OUTPUT VARIABLES
C
C*** RUN,TON,TOFF,GA: SAME AS INPUT LISTING
C*** TM=FLUIDIZING TIME=MAXIMUM SOLIDS TRANSFER TIME, SECONDS
C*** WP=TRANSPORT GAS INPUT RATE DURING PULSE, KG/S
C*** WH=HORIZONTAL GAS FLOW RATE DURING PULSE, KG/S
C*** E1=VERTICAL VOIDAGE AT START OF PULSE
C*** E3=DILUTE PHASE VOIDAGE
C*** PD=HORIZONTAL PRESSURE LOSS, KILOPASCALS
C*** SRAT=PREDICTED RATIO OF SOLIDS FLOW RATE TO GAS INPUT RATE, KG/KG
C*** GSP=PREDICTED SOLIDS FLOW RATE, KG/S
      WRITE (IOUT,600) RUN,TON,TOFF,TM,GA,WP,WH,E1,E3,PD,SRAT,GSP
  600 FORMAT (1H ,I4,3F5.2,3F8.4,2F6.2,F6.1,F6.0,F8.2)
 1000 CONTINUE
 2000 CONTINUE
       CALL EXIT
      END
```

APPENDIX E

COMPARISON OF EXPERIMENTAL SOLIDS TRANSFER RATES AND MODEL PREDICTIONS - 1978 TESTS

COMPARISON OF EXPERIMENTAL AND PREDICTED SOLIDS FLOW RATES

Run No. -	On Time, s	Off Time, s	Fluid-izing Time, s	ΔP (P_1-P_3) kPa	ε_1 -	ε_3 -	Measured Solids Flow, kg/s	Predicted Solids Flow, kg/s
1	.10	2.00	.32	3.29	.450	.611	1.56	2.29
2	.10	2.00	.32	3.44	.449	.615	2.60	2.54
3	.50	2.00	.34	2.07	.449	.815	3.45	3.00
4	.50	2.00	.34	2.17	.449	.815	2.41	3.11
6	.25	2.00	.33	2.54	.448	.757	1.57	3.42
7	.25	2.00	.33	2.46	.448	.753	2.39	3.16
8	1.00	2.00	.34	2.07	.447	.813	2.17	2.48
9	1.00	2.00	.34	2.07	.447	.811	2.57	2.46
10	.75	2.00	.34	2.07	.447	.814	2.03	2.73
11	.75	2.00	.34	2.07	.446	.812	2.62	2.70
12	.10	2.00	.32	3.44	.446	.611	2.75	2.55
13	.10	2.00	.32	3.23	.446	.604	2.41	2.19
14	.05	2.00	.31	4.45	.445	.447	2.76	2.05
15	.05	2.00	.31	4.02	.445	.445	1.83	1.62
16	.50	2.00	.34	2.07	.445	.815	2.82	3.02
17	.50	2.00	.34	2.07	.445	.815	1.45	3.02
18	.20	2.00	.33	2.65	.444	.724	2.55	2.97
19	.20	2.00	.33	2.65	.444	.724	1.57	2.99
20	2.00	2.00	.34	2.07	.444	.809	3.04	1.84
21	2.00	2.00	.34	2.07	.443	.808	1.92	1.84
22	1.00	2.00	.34	2.07	.443	.812	2.39	2.47
28	2.00	2.00	.34	2.07	.441	.809	1.85	1.85
29	2.00	2.00	.34	2.07	.441	.808	2.04	1.85
30	.50	2.00	.34	2.07	.440	.813	3.14	3.02
31	.50	2.00	.34	2.07	.440	.814	2.82	3.03
32	.20	2.00	.33	2.65	.440	.720	3.46	2.98
33	.20	2.00	.33	2.65	.439	.721	2.52	2.99
34	1.20	2.40	.34	2.39	.439	.746	2.18	2.52
35	1.20	2.40	.34	2.39	.439	.747	2.58	2.52
36	.10	2.00	.32	3.25	.438	.600	2.81	2.22
37	.10	2.00	.32	3.28	.438	.600	2.38	2.27
38	3.00	2.00	.34	2.07	.438	.807	1.81	1.48
39	2.80	1.85	.34	2.07	.437	.828	1.15	1.51
40	1.00	2.00	.34	2.07	.437	.811	2.14	2.49
41	1.00	2.00	.34	2.07	.437	.809	2.76	2.48
42	1.50	2.00	.34	2.07	.436	.808	3.19	2.12
43	1.50	2.00	.34	2.07	.436	.809	1.98	2.13
44	2.50	2.00	.34	2.07	.436	.808	2.15	1.65
45	2.50	2.00	.34	2.07	.435	.806	2.28	1.65

COMPARISON OF EXPERIMENTAL AND PREDICTED SOLIDS FLOW RATES

Run No. -	On Time, s	Off Time, s	Fluid-izing Time, s	ΔP (P_1-P_3) kPa	ε_1 -	ε_3 -	Measured Solids Flow, kg/s	Predicted Solids Flow, kg/s
46	4.00	2.00	.34	2.07	.435	.805	1.51	1.24
47	4.00	2.00	.35	2.07	.435	.806	1.13	1.24
48	1.00	1.00	.27	.92	.696	.946	.06	1.07
49	1.00	1.00	.28	1.03	.656	.944	1.27	1.20
50	2.00	1.00	.32	1.20	.556	.938	2.05	1.00
51	2.00	1.00	.31	1.23	.596	.939	.21	.95
52	.50	1.00	.27	.98	.696	.947	.14	1.53
53	.50	1.00	.27	.98	.695	.947	1.13	1.52
54	3.00	1.00	.33	1.36	.525	.935	1.88	.83
55	3.00	1.00	.32	1.18	.565	.938	.88	.73
56	.20	1.00	.28	1.47	.641	.875	2.87	2.77
57	.20	1.00	.28	1.48	.641	.876	3.11	2.84
58	1.50	1.00	.31	1.22	.595	.939	1.79	1.15
59	1.50	1.00	.29	1.02	.644	.943	.31	.98
60	.10	1.00	.33	2.51	.455	.726	2.75	2.81
61	.10	1.00	.33	2.53	.455	.727	3.06	2.85
62	2.50	1.00	.33	1.34	.534	.936	1.84	.93
63	2.50	1.00	.31	1.24	.584	.939	.33	.84
64	.75	1.00	.27	.97	.694	.946	.00	1.27
65	.75	1.00	.28	.96	.673	.945	2.32	1.29
66	4.00	1.00	.33	1.38	.513	.935	1.27	.68
67	4.00	1.00	.32	1.30	.553	.937	.45	.62
68	.50	1.50	.35	1.84	.428	.878	2.90	2.96
69	.50	1.50	.35	1.83	.428	.877	2.73	2.93
70	1.00	1.50	.35	1.81	.427	.875	3.12	2.30
71	1.00	1.50	.35	1.82	.427	.876	2.14	2.31
72	.20	1.50	.34	2.46	.427	.753	2.72	3.40
73	.20	1.50	.34	2.47	.426	.753	2.97	3.44
74	1.50	1.50	.35	1.81	.426	.874	2.23	1.91
75	1.50	1.50	.35	1.81	.426	.875	2.27	1.92
76	.20	1.50	.34	2.45	.425	.752	4.08	3.37
77	.20	1.50	.34	2.45	.425	.751	3.06	3.37
78	2.00	1.50	.35	1.81	.425	.873	2.14	1.64
79	2.00	1.50	.35	1.81	.424	.874	2.36	1.64
80	.10	1.50	.33	2.98	.424	.644	3.40	2.54
81	.10	1.50	.33	2.98	.424	.644	3.12	2.52
82	3.10	1.50	.35	1.81	.423	.873	1.50	1.25
83	3.10	1.50	.35	1.81	.423	.873	1.76	1.25
84	.40	1.50	.35	1.84	.423	.878	2.99	3.14
85	.40	1.50	.35	1.84	.423	.878	3.25	3.15
86	.20	3.00	.33	3.00	.422	.644	3.73	2.58
87	.20	3.00	.33	2.98	.422	.643	2.63	2.54
88	.80	3.00	.34	2.79	.422	.640	2.53	3.09
89	.80	3.00	.34	2.79	.421	.642	3.28	3.11
90	2.00	3.00	.34	2.79	.421	.635	2.18	2.34

COMPARISON OF EXPERIMENTAL AND PREDICTED SOLIDS FLOW RATES

Run No. -	On Time, s	Off Time, s	Fluid-izing Time S	ΔP (P_1-P_3) kPa	ε_1 -	ε_3 -	Measured Solids Flow, kg/s	Predicted Solids Flow, kg/s
91	2.00	3.00	.34	2.79	.421	.633	1.98	2.34
92	.40	2.90	.34	2.74	.420	.663	2.43	3.50
93	.40	2.90	.34	2.76	.420	.665	2.62	3.57
94	1.00	3.00	.34	2.79	.420	.640	3.43	2.95
95	1.00	3.00	.34	2.78	.419	.638	2.94	2.94
96	.60	2.90	.34	2.72	.419	.660	3.18	3.26
97	.60	2.90	.34	2.73	.419	.662	3.87	3.30
98	1.50	3.10	.34	2.85	.418	.617	2.24	2.64
99	1.50	3.10	.34	2.86	.418	.613	2.10	2.64
100	.40	.50	.05	.09	.990	.993	.34	.01
101	.40	.50	.05	.09	.990	.993	.00	.01
102	.40	1.60	.35	1.91	.417	.865	5.44	3.25
103	.40	1.60	.35	1.91	.417	.865	3.83	3.24
104	.40	1.00	.27	.99	.687	.946	.77	1.74
105	.40	1.00	.27	.99	.687	.946	.52	1.76
106	.40	1.80	.35	2.07	.416	.838	4.88	3.34
107	.40	1.80	.35	2.07	.415	.838	4.16	3.32
108	.40	1.40	.35	1.77	.422	.890	3.38	3.14
109	.40	1.40	.35	1.77	.421	.890	4.03	3.15
110	.40	1.20	.32	1.36	.553	.920	1.84	2.41
111	.40	1.20	.32	1.37	.553	.921	2.78	2.44
112	.10	.50	.11	.35	.950	.983	.57	.89
113	.10	.50	.11	.35	.950	.983	.92	.88
114	.20	.50	.18	.46	.870	.985	.00	.95
115	.20	.50	.05	.00	.990	.993	.00	.03
116	.20	1.60	.34	2.51	.412	.737	4.85	3.38
117	.20	1.60	.34	2.52	.412	.738	4.33	3.41
118	.20	1.20	.34	2.31	.421	.777	4.09	3.78
119	.20	1.20	.34	2.31	.421	.777	5.87	3.78
120	.20	1.00	.29	1.49	.625	.869	5.13	2.86
121	.20	1.00	.28	1.51	.625	.870	3.89	2.96
122	.20	.80	.21	.77	.812	.942	1.29	1.95
123	.20	.80	.21	.77	.812	.942	.53	1.96
124	.20	1.40	.34	2.43	.410	.753	4.90	3.58
125	.20	1.40	.34	2.43	.410	.754	4.08	3.59
126	.20	1.80	.34	2.60	.409	.719	3.77	3.24
127	.20	1.80	.34	2.60	.409	.719	4.57	3.25
128	.10	.90	.30	1.92	.575	.799	4.32	2.50
129	.10	.90	.30	1.95	.575	.800	3.36	2.59
130	.10	.80	.25	1.36	.714	.874	3.46	2.18
131	.10	.80	.25	1.33	.713	.873	2.68	2.05
132	.10	.70	.19	.79	.842	.935	2.75	1.42
133	.10	.70	.19	.84	.842	.936	1.89	1.69
134	.10	.60	.11	.33	.947	.980	.57	.90
135	.10	.60	.11	.37	.947	.980	.91	.81

COMPARISON OF EXPERIMENTAL AND PREDICTED SOLIDS FLOW RATES

Run No. -	On Time, s	Off Time, s	Fluid-izing Time S	ΔP (P_1-P_3) kPa	ε_1 -	ε_3 -	Measured Solids Flow, kg/s	Predicted Solids Flow, kg/s
136	1.00	1.00	.28	.96	.681	.945	1.50	1.14
137	1.00	1.00	.28	.96	.681	.945	1.22	1.12
138	1.00	1.80	.35	2.07	.405	.835	3.45	2.58
139	.40	1.80	.35	2.17	.405	.840	5.66	3.87
140	.40	1.80	.35	2.07	.405	.841	6.55	3.67
141	.20	1.50	.34	2.71	.404	.750	6.74	4.30
142	.20	1.50	.34	2.68	.404	.749	5.53	4.21
143	.60	2.70	.34	2.69	.404	.701	3.87	3.60
144	.60	2.70	.34	2.64	.403	.699	4.80	3.46
145	1.00	3.00	.34	2.79	.403	.643	2.38	3.07
146	1.00	3.00	.34	2.83	.403	.645	2.23	3.16
147	.40	1.60	.35	2.07	.402	.866	3.16	3.89
148	.40	1.60	.35	2.07	.402	.865	5.05	3.70
149	.40	1.40	.36	1.84	.409	.891	3.35	3.52
150	.40	1.40	.36	1.90	.408	.891	4.65	3.78
151	.20	1.40	.34	2.69	.401	.758	5.52	4.54
152	.20	1.40	.34	2.63	.401	.756	7.65	4.34
153	.20	1.00	.28	1.68	.618	.871	4.09	3.81
154	.20	1.00	.29	1.64	.617	.870	3.65	3.64
155	.20	.80	.21	.87	.809	.942	3.02	2.63
156	.20	.80	.21	.89	.809	.943	1.46	2.79
157	.10	1.00	.33	3.02	.424	.722	4.35	4.38
158	.10	1.00	.33	2.88	.421	.718	3.91	3.90
159	.10	.80	.25	1.54	.710	.875	.00	2.94
160	.10	.80	.24	1.65	.716	.879	.00	3.40
161	1.00	2.00	.36	2.07	.398	.810	2.71	2.70
162	1.00	2.00	.36	2.07	.398	.810	1.20	2.74
163	1.00	1.60	.36	1.93	.397	.864	4.16	2.64
164	1.00	1.60	.36	1.90	.397	.864	1.81	2.57
165	.40	2.00	.35	2.32	.397	.811	5.32	4.05
167	.40	2.00	.35	2.31	.396	.811	4.52	4.03
168	.40	2.00	.35	2.34	.396	.811	3.09	4.13
170	.40	2.00	.35	2.30	.395	.811	4.65	3.97
171	.40	2.00	.36	2.17	.395	.809	5.37	3.55
172	.40	2.00	.36	2.18	.394	.809	4.30	3.58
173	.40	2.00	.36	2.07	.394	.809	3.50	3.37
174	.40	2.00	.36	2.07	.394	.808	3.93	3.35
175	.40	2.00	.36	2.07	.393	.808	3.74	3.33
176	.40	2.00	.36	2.07	.393	.809	2.61	3.36
177	.40	2.00	.36	2.07	.393	.810	3.92	3.40
178	.40	2.00	.36	2.07	.392	.811	4.86	3.47
179	.40	2.00	.36	2.20	.392	.810	4.57	3.66
180	.40	2.00	.36	2.17	.392	.810	3.89	3.57

COMPARISON OF EXPERIMENTAL AND PREDICTED SOLIDS FLOW RATES

Run No. -	On Time, s	Off Time, s	Fluid-izing Time, s	ΔP (P_1-P_3) kPa	ε_1 -	ε_3 -	Measured Solids Flow, kg/s	Predicted Solids Flow, kg/s
181	.40	2.00	.36	2.07	.391	.807	3.98	3.32
182	.40	2.00	.36	2.07	.391	.807	3.53	3.32
183	.40	2.00	.36	2.07	.391	.808	3.33	3.37
184	.40	2.00	.36	2.07	.390	.807	3.23	3.34
185	.40	2.00	.36	2.07	.390	.805	1.92	3.29
186	.40	2.00	.36	2.07	.390	.802	1.08	3.27
187	.20	1.20	.34	2.28	.392	.752	2.37	3.66
188	.20	1.20	.35	2.28	.391	.755	1.12	3.66
189	.20	1.20	.34	2.29	.391	.760	3.75	3.72
190	.20	1.20	.35	2.29	.391	.759	2.90	3.70
191	.20	1.20	.34	2.30	.390	.761	5.41	3.77
192	.20	1.20	.34	2.31	.390	.762	2.99	3.78
193	.20	1.20	.34	2.35	.390	.765	5.80	3.94
194	.20	1.20	.34	2.33	.390	.764	5.07	3.89
195	.20	1.20	.34	2.39	.390	.767	5.09	4.11
196	.20	1.20	.34	2.40	.390	.767	5.10	4.15
197	.40	1.80	.36	2.07	.386	.833	4.59	3.35
198	.40	1.80	.36	2.07	.386	.832	3.53	3.35
199	.40	1.80	.36	2.06	.386	.832	2.55	3.32
200	.40	1.80	.36	2.06	.385	.831	3.49	3.32
201	.40	1.60	.36	1.84	.385	.859	2.39	3.18
202	.40	1.60	.36	1.85	.385	.860	2.63	3.20
203	.40	1.40	.36	1.71	.391	.885	2.71	3.08
204	.40	1.40	.37	1.70	.391	.885	2.53	3.08
205	.40	1.20	.33	1.31	.530	.917	2.87	2.34
206	.40	1.20	.33	1.31	.530	.917	1.84	2.35
207	.40	2.00	.36	2.07	.383	.805	2.73	3.32
208	.40	2.00	.36	2.07	.383	.804	1.89	3.31
209	.40	2.00	.36	2.07	.382	.807	3.87	3.38
210	.40	2.00	.36	2.07	.382	.806	2.90	3.36
211	.40	2.00	.36	2.07	.382	.806	3.06	3.36
212	.40	2.00	.36	2.07	.381	.804	3.36	3.33
213	.40	1.80	.36	2.06	.381	.832	3.63	3.35
214	.40	1.80	.36	2.06	.381	.832	3.20	3.36
215	.40	1.60	.37	1.85	.380	.861	3.57	3.25
216	.40	1.60	.37	1.84	.380	.860	2.66	3.22
217	.40	1.40	.37	1.71	.387	.886	1.90	3.12
218	.40	1.40	.37	1.71	.386	.886	2.37	3.14
219	.40	1.20	.33	1.31	.527	.917	3.14	2.38
220	.40	1.20	.33	1.31	.526	.917	2.38	2.37
221	.40	1.00	.28	.94	.667	.943	1.32	1.61
222	.40	1.00	.28	.95	.667	.944	3.00	1.68
223	.20	1.00	.30	1.46	.597	.856	3.57	2.77
224	.20	1.00	.30	1.46	.596	.855	3.07	2.77

COMPARISON OF EXPERIMENTAL AND PREDICTED SOLIDS FLOW RATES

Run No. -	On Time, s	Off Time, s	Fluid-izing Time, s	ΔP (P_1-P_3) kPa	ε_1 -	ε_3 -	Measured Solids Flow, kg/s	Predicted Solids Flow, kg/s
225	.20	.80	.22	.77	.799	.937	1.45	1.76
226	.20	.80	.22	.77	.799	.936	2.70	1.73
227	.20	.60	.17	.35	.888	.982	.39	.79
228	.20	.60	.19	.38	.858	.980	1.02	.89
229	.20	1.40	.36	2.37	.376	.732	2.70	3.51
230	.20	1.40	.36	2.37	.376	.733	3.46	3.52
231	.20	1.80	.35	2.52	.375	.695	3.01	3.12
232	.20	1.80	.35	2.52	.375	.694	2.57	3.12
233	1.00	2.00	.36	2.07	.375	.798	2.28	2.66
234	1.00	2.00	.36	2.07	.374	.801	2.52	2.66
235	1.00	1.80	.37	1.95	.374	.830	2.62	2.57
236	1.00	1.80	.37	1.95	.374	.828	2.81	2.57
237	1.00	1.60	.37	1.83	.373	.856	2.76	2.46
238	1.00	1.60	.37	1.83	.373	.857	2.60	2.47
239	1.00	1.40	.37	1.69	.380	.884	2.05	2.33
240	1.00	1.40	.37	1.69	.379	.882	1.68	2.32
241	.40	2.00	.36	2.07	.372	.802	1.22	3.35
242	.40	2.00	.36	2.07	.372	.802	1.88	3.35
243	.40	2.00	.36	2.07	.371	.804	2.71	3.40
244	.40	2.00	.36	2.07	.371	.805	3.44	3.42
245	.40	1.80	.36	2.06	.371	.832	3.20	3.42
246	.40	1.80	.37	1.96	.370	.832	4.38	3.34
247	.40	1.40	.37	1.70	.377	.886	3.25	3.17
248	.40	1.40	.37	1.70	.377	.886	3.26	3.17
249	.40	1.20	.33	1.31	.519	.917	2.85	2.43
250	.40	1.20	.33	1.31	.519	.918	2.66	2.45
251	.40	1.00	.28	.95	.662	.944	1.89	1.70
252	.40	1.00	.28	.94	.661	.944	2.68	1.70
253	1.00	2.00	.36	2.07	.368	.800	2.71	2.69
254	1.00	2.00	.36	2.07	.368	.799	3.18	2.68
255	1.00	1.60	.37	1.82	.368	.857	3.50	2.48
256	1.00	1.60	.37	1.82	.367	.858	2.80	2.49
257	1.00	1.20	.33	1.30	.517	.916	.47	1.73
258	1.00	1.20	.33	1.29	.517	.916	2.66	1.72
259	1.00	1.40	.37	1.68	.373	.883	2.62	2.34
260	1.00	1.40	.37	1.68	.373	.884	3.00	2.35

COMPARISON OF EXPERIMENTAL AND PREDICTED SOLIDS FLOW RATES

Run No. -	On Time, s	Off Time, s	Fluid-izing Time, s	ΔP (P_1-P_3) kPa	ε_1 -	ε_3 -	Measured Solids Flow, kg/s	Predicted Solids Flow, kg/s
261	1.00	1.80	.37	1.94	.366	.830	2.86	2.60
262	1.00	1.80	.37	1.93	.365	.829	4.06	2.59
263	1.00	1.00	.28	.93	.659	.943	2.53	1.15
264	1.00	1.00	.28	.93	.659	.943	.54	1.16
265	.20	1.40	.36	2.37	.364	.728	3.59	3.58
266	.20	1.40	.36	2.37	.364	.728	3.98	3.59
267	.20	1.00	.30	1.48	.585	.852	3.57	2.88
268	.20	1.00	.30	1.48	.585	.852	3.48	2.89
269	.20	.80	.22	.76	.794	.934	3.23	1.73
270	.20	.80	.22	.77	.794	.935	3.20	1.78
271	.20	.60	.15	.37	.917	.983	.00	.70
272	.20	.60	.15	.38	.907	.982	.00	.74

TECHNICAL REPORT DATA
(Please read Instructions on the reverse before completing)

1. REPORT NO. EPA-600/7-79-021	2.	3. RECIPIENT'S ACCESSION NO.
4. TITLE AND SUBTITLE Solids Transport Between Adjacent CAFB Fluidized Beds		5. REPORT DATE January 1979
		6. PERFORMING ORGANIZATION CODE
7. AUTHOR(S) D. M. Bachovchin, P. R. Mulik, R. A. Newby, and D. L. Keairns		8. PERFORMING ORGANIZATION REPORT NO.
9. PERFORMING ORGANIZATION NAME AND ADDRESS Westinghouse Research and Development Center Pittsburgh, Pennsylvania 15235		10. PROGRAM ELEMENT NO. EHE623A
		11. CONTRACT/GRANT NO. 68-02-2142
12. SPONSORING AGENCY NAME AND ADDRESS EPA, Office of Research and Development Industrial Environmental Research Laboratory Research Triangle Park, NC 27711		13. TYPE OF REPORT AND PERIOD COVERED Final; 7/75 - 8/78
		14. SPONSORING AGENCY CODE EPA/600/13

15. SUPPLEMENTARY NOTES IERL-RTP project officer is Samuel L. Rakes, MD-61, 919/541-2825.

16. ABSTRACT The report gives results of an experimental investigation of a pulsed, dense-phase pneumatic transport system for controlled circulation between adjacent fluidized beds. A model was developed to predict performance. The program provides technical support for EPA's program to demonstrate the Chemically Active Fluid Bed (CAFB) Process, being developed to produce a clean, low heating value fuel gas from fossil fuels. A cold model test facility, capable of transporting up to about 6.3 kg/s, was built and operated to demonstrate effects of key parameters. Generated data were utilized in the development of a mathematical model of the system which allows projection of the effects of key variables. Solids flow is controlled by pulsed air input, whose on-time (<0.3 to 0.4 s) and off-time (1.5 to 2.0 s) should be controlled for best performance. The system pressure balance should also be carefully controlled. Expected demonstration plant bed-material density may result in higher air requirements than was predicted in the plant design. Wider legs and more nozzles or greater transport-gas capacity may alleviate this difficulty.

17. KEY WORDS AND DOCUMENT ANALYSIS

a. DESCRIPTORS	b. IDENTIFIERS/OPEN ENDED TERMS	c. COSATI Field/Group
Pollution	Pollution Control	13B
Fluidized Bed Processors	Stationary Sources	13I, 07A
Solids Flow	Chemically Active Fluid Beds	20D
Gasification		13H
Fossil Fuels		21D
Mathematical Models		12A

18. DISTRIBUTION STATEMENT Unlimited	19. SECURITY CLASS (This Report) Unclassified	21. NO. OF PAGES 173
	20. SECURITY CLASS (This page) Unclassified	22. PRICE

EPA Form 2220-1 (9-73)